Target indicators and mechanistic function of epidrugs with activity against multiple stages of *Plasmodium falciparum* parasites

Daniel Francis Luke Opperman

Submitted in fulfilment of the requirements of the degree

*Magister Scientia*e

(Specialisation in Biochemistry)

In the Faculty of Natural and Agricultural Sciences

Department of Biochemistry, Genetics and Microbiology

Division of Biochemistry

University of Pretoria

South Africa

2021

The financial assistance of the National Research Foundation (NRF) towards this research is hereby acknowledged. Opinions expressed and conclusions arrived at, are those of the author and are not necessarily to be attributed to the NRF.

UNIVERSITEIT VAN PRETORIA
UNIVERSITY OF PRETORIA
YUNIBESITHI YA PRETORIA

Submission Declaration

I, Daniel Francis Luke Opperman, declare that the dissertation, which I hereby submit for the degree *Magister Scientiae* in the Department of Biochemistry, Genetics and Microbiology at the University of Pretoria, is my own work and has not previously been submitted by me for a degree at this or any other tertiary institution.

Signature: _____

Date: 10-12-2021

UNIVERSITEIT VAN PRETORIA
UNIVERSITY OF PRETORIA
YUNIBESITHI YA PRETORIA

Declaration of Originality

University of Pretoria

Faculty of Natural and Agricultural Sciences

Department of Biochemistry, Genetics and Microbiology

Division of Biochemistry

Full names of student: Daniel Francis Luke Opperman

Student number: 13009631

Declaration:

1. I understand what plagiarism is and am aware of the University's policy in this regard.
2. I declare that this dissertation is my own original work. Where other people's work has been used (either from a printed source, Internet or any other source), this has been properly acknowledged and referenced in accordance with departmental requirements.
3. I have not used work previously produced by another student or any other person to hand in as my own.
4. I have not allowed, and will not allow, anyone to copy my work with the intention of passing it off as his or her own work.

Signature: 

Date: 10-12-2021

Table of Contents

List of Figures

List of Tables

List of Abbreviations

2-oxoglutarate	2-OG
ACT	Artemisinin-based combination therapy
ApiAP2	Apicomplexan Apetala 2
BCA	Bicinchoninic acid
BLAST	Basic Local Alignment Search Tool
BSA	Bovine serum albumin
CARM1	Coactivator-associated arginine methyltransferase 1
CRT	Chloroquine resistance transporter
CSP	Circumsporozoite protein
DARTS	Drug affinity responsive target stability
DMSO	Dimethyl sulfoxide
EIA	Exflagellation inhibition assay
ELISA	Enzyme-linked immunosorbent assay
epidrugs	Epigenetic drugs
GCN5	General control non-repressed protein 5
GMQE	Global model quality estimate
HAT	Histone acetyltransferase
HATi	Histone acetyltransferase inhibitor
HDAC	Histone deacetylase
HDACi	Histone deacetylase inhibitors
HDM	Histone demethylase
HDMi	Histone demethylase inhibitor
HEPES	4-(2-hydroxyethyl)-1-piperazineethanesulfonic acid
HKMT	Histone lysine methyltransferase
HKMTi	Histone lysine methyltransferase inhibitors
HRP	Horseradish peroxidase
IC_{50}	Half-maximal inhibitory concentration
IDC	Intra-erythrocytic development cycle
Jmj	Jumonji domain-containing
JMJD	Jumonji domain-containing
KDM	Lysine demethylase
LC-MS	Liquid chromatography-mass spectrometry
LSD	Lysine-specific demethylase
MoA	Mode of action
NMR	Nuclear magnetic resonance
PBS	Phosphate-buffered saline
PfEMP1	Erythrocyte membrane protein 1
PfHP1	Heterochromatin protein 1
PRMT	Protein arginine methyltransferase
PTM	Post-translational modification
RMSD	Root-mean-square deviation
SAM	*S*-adenosylmethionine
SDS-PAGE	Sodium dodecyl sulphate-polyacrylamide gel electrophoresis
SET	Su(var)3–9-‘ Enhancer of zeste-Trithorax
Sir2A	Sirtuin 2A
Sir2B	Sirtuin 2B
Sirtinol	Sir two inhibitor naphthol
SMFA	Standard membrane-feeding assay
SUMO	Small ubiquitin-like modifier
TCA	Trichloroacetic acid
TCP	Target candidate profile
TPP	Target product profile
WHO	World Health Organisation

Acknowledgements

I would like to thank my supervisor, Professor Lyn-Marié Birkholtz, for her mentorship, time and support and her contagious passion for science, which has enabled me to pursue my ambitions in a way that would not otherwise have been possible.

My sincere gratitude also goes to my co-supervisor, Dr Janette Reader, for her assistance and guidance and for her efforts in reading my dissertation.

My heartfelt thanks go to my mother, Ilse Opperman, to whom I am profoundly grateful, for her unending encouragement and support throughout my studies, both in trying times and through my successes.

My sincerest thanks to Shanté and Henrico, who have become dear friends, for three years of incredible friendship, support, lunches at Adlers and for our weekly quiz nights. Thank you for making the stresses of postgraduate studies bearable and for making the good times all the better.

To Brendon, one of my closest friends for more than a decade, for his constant investment in my studies and successes, for the great times spent over coffee that allowed me to recharge my batteries and more easily deal with the rigours of my MSc.

I will forever be grateful to the M^2PL group, for their bottomless well of knowledge and expertise and their incredible generosity in sharing it.

I am also grateful towards the NRF for funding my degree through the Grantholder-linked bursary, enabling me to pursue my studies.

Finally, I would like to thank all of those in my life whom I have not mentioned by name but who have supported me through the years.

Summary

Resistance to the most widely used drugs in the treatment of malaria, those in artemisinin-based combination therapies, has emerged, most recently in Africa. Development of new drugs that exploit unique structures with new modes of action (MoA) is therefore critical. There is also a need for the development of compounds with transmission-blocking activity, in addition to the clearance of symptom-causing stages associated with drugs currently part of the chemotherapeutic toolbox. A promising avenue of research in this regard is into epigenetic drugs ("epidrugs"), which target epigenetic mechanisms of transcriptional control, resulting in parasite death through perturbation of gene expression.

A selection of compounds with demonstrated epigenetic perturbation in human cancer cell lines have shown favourable inhibitory profiles against *Plasmodium falciparum* parasites. For a number of these compounds, the specific mode of action remained to be elucidated and characterised. This dissertation has contributed to our understanding of these compounds' modes of action, demonstrating perturbation of histone post-translational modifications, and revealing possible binding modes to putative targets through *in silico* predictions. Findings confirmed histone deacetylase inhibition for both Scriptaid and Sirtinol, with histone deacetylase 1 (PfHDAC1) and sirtuin 2A (PfSir2A), respectively, indicated as the targets of these compounds through *in silico* docking studies. ML324 was found to exhibit histone demethylase activity in *P. falciparum* late-stage gametocytes, with PfJmj3 indicated as the target of this compound. Finally, the potential of these compounds as transmission-blocking drugs has been revealed through exflagellation inhibition assays and confirmed with standard membrane-feeding assays. These results underscore the potential of epigenetic transcriptional control as a targetable biology, and of epidrugs to contribute towards addressing the development of drug resistance by *P. falciparum*. The findings demonstrated in this dissertation may lay the groundwork for future drug development efforts for which the epigenetic drugs discussed here may serve as chemical scaffolds.

Chapter 1: Literature review

1.1. Malaria as a pathogenic disease and its global impact

Malaria is a disease of poverty that has had a profound effect on humanity, presenting an extreme socioeconomic burden in developing countries. Approximately 229 million cases of malaria occurred in 2019, resulting in approximately 409 000 deaths, with the overwhelming majority of these in Africa, according to the World Health Organisation (WHO) [1]. While there is an observable downwards trend in the number of malaria cases and deaths year-on-year, this decrease has begun to slow, and it is predicted that the COVID-19 pandemic, which caused widespread disruptions to essential malaria services, may itself result in reversion of gains made over the past decades in the fight against malaria [1].

Malaria is prevalent in poorer countries, where access to healthcare may be more limited and living conditions are inadequate, and is additionally associated with an economic impact, where illness and death may deprive families of an income. For these reasons malaria is regarded a disease of poverty [2]. While the list of countries that have achieved malaria elimination continues to grow (Fig. 1.1), with numerous having been certified malaria free and a number having had no indigenous cases for a number of years [1], a large percentage of the world's population continue to live under threat of malaria and its consequences, necessitating strategies to address the severe burden this disease presents to global health.

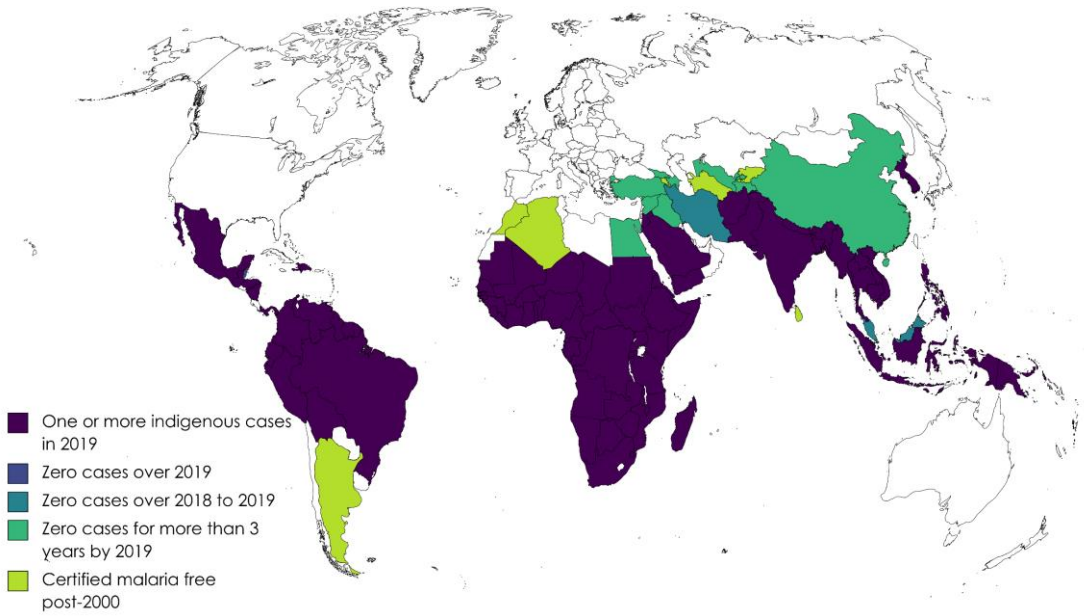

Figure 1.1: State of malaria elimination progress since 2000. Numerous countries have achieved elimination, while others are on the cusp of doing so. Much of the world, however, still suffers under the burden of this disease. Countries that have achieved elimination since 2020 are indicated in light green, while those that continue to see indigenous cases are indicated in purple. Figure adapted from the World Health Organisation World Malaria Report 2020. Map created using MapChart, available at the URL https://mapchart.net/.

1.2. The aetiological *Plasmodium* parasite

In the majority of cases, malaria in Africa is caused by the species *Plasmodium falciparum*, which is responsible for the most severe form of the disease and has the most extensive socioeconomic impact [3], while in Asia it is predominantly caused by *Plasmodium vivax* [4]. Several other clinically less relevant species are also known to cause malaria in humans, including *Plasmodium malariae*, *Plasmodium ovale* [5] and *Plasmodium knowlesi* [6]. *Plasmodium* parasites, alongside other clinically relevant protozoans such as *Toxoplasma* and *Babesia*, belong to the protozoan phylum Apicomplexa [7]. The symptoms of malaria are most serious in children younger than five years old and pregnant women [8], and include a characteristic cyclical fever, chills with drenching sweats, muscle aches and headaches. In the most severe cases it can progress to cerebral malaria, hypoglycaemia, anaemia and metabolic acidosis [9].

In large part, the difficulty in achieving malaria elimination lies in the exceedingly complex life cycle of *Plasmodium* species in comparison to many other pathogens. Transmission of the disease is mediated through parasite transfer, occurring upon being bitten by infected females of the mosquito genus *Anopheles*. Female mosquitoes, like males, are nectarivores but, while carrying eggs, will seek a blood meal to provide nutrients essential for egg development [10].

All *Plasmodium* species are associated with both a symptom-causing asexual cycle and an asymptomatic sexual cycle [11] (Fig. 1.2). Sporozoites are injected into dermal capillaries of the human secondary host upon being bitten by an infected mosquito, the primary host [12]. The injected sporozoites then make their way through the circulatory system to the liver, where they infect hepatocytes, forming hepatic schizonts [13]. Through hepatic schizogony, thousands of merozoites are produced and released [14]. These merozoites may proceed to infect erythrocytes and, in the case of *P. falciparum*, also reticulocytes, thus initiating the asexual, intra-erythrocytic development cycle (IDC) [15]. The process of erythrocytic invasion occurs through the binding of a merozoite to the erythrocyte, reorientation of the merozoite until the apical end makes contact with the erythrocyte, and finally entry of the merozoite into the cell [16]. Prior to entering the erythrocyte, the merozoite is vulnerable, but is able to evade the immune system due to polymorphic, redundant surface proteins, as well as a rapid invasion process [15, 17]. As the parasite proceeds through the IDC, its nutritional needs are met through ingestion and metabolism of haemoglobin from the host cell, with the toxic haem prosthetic group being converted to nontoxic haemozoin crystals, a process that occurs in the food vacuole [18]. The first stage of the IDC is the ring stage, which is followed by the trophozoite stage. This progresses to the schizont stage, where asynchronous, endomitotic replication, termed schizogony, produces 16 to 32 merozoites per schizont [19], each of which may infect further erythrocytes [20, 21]. In *P. falciparum*, this cycle takes place over a 48 h period, with the rupturing of schizonts at the end of each cycle corresponding to the 48 h fever cycle characteristic of falciparum malaria [9].

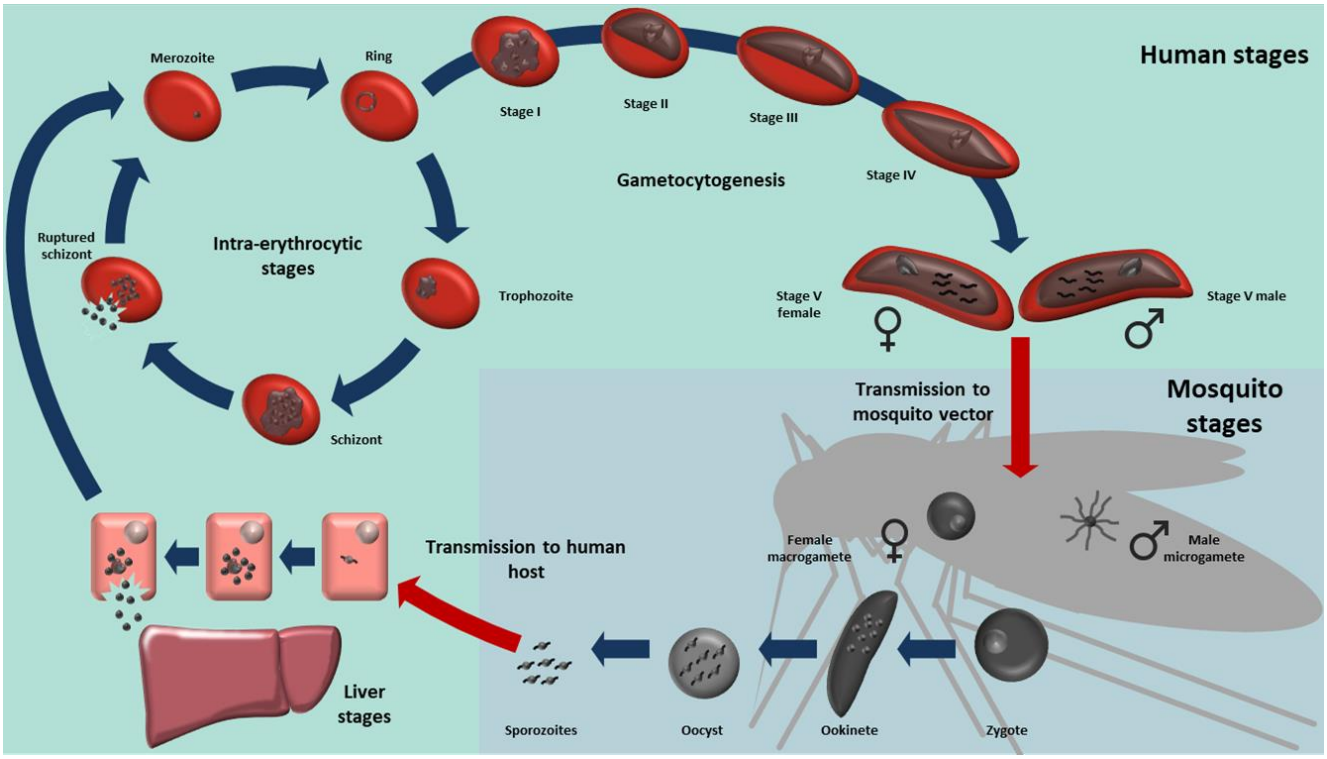

Figure 1.2: The life cycle of *P. falciparum*. Malaria infection occurs upon injection of sporozoites as an infected mosquito takes a blood meal. The sporozoites proceed to the liver, where they infect hepatocytes. After schizogony, merozoites are released into the bloodstream as the erythrocyte ruptures. Each of these may continue the infection cycle in another erythrocyte. A percentage of these parasites commit to gametocytogenesis. Gametocytes progress through five stages and stage V gametocytes are ingested by mosquitoes taking a blood meal. Stage V gametocytes undergo gametogenesis, resulting in the formation of male microgametes and female macrogametes. One male and one female gamete fuse to form a zygote, which matures to produce an ookinete. This ookinete then develops into an oocyst in which sporogony occurs, forming sporozoites, which travel to the salivary ducts and are injected into the secondary host when the mosquito takes another blood meal, thus transmitting the parasite.

A proportion of IDC-stage parasites, amounting to less than 10 %, commit to sexual differentiation in a stochastic manner and undergo gametocytogenesis [22]. In *P. falciparum*, gametocytogenesis proceeds through five stages (I-V) [23]. Early stages sequester in bone marrow, precluding splenic clearance of the gametocytes [24], while the mature stage V gametocytes are released and reach the dermal capillaries, where they may once more be taken up by a female mosquito taking a blood meal, enabling parasite transmission [25]. In the mosquito gut, the parasite is exposed to a drop in pH through contact with xanthurenic acid, as well as a decrease in temperature, triggering gametogenesis and resulting in the formation of male microgametes and female macrogametes [26]. One macrogamete and one microgamete fuse to form a zygote, completing the sexual reproduction cycle [27]. This zygote differentiates, forming an ookinete that is able to penetrate the gut wall [28], whereupon an oocyst is formed in the gut epithelium, leading to asexual sporogony. The sporozoites continue to the salivary glands, from where they are injected into a human secondary host upon further blood meals, completing the parasite life cycle [29]. This coordinated progression through the life cycle in *P. falciparum* occurs primarily through the Apicomplexa Apetala 2 (ApiAP2) group of transcription factors [30, 31] as well as

through epigenetic mechanisms whose important role is becoming increasingly apparent [11] and which may also control ApiAP2 member activity.

1.3. Malaria control – general strategies targeting the parasite

Malaria may be addressed from a vector-control basis, which is the mainstay of decreasing malaria transmission and is typically accomplished using indoor residual spraying and insecticide-treated nets [32]. Unfortunately, resistance to many of the most commonly used insecticides is starting to show in many mosquito populations [33, 34]. A diagnosis of malaria is suspected based on patient signs and symptoms as well as their country of origin or travel history. Diagnosis is confirmed by physical observation of parasite presence through thin- or thick-smear microscopy of blood obtained from the patient [35]. Another common method is the rapid diagnostic test [36], but this has characteristic drawbacks, including poor detection of low-parasitaemia infections, though it is able to provide rapid results with little training required for the administration of tests.

Treatment regimens differ depending on the particular aetiological species of *Plasmodium*, as well as the characteristics of the disease course, namely whether the malaria is severe or uncomplicated [37]. The primary method of treatment of endemic uncomplicated malaria is artemisinin-based combination therapy (ACT), in which a fast-acting artemisinin derivative such as artesunate, artemether or dihydroartemisinin is administered to the patient in combination with a longer half-life partner, such as amodiaquine or lumefantrine, allowing residual parasite clearance and minimising the risk of resistance development [37]. Another strategy that is being explored is vaccination to prevent the establishment of malaria infection. To date, the only licensed vaccine against malaria is the recombinant RTS,S/AS01 vaccine, developed by GlaxoSmithKline and marketed as Mosquirix, which directs immunogenic attack against the circumsporozoite protein PfCSP. However, this vaccine requires multiple administrations and has low efficacy (~30 %) [38], though it is predicted that it may still have a dramatic impact on mortality and morbidity of children under the age of five years in high-transmission areas, if used in combination with other interventions [39]. Other vaccines targeting malaria are currently in clinical trials, such as the R21 vaccine which, like RTS,S/AS01, is a recombinant vaccine and is in stage II clinical trials [40], and the PfSPZ live attenuated vaccine, which is in phase III clinical trials [41]. The difficulties in developing a malaria vaccine stem from the complex nature of the *P. falciparum* life cycle, involving two hosts and multiple stages [42]. Mass surveillance also constitutes an extremely important strategy in malaria epidemiology, allowing the identification of high-transmission areas and the focussing of resources, and timely identification of the emergence of drug resistance.

1.4. Chemotherapeutics targeting the aetiological organisms of malaria

Resistance to mainstays of antimalarial therapeutics requires urgent attention. Most populations of *P. falciparum* show resistance to chloroquine [43], once the most widely used medicine for the treatment of malaria throughout the world. Resistance to this medication first appeared in Thailand, from where it spread, and is now globally prevalent. The primary mechanism involved in chloroquine resistance is the chloroquine resistance transporter (PfCRT) protein, which is found in the food vacuole membrane

of the IDC-stage parasite and rapidly exports chloroquine, mitigating its toxicity to the parasite [44]. While treatment with ACT has since largely replaced chloroquine treatment, resistance to artemisinin has now also emerged and is already evident along the Thai-Cambodian border [45]. This is troublesome, as ACT is the mainstay of falciparum malaria treatment and the development of resistance may result in the loss of many lives and may prove a major setback in the fight against malaria [46]. Notably, while mutations conferring resistance to artemisinin derivatives have previously been observed, the first convincing indications of clinical malaria resistance in Africa have now been reported, mediated through *kelch13* mutations [47]. This is a foreboding sign that underscores the increasingly important task of combating this resistance through surveillance and investment into drug discovery efforts.

To combat the rise in resistance to antimalarial therapeutics, new strategies have been proposed to aid in the discovery and refinement of antimalarial drugs and effective combination therapies, namely target candidate profiles (TCP), which describe the ideal and minimum attributes for candidate drug molecules, and target product profiles (TPP), which describe the ideal and minimum attributes necessary for combination therapies. These aim to set clearly defined targets for the discovery of new drugs and the development and refinement of effective combination therapy formulations [48]. They must necessarily be in constant flux due to the changing nature of the parasite, as resistance is developed and patterns of transmission change, and changes in the understanding of the parasite occur over time as new aspects of parasite biology are discovered [49]. An effective medication must be orally bioactive, bioavailable, safe, clear asexual parasites, prevent transmission and confer chemoprotection [49]. Two main foci in this regard are TCP-1 and TCP-5, which respectively refer to the targeting of asexual, symptom-causing parasites and gametocytes, thus conferring transmission blocking.

Due to increasing resistance to artemisinin and its derivatives, the development of novel drugs and the discovery of new drug targets for malaria treatment is essential. Drug discovery may follow different avenues, including phenotypic screening, in which compounds are screened for inhibitory activity in malaria parasites, or target-based screening, where putative drug targets in the parasites are screened for inhibition by a variety of drugs [50]. However, in both instances, any new antimalarial will need to target a unique pathway or protein in malaria parasites to delay resistance development and to guide combination therapies.

Because many enzymes involved in epigenetic regulation in *P. falciparum* appear to be distinct from those in humans, and because of the reliance of *P. falciparum* on these enzymes for the regulation of various processes, they may be good potential drug targets [51]. In addition, transmission blocking is an important aspect of malaria control, as the clearance of symptom-causing asexual stages may leave the patient still harbouring transmissible gametocyte stages [52]. This may be addressed by the development of drugs targeting those stages. The ability of epidrugs to perturb the tight transcriptional control characteristic of these parasites, resulting in parasite death and therefore clearance of asexual parasites as well as transmission blocking, should therefore be explored [48].

1.5. Transcriptional control in *P. falciparum*

Control of gene expression may be mediated at multiple levels: transcriptional, post-transcriptional, translational and post-translational [53]. Progression through the parasite life cycle is tightly controlled, with stage-specific gene activation following a "just-in-time" model in asexual stages [54], whereby genes are expressed only as needed and in a highly stage-specific manner, highlighting the importance of transcriptional control in *P. falciparum*. An even more specialised expression profile is seen throughout gametocyte development. Increased transcript abundance is found for only 45 % of genes throughout sexual differentiation, compared to 80-95 % in asexual development [55]. This reveals a more specialised transcriptional program in the sexual stages and validates this tight transcriptional control in sexual development, with a number of genes showing increased transcription levels in gametocyte stages or clear developmental regulation throughout gametocytogenesis.

Despite the observed tight transcriptional control, few transcription factors have been discovered in *P. falciparum* parasites beyond the ApiAP2 family of DNA-binding proteins, indicating that other factors must be important in mediating this control, of which a proposed mechanism is epigenetic transcriptional regulation [56].

1.6. Epigenetic control of transcription – a general overview with specifics in *P. falciparum*

The epigenome consists of heritable chemical changes to the genome, independent of the underlying DNA sequence, that allow for tight transcriptional regulation in a manner that is fully reversable. A number of modifier proteins coordinate this complex epigenetic programming [51], effecting downstream transcriptional changes. Genetic material is organised into chromatin, which is composed of multiple nucleosomes, each made up of DNA wrapped around a histone octamer. Epigenetic control of transcription in eukaryotes may occur at different levels (Fig. 1.3). For example, at the DNA level, bases may be methylated by DNA methyltransferases to form a 5-methylcytosine product. This alters transcription levels, largely through the prevention of transcription factor binding or through the recruitment of other proteins, including adaptor proteins, that themselves recruit other modifier proteins such as histone deacetylases that may change the chromatic state, with gene silencing as the downstream functional consequence [57]. At the nucleosome level, canonical histone proteins may be replaced with histone variants. *P. falciparum* possess four canonical histones, H2A, H2B, H3 and H4. The first three of these may be replaced with variant histones, respectively H2A.Z, H2Bv and H3.3 and H3Cen, each of which are implicated in gene regulation changes [58]. In contrast to higher eukaryotes, linker histone H1 is not found in the *P. falciparum* proteome [58]. Each histone monomer has a histone tail that may undergo post-translational modification [59], and lysine residues in histone protein tails may be acetylated or methylated, amongst other post-translational modification (PTMs) (Fig. 1.3).

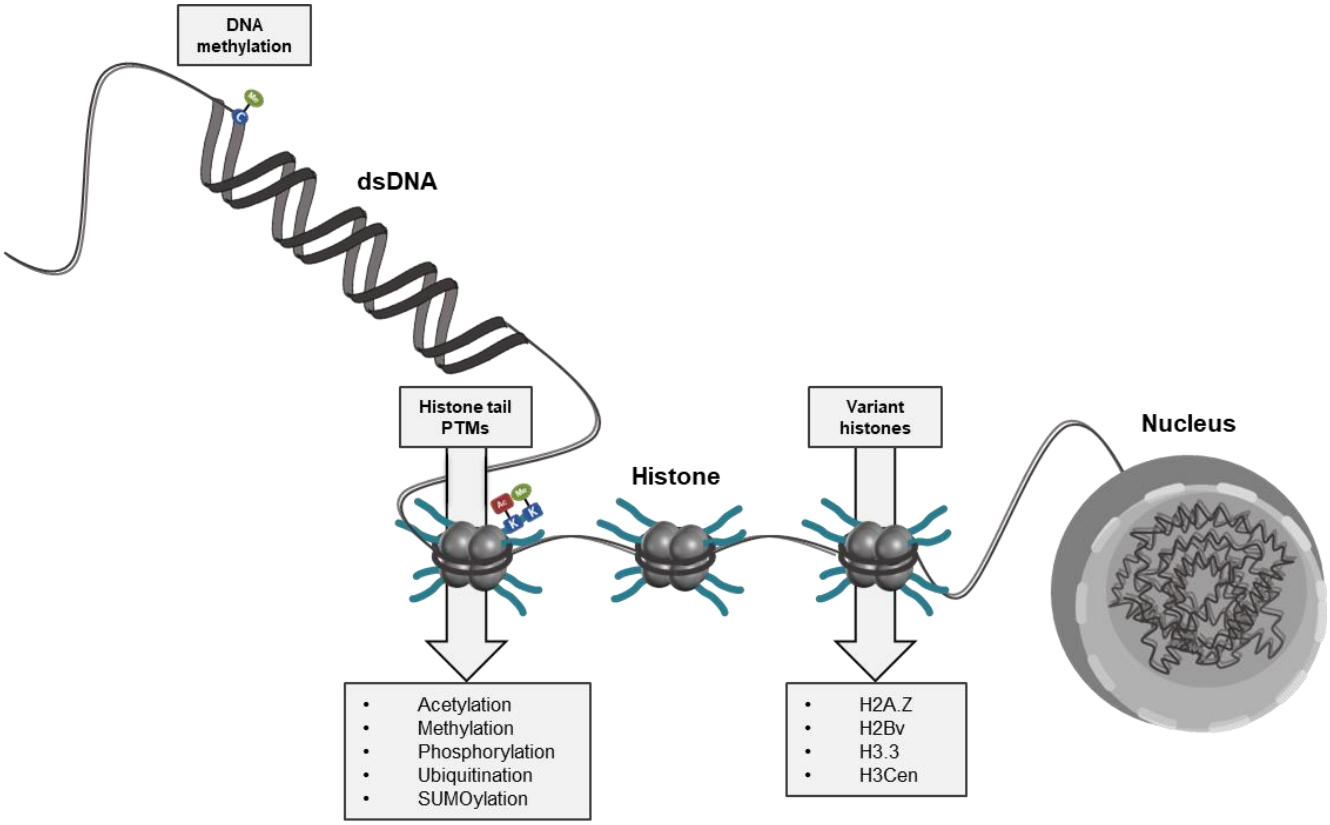

Figure 1.3: The levels of epigenetic control of transcription. Epigenetic control can, for example, occur at the DNA level, where bases may be methylated, or at the nucleosome level, which may include histone PTMs or replacement of core histones with variant histones.

Such perturbations of the epigenome may result in the conversion of transcriptionally active euchromatin to transcriptionally repressed heterochromatin or *vice versa*. These two states are characterised by their accessibility to DNA-binding effector proteins such as RNA polymerases [56, 60] (Fig. 1.4). Epigenetic changes may also recruit particular epigenetic readers to exert downstream effects [61]. Proteins involved in the epigenetic control of transcription include writers, which carry out the addition of epigenetic modifications (particularly to histone N-terminal tails) and erasers, which remove these modifications. Reader proteins are able to detect these modifications and react accordingly in effecting gene transcription [62] (Fig. 1.4). The histone code is the distinct histone PTM pattern of mostly acetylation and methylation, associated with particular chromosomal states and resulting in distinct patterns of gene expression [59]. Acetylation of lysine residues in histone tails increases the rate of transcription by diminishing the positive charge associated with these, inducing the conversion of heterochromatin to euchromatin [63]. Methylation of histone tail lysine residues may either increase or decrease the rate of transcription, depending both on the position and the degree of methylation, with the addition of between one and three methyl groups possible [61]. Other histone PTMs may also effect this epigenetic control. For example, serine and threonine residues may be phosphorylated [64] and arginine residues may be methylated [58, 65], whilst lysine residues may be ubiquitylated [66], or sumoylated through the addition of small ubiquitin-like modifiers (SUMO) [67].

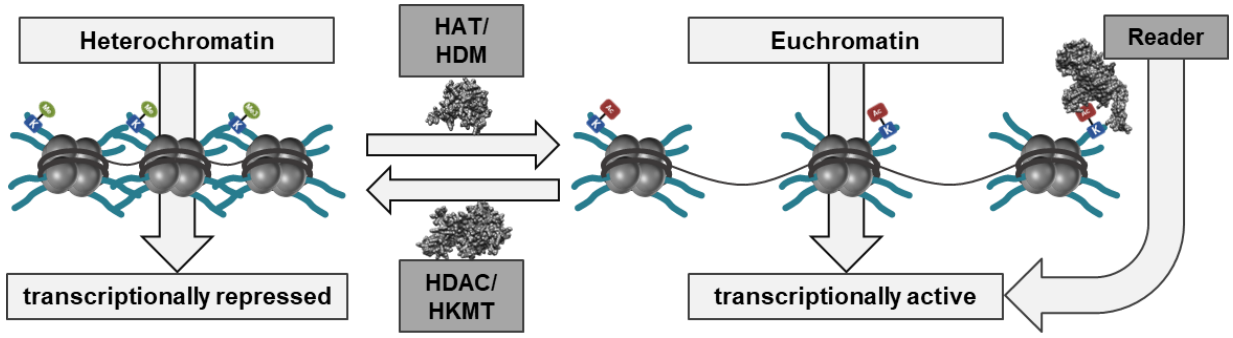

Figure 1.4: Histone PTMs and the conversion of heterochromatin to euchromatin. Certain histone tail PTMs, such as lysine acetylation or methylation, facilitate the conversion of heterochromatin to euchromatin, or the reverse. In heterochromatin, transcription is repressed while in euchromatin transcription is active. Ac – acetylation, in red. Me – methylation, in green. HAT: histone acetylatransferase. HDM: histone demethylase. HDAC: histone deacetylase. HKMT: histone lysine methyltransferase.

Validating the importance of epigenetic transcriptional regulation in *P. falciparum* is the defined pattern of histone PTMs, both activating and repressing, found to be associated with each developmental stage of the parasite [68]. These histone PTMs show a dynamic pattern associated with stage differentiation, and a clear distinction is seen in histone PTMs associated with different developmental outcomes (Fig. 1.5). The acetylation mark H3K9ac has been associated with transcriptional permissiveness in *P. falciparum*, with a high observed occupancy in the promotor regions of actively transcribed genes. H3K9ac is enriched in the trophozoite and schizont stages of the parasite and is almost completely depleted in mature gametocytes (Fig. 1.5). Conversely, a high occupancy of H3K9me3 is observed in the promotor regions of transcriptionally silent genes, especially in gametocyte developmental stages [69] (Fig. 1.5). These histone PTMs therefore exert opposing effects on gene regulation. Antigenic variation of erythrocyte membrane protein 1 (PfEMP1), encoded by *var* genes in a clonally-variant manner, is controlled in an antagonistic fashion by silencing H3K9me3 PTMs and activating di- and trimethylation of H3K4 and acetylation of H3K9, facilitating evasion of the host immune system [70]. The transcription factor PfAP2-G is instrumental in committing asexual parasites to sexual development. The *pfap2-g* locus appears to be maintained in a silenced, heterochromatic state through high abundance of the histone PTM H3K9me3 with concomitant binding of heterochromatin protein 1 (PfHP1) in uncommitted asexual parasites [71]. This underlines the importance of epigenetic control in sexual commitment. Di- and trimethylation of H3K36 appear to control early gametocyte development through the silencing of genes involved in asexual proliferation and sexual commitment [72].

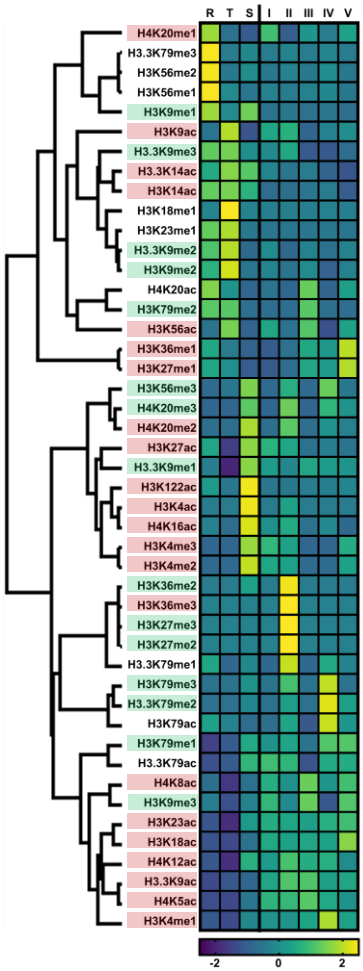

Figure 1.5 Relative abundance (z-score) of histone PTMs throughout asexual and gametocyte development. Histone PTMs phase ordered after hierarchical clustering of Z-scores with Pearson correlation on average linkages. PTMs known to induce conversion to euchromatin are highlighted in red while those known to induce conversion to heterochromatin are highlighted in green, based on available data for *P. falciparum* or in other model organisms. Figure adapted from Coetzee *et al*. 2017 using GraphPad Prism 9.

1.7. Epigenetic control of transcription as a targetable biology in *P. falciparum*

The importance of epigenetic control for development and differentiation of *P. falciparum* parasites implies that this process may be targetable. As it is involved in both asexual proliferation and in sexual differentiation, perturbation of epigenetic processes may meet the criteria for both TCP-1 and TCP-5. The *P. falciparum* genome encodes several and diverse reader and writer proteins that could be targets for chemotherapeutic interventions (Fig. 1.6). This includes ten Su(var)3-9-'Enhancer of zeste-Trithorax (SET) domain-containing histone lysine methyltransferases (HKMTs) (PfSET1-10), five histone demethylases (HDMs, including lysine-specific demethylase 1 and 2, PfLSD1 and PfLSD2)) and Jumonji C domain-containing demethylases 1-3 (PfJmjc1, PfJmjc2 and PfJmj3). Regarding acetylation marks, four histone acetyltransferases (HATs) including PfMYST, PFL1345c, general control non-repressed protein 5 (PfGCN5) and PfHAT1 - and five histone deacetylases (HDACs), including the class I HDACs PfHDAC1 and PfHDAC2, class II HDAC PfHDAC3 and class III HDACs PfSir2A and PfSir2B (sirtuin 2A and 2B) are present [61].

In comparison to the lysine modifiers, effector proteins of histone tail arginine residues are more sparsely characterised. These include protein arginine methyltransferase 1 (PfPRMT1), which appears to be involved in methylation of arginine residues in histones H2A and H4 [65], PfPRMT5 [53] and a putative coactivator-associated arginine methyltransferase 1 (PfCARM1), also known as PfPRMT4 [65]. These epigenetic modulators are differentially expressed throughout the parasite life cycle, indicating their importance in stage-specific processes [55] (Fig. 1.6). PfLSD2 and PfSET3 appear to be involved in gametocytogenesis and PfSir2A appears to have a role in late-stage gametocytes and possibly in gametogenesis, evidenced by respective increases in transcript abundances. PfJmjC2, by contrast, is upregulated in asexual development (Fig. 1.6).

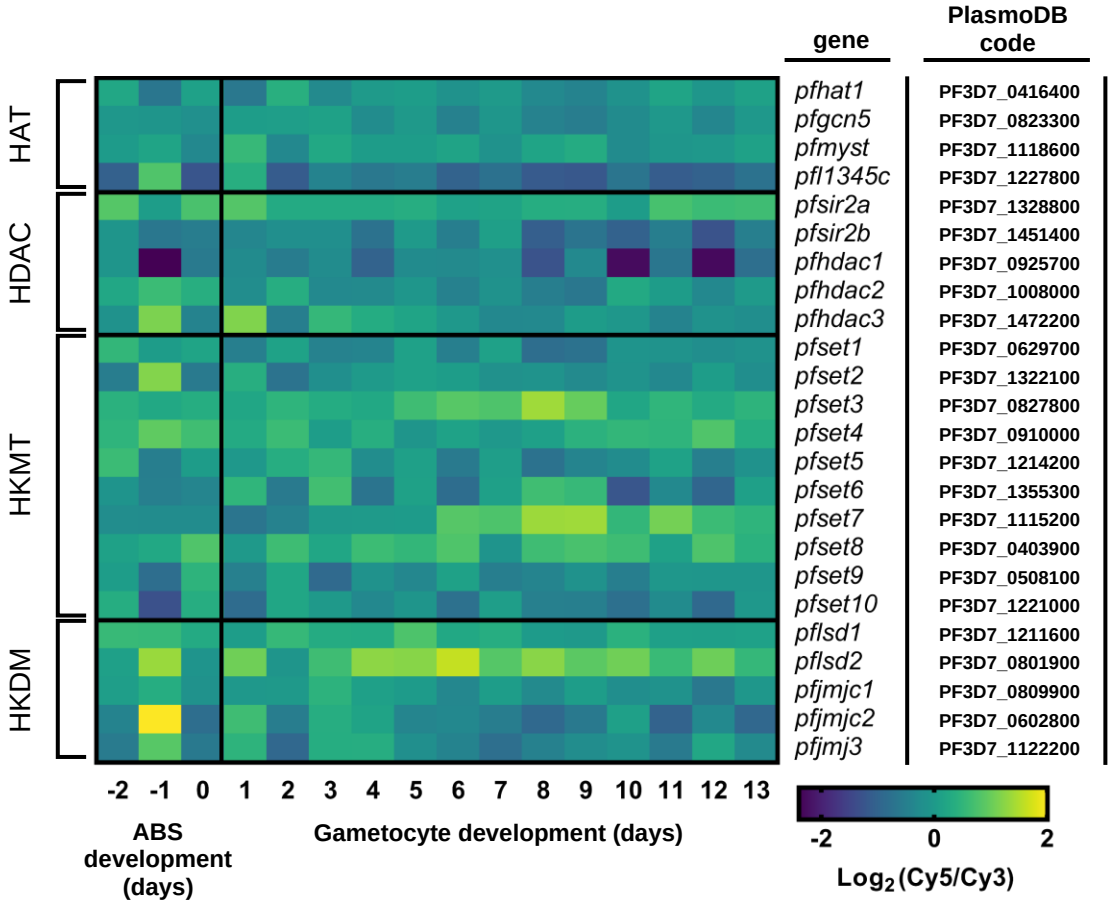

Figure 1.6: Expression profiles of epigenetic modifier proteins encoded by the *P. falciparum* genome. Signal represents the $\log_2$ ratio of Cy5-labelled sample RNA to Cy3-labelled reference pool RNA. Data extracted from van Biljon *et al*. (2019). Transcription levels are shown for different parasite stages, from day -2 to day 13 post-induction of gametocytogenesis. Figure generated using GraphPad Prism 9.

The diversity and importance of epigenetic effectors that confer these modifications indicates that this biology may be targetable with small molecule inhibitors of these protein effectors. Such compounds, termed “epidrugs”, may inhibit writers and erasers such as DNA methyltransferases or histone modifiers such as HDACs and HKMTs [73], amongst others. Some epidrugs exhibit antitumour activity in certain cancers by targeting of epigenetic effector proteins [74].

1.8. Epidrugs as antimalarial agents

To comply with the criteria proposed as TCP-1, where a drug should clear asexual, symptom-causing stages, and TCP-5, where a drug should target transmitted stages for transmission blocking, novel targetable proteins controlling important processes must be found and investigated, particularly those involved in proliferation and differentiation throughout the parasite life cycle. Since epigenetic regulation is a clear contributor to developmental processes involved in both *P. falciparum* parasite proliferation and differentiation, investigation of this as a targetable biology is well supported. The repurposing of drugs for other diseases holds several benefits over the *de novo* development of such compounds. This is generally a significantly more cost-effective approach, and such compounds often also have established safety profiles in humans, with the result that less time may be spent in the developmental pipeline [75]. It is therefore prudent to investigate epidrugs, previously evaluated as chemotherapeutics for the treatment of cancer, in targeting *P. falciparum* parasites.

Some epidrugs have been approved for use against certain cancers, such as peripheral T-cell lymphoma, and trials are underway for the treatment of other cancers with epidrugs [76], however, none have yet been approved for use in the treatment of malaria. In a previous study, compounds in the Cayman Epigenetic Screening Library that were previously used in cancer research, were screened in *P. falciparum* against asexual stages, early- and late-stage gametocytes [77]. These drugs belonged to several inhibitor classes, with the majority in the HDAC inhibitor (HDACi) or HKMT inhibitor (HKMTi) classes. In addition, epidrugs included in the MMV Pandemic Response Box were also screened against multiple stages of *P. falciparum* parasites [78]. A number of the compounds from these screens were found to have favourable inhibition profiles, some exhibiting pan-activity and others stage-specific inhibition (Fig. 1.7). Pan-activity, activity against asexual, early- and late-stage gametocytes, involves targeting of a biological process important to each of these life cycle stages, while stage-specific inhibition indicates that the targeted process may be essential to that stage alone. Such a compound may, for example, target a process involved in preparing late-stage gametocytes for gametogenesis, a process that would be absent in the asexual stages.

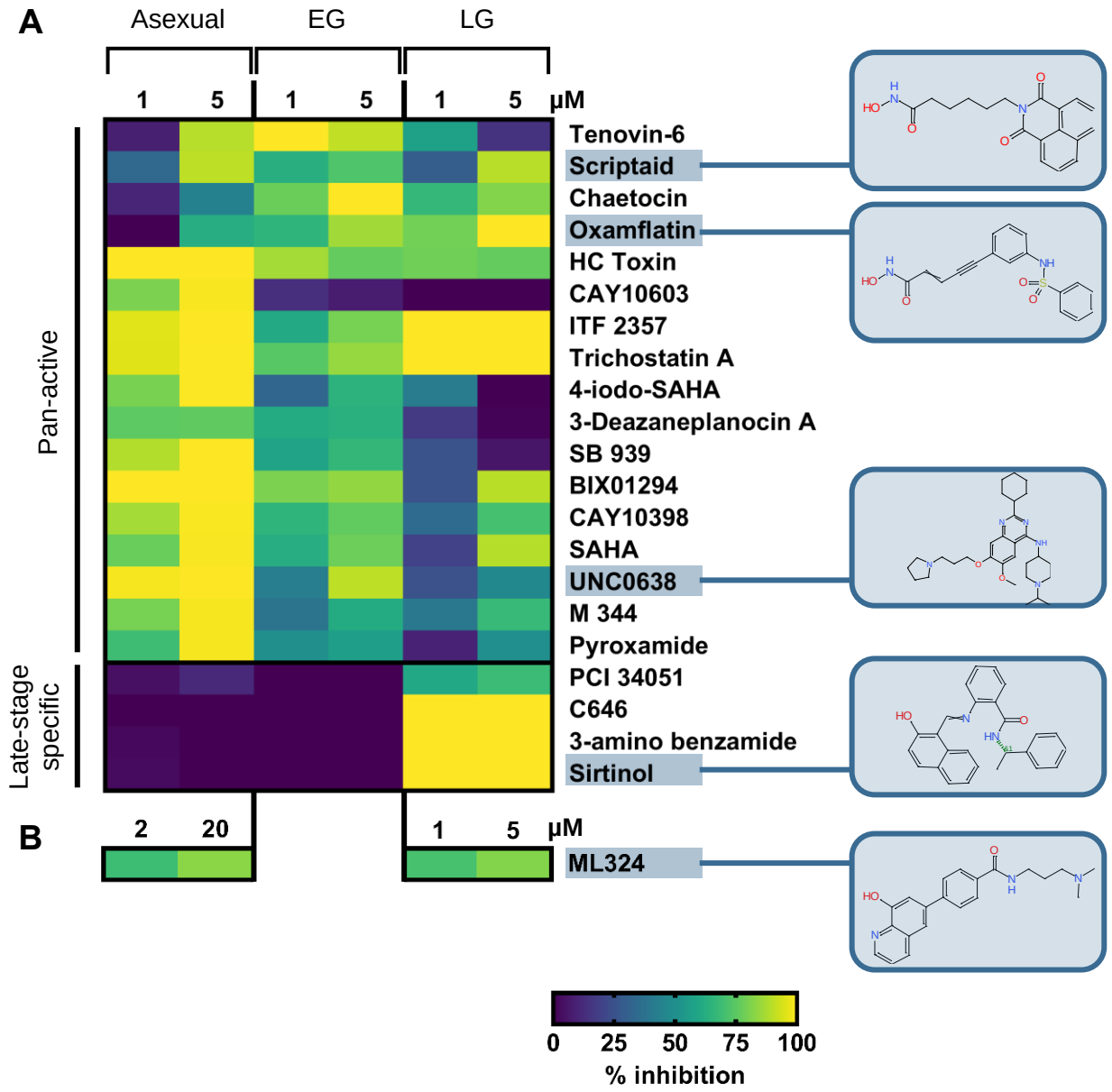

Figure 1.7: Epidrugs with favourable inhibitory profiles selected for investigation of modes of action. (A) Dual point data for epidrugs from the Cayman Epigenetics Screening Library screened against *P. falciparum*. Screening was performed using SYBR Green I-based fluorescence assays with asexual parasites of the 3D7 strain under 96 h of drug pressure. For early-stage (EG) and late-stage (LG) gametocytes, data were obtained with a pLDH assay using the NF54 strain, with 72 h of drug pressure. Epidrugs with favourable inhibitory fingerprints (targeting symptomatic asexual parasites and transmissible late-stage gametocytes) were selected for further investigation, namely the pan-active HDACi Scriptaid and Oxamflatin and HKMTi UNC0638 and the late-stage gametocyte-specific HDAC inhibitor Sirtinol. Figure adapted from Coetzee *et al*., 2020. **(B)** Dual point data for ML324 from the MMV Pandemic Response Box screened against *P. falciparum* (Reader *et al.*, 2021). Screening was performed using pLDH assays with asexual parasites of the NF54 strain under 72 h of drug pressure. For late-stage gametocytes, data were obtained with a PrestoBlue assay using the NF54 strain, under 48 h of drug pressure. Inhibition data of drugs at 2 and 20 µM (ML324-treated asexual stages) and 1 and 5 µM (asexual stages from Cayman Epigenetic Screening Library and late-stage gametocytes) concentrations were used to construct a heatmap, with colour intensity indicative of % inhibition. Drugs were clustered according to similarity in inhibition profile. Figure generated using GraphPad Prism 9.

Of the compounds screened in these studies, a subset has been investigated further, with some validated as inhibitors of epigenetic modulators in *P. falciparum* parasites. This includes the HKMTi BIX01294, which modulates downstream gene expression in *P. falciparum* by targeting of a G9a HKMT

[79]. The HDMi JIB-04, on the other hand, exerts its anti-plasmodial activity through targeting of Jumonji demethylases [80]. These examples validate epigenetic regulation of transcription as a viable targetable biology in malaria parasites. However, the data from these screens provide a wide variety of additional compounds that could be investigated further. Several compounds showed interesting activity profiles, including Scriptaid, Oxamflatin, Sirtinol and ML324. Each of these compounds show a preference towards gametocyte stages, a characteristic not previously explored for these. Inhibition of epigenetic writers and erasers by these compounds is expected to perturb PTMs effected by these epigenetic modifiers, confirming an epigenetic MoA of these compounds in *P. falciparum*.

Amongst the HDACi (Table 1.1), Oxamflatin inhibits HDACs in mouse and human cancer cells [81]. It additionally shows inhibitory activity against MKN-45 human gastric cancer cell lines [82] and induces apoptosis in human endometrial cancer cells [83]. Oxamflatin is an HDACi that exhibits pan-activity, as well as potent male gamete exflagellation inhibition [77]. Additionally, Oxamflatin reduces the 3:1 ratio of female to male late-stage gametocytes, indicating that this drug perturbs female-specific biological processes. This is critical as male gametocytes are more sensitive to drugs [84].

Scriptaid is an inhibitor of HDACs in human cancer cell lines, active against colon cancer cell lines [85] and inhibiting growth of oestrogen receptor α-negative breast cancer cells [86]. A pan-active inhibitory fingerprint, with potent male gamete inhibition, is associated with Scriptaid treatment in *P. falciparum* cells. The slight preference for late-stage gametocytes [77] supports the exploration of this compound as a repurposed transmission-blocking epidrug.

Sirtinol (Sir two inhibitor naphthol) is an HDACi, particularly targeting NAD^+-dependent HDACs, termed sirtuins [87]. Sirtinol specifically inhibits SIRT1 [87] and SIRT2, [88], arresting growth of human MCF-7 breast cancer cell lines and H1299 cancer cells [89]. In *P. falciparum*, Sirtinol showed potent inhibition of late-stage gametocytes as well as potent male gamete exflagellation. The expression of Sir2A, the proposed target of Sirtinol, is upregulated in stage V gametocytes (Fig. 1.6). Sirtinol has high specificity towards *P. falciparum* [77] as well as against promastigote and amastigote stages in *Leishmania donovanii* parasites [90]. Based on these findings, the use of Sirtinol as a transmission-blocking drug needs to be investigated.

ML324 is an inhibitor of Jumonji domain-containing HDMs [91] and, through targeting of the Jumonji demethylase JMJD2, has shown potent antiviral activity in inhibiting infection initiation and spread of such viruses as herpes simplex virus and human cytomegalovirus [91]. Activity has also been demonstrated against head and neck squamous cell carcinomas [92]. Three putative Jumonji demethylases have been annotated in *P. falciparum* to date [80]. Screens of ML324 against *P. falciparum* have shown good activity against late-stage gametocytes, with potent inhibition of male gamete exflagellation and reduction of oocyst intensity, indicating strong transmission-blocking activity by this compound [78]. ML324 has shown inhibition of the catalytic effect of Jumonji demethylase PfJmj3 in converting 2-oxoglutarate to succinate [80].

Lastly, the HKMTi UNC0638 inhibits G9a methyltransferases in human cell lines [93] as well as invasion and proliferation of certain breast cancers [94]. This compound has additionally shown activity against *B. divergens* [95]. Immunoblotting performed in this study supported histone methyltransferase activity as the means whereby this compound exerts its inhibitory activity in *P. falciparum*, as is the case in cancer cells, and SMFAs indicated good transmission-blocking potential.

This dissertation aims to elucidate the MoA of the selected compounds presented in Table 1.1. In addition to the HDMi ML324, another potent KDM4B inhibitor, f1iii (P. Woster, Medical University of South Carolina, unpublished), was included to expand the chemical footprint for inhibition of HDMi in *P. falciparum*. Similarly, UNC0379 was included as a second HKMTi targeting human SET lysine methyltransferases. UNC0379 actively supresses various cancers, including human multiple myelomas [96] and ovarian cancer [97].

Identifying the targets of potential drugs and hence their MoA allows rational drug design and minimises off-target effects. Compounds for which the target is associated with a risk of resistance development may be excluded from the discovery pipeline. The compounds listed in Table 1.1 all inhibit parasites, such that they should be further investigated as possible drugs blocking transmission and eliminating malaria. Such findings may contribute to efforts towards malaria treatment and elimination by exploiting the unique structures and MoA of these compounds.

Table 1.1: Compounds previously reported as targeting epigenetic processes in human cancer cells and investigated here as epidrugs targeting *P. falciparum* parasites.

Inhibitor class	Compound name	Chemical structure	Target in human cell lines	*P. falciparum* asexual IC_{50} (µM) [Ref]	*P. falciparum* late-stage gametocyte IC_{50} (µM) [Ref]
HDACi	**Scriptaid**	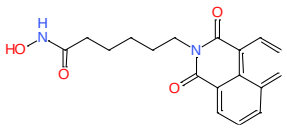	HDACs [85]	0.5 [98]	0.820 [77]
	Sirtinol	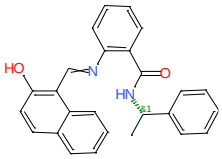	Sirtuin deacetylase SIRT1 [87] Sirtuin deacetylase SIRT2 [88]	0.37 [77]	0.130 [77]
	Oxamflatin	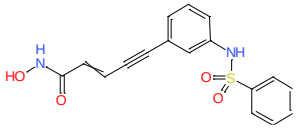	HDACs [81]	3.7 [77]	3.001 [77]
HDMi	**ML324**	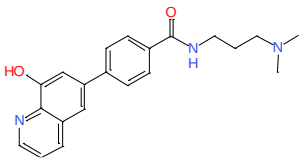	KDM4A [91] KDM4B [99] KDM4E [91]	>6 [78]	0.08 [78]
	f1iii	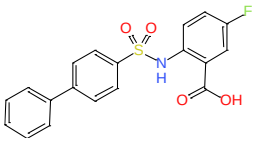	KDM4B (P. Woster, unpublished)	ND	0.009 (J Reader, unpublished)
HKMTi	**UNC0638**	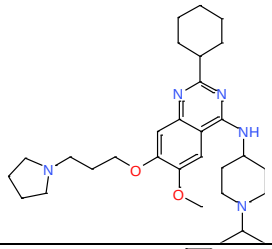	G9a [93, 94]	0.0283 [77]	0.442
	UNC0379	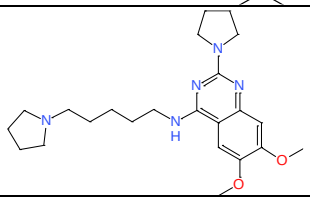	SET8 [100]	(Unpublished)	(Unpublished)

Hypothesis

The selected compounds kill *P. falciparum* parasites through perturbation of histone post-translational modification levels by inhibiting epigenetic writers or erasers.

Aim

To investigate the modes of action of epidrugs with unique life cycle fingerprints using complementary biochemical and *in silico* bioinformatics approaches

Objectives

Objective 1: To identify target indicators for the compounds of interest for target deconvolution

Objective 2: To prove that epidrug inhibition is associated with changes in epigenetic status of the parasite through immunoblot analysis of histone tail acetylation and methylation status

Objective 3: To confirm transmission-blocking activity of compounds of interest using exflagellation inhibition and standard membrane-feeding assays

Research outputs

Peer-reviewed publications

Reader, J., van der Watt, M. E., Taylor, D., Le Manach, C., Mittal, N., Ottilie, S., Theron, A., Moyo, P., Erlank, E., Nardini, L., Venter, N., Lauterbach, S., Bezuidenhout, B., Horatschek, A., van Heerden, A., Spillman, N. J., Cowell, A. N., Connacher, J., Opperman, D., Orchard, L. M., Llinás, M., Istvan, E. S. Goldberg, D. E., Boyle, G. A., Calvo, D., Mancama, D., Coetzer, T. L., Winzeler, E. A., Duffy, J., Koekemoer, L. L., Basarab, G., Chibale, K., and Birkholtz, L.-M. (2021) Multistage and transmission-blocking targeted antimalarials discovered from the open-source MMV Pandemic Response Box, Nature Communications 12, 1-15.

Poster presentations

Opperman, D. F. L., Connacher, J., Birkholtz, L. M. Mechanistic insights into the activity of selected epigenetic drugs targeting *Plasmodium falciparum* parasites. SAMRC Office of Malaria Research 6th Malaria Research Conference 2021. Poster presentation. Pretoria, South Africa, 2021.

Chapter 2: Experimental procedures

2.1. Modelling of putative compound targets using bioinformatics approaches

Protein structural models were generated for putative targets of the compounds under investigation in this study. First, putative antiplasmodial drug targets were identified by sequence homology to related human proteins (Table 2.1) using the BlastP function in PlasmodDB (https://plasmodb.org) and the Expect (E) value. Scriptaid [85] and Oxamflatin [81] exhibit HDACi activity in human cells, though their respective targets are unknown. In addition to the sirtuin HDACs, three other established HDACs (PfHDAC1-3) were investigated as potential targets using molecular docking. As ML324 inhibits recombinantly expressed PfJmj3 *in vitro* [80], theoretical models of PfJmjC1, PfJmjC2 and PfJmj3 were derived to evaluate binding of ML324.

Table 2.1: *P. falciparum* homologues of compound targets in human cell lines.

Compound	Inhibitor target (human cell lines)	Homologous proteins (*P. falciparum*)	PlasmoDB code	E value
Sirtinol	Sirtuin deacetylase SIRT1 [87]	PfSir2A	PF3D7_1328800	5e-19
	Sirtuin deacetylase SIRT2 [88]	PfSir2A		1e-18
ML324	KDM4A [91]	PfJmjC1	PF3D7_1122200	2e-13
	KDM4B [99]	PfJmjC1		1e-14
	KDM4E [91]	PfJmjC1		7e-15
UNC0379	SET8 [96]	PfSET8	PF3D7_0403900	5e-28
UNC0638	G9a [93]	PfSET2	PF3D7_0827800	2e-15

Theoretical structural models for the proposed drug targets identified above were generated by homology modelling using the web-based SwissModel server [101]. This software uses the input amino acid sequence of the protein of interest to generate a structural model based on the experimentally-determined structure of a homologous protein obtained through experimental methods such as X-ray crystallography, cryogenic electron microscopy or nuclear magnetic resonance (NMR) [101]. This was done for all potential drug targets except PfSir2A, as a crystal structure is already available [102]. The template providing the highest initial global model quality estimate (GMQE) was selected for modelling (Table 2.2).

Table 2.2: Templates used for modelling of *P. falciparum* putative drug targets in SwissModel.

Model	Accession Number.	Template	Organism	GMQE	Sequence identity (%)
PfHDAC1	Q7K6A1_PLAF7	6who.1.A	*Homo sapiens*	0.71	62.60
PfHDAC2	Q8IJW3_PLAF7	1zz0.1.A	Alcaligenaceae bacterium FB188	0.00	38.84
Putative PfHDAC3	A0A144A4T0_PLAF7-	1zz0.1.A	Alcaligenaceae bacterium FB188	0.00	26.92
PfJmjC1	Q8IAT4_PLAF7	5ykn.1.A	*Arabidopsis thaliana*	0.25	29.56
PfJmjC2	C6KSM8_PLAF7-	3al5.1.B	*Homo sapiens*	0.27	28.74
PfJmj3	Q8IIE4_PLAF7	2xum.1.A	*Homo sapiens*	0.31	21.81
PfSET8	Q8I1Z0_PLAF7	4ldg.1.A	*Cryptosporidium parvum* Iowa II	0.11	43.09
PfSET2	SETVS_PLAF7	5v21.1.A	*Homo sapiens*	0.00	34.7

Secondly, models for these proteins were also obtained from DeepMind's AlphaFold2 repository of *P. falciparum* protein structures. AlphaFold2 follows a machine learning approach to *in silico* protein structure elucidation with accuracy on an atomic scale without the use of a template, and based on physical and biological principles as applied to protein folding [103]. Low-confidence regions of each model were trimmed using UCSFChimera v. 1.15 [104]. All models were validated using MolProbity v. 4.5.1 (http://molprobity.biochem.duke.edu/) [105]. This was achieved by uploading the coordinate file in Protein Data Bank file format (.pdb) generated through modelling to the MolProbity online utility, followed by the addition of explicit hydrogen atoms. As the orientation of asparagine (Asn), glutamine (Gln) and histidine (His) amino acid residues may be poorly captured in structures generated using X-ray crystallography and NMR, these residues were flipped 180° where such evidence existed. Finally, intramolecular steric interactions and geometric analyses were performed to evaluate model quality. For each protein, either the SwissModel or the AlphaFold2 model was selected for docking on this basis, with the quality of the active site-containing domain and the completeness of the model prioritised. Ramachandran plots of peptide backbone dihedral angles were generated and any outliers from energetically favoured conformations were noted.

2.2. Exploration of target indicators for epidrugs using *in silico* molecular docking

Epidrugs were docked to their proposed plasmodial target structures to assess possible binding modes and binding energies of the epidrugs under investigation to their putative targets in *P. falciparum*. Structural models were processed using the Dock Prep utility of UCSFChimera v. 1.15 [104]. This involved deleting solvent molecules and non-complexed ions, complementing incomplete sidechains, and assigning partial charges to atoms as required. Resulting files were saved in .pdb format. Coordinate data contained within these files were then submitted to SwissDock where ligand 3D structures from the ZINC database were specified for docking. This approach calculates binding modes and energies in iterated clusters using CHARMM22 force fields [106, 107]. Binding modes of ligands complexed to models resulting from the docking simulation were evaluated and visualised using the ViewDock utility in UCSF Chimera and corresponding CHARMM22 force field binding energies were ascertained. Protein domain and active site predictions from InterPro (https://www.ebi.ac.uk/interpro/) were used to rationalise the results.

2.3. Statements of ethical clearance

In vitro experiments involving the cultivation of live *P. falciparum* parasites were performed at the Malaria Parasite Molecular Laboratory (M^2PL) biosafety level 2 (BSL2) malaria culture facility. This was carried out under an umbrella ethical clearance to Prof L Birkholtz for work on human malaria parasites from the Faculty of Natural and Agricultural Sciences Ethics Committee (ref. 180000094), with additional clearance from the Faculty of Health Science Ethics Committee for the use of human erythrocytes (ref. 506/2018).

2.4. *In vitro* drug-sensitive *P. falciparum* parasite cultivation

2.4.1. *In vitro* cultivation of asexual stages

All parasites were cultivated *in vitro* in BSL2 laminar flow hoods under sterile conditions. Drug-sensitive NF54 *P. falciparum* parasite strains were maintained at 5 % haematocrit in human erythrocytes (A^+ or O^+ blood type) in RPMI-1640 cell culture medium (Sigma Aldrich, USA) supplemented with 23.81 mM sodium bicarbonate, 0.2 % (w/v) glucose, 0.024 $mg.mL^{-1}$ gentamycin, 25 mM 4-(2-hydroxyethyl)-1-piperazineethanesulfonic acid (HEPES) and 0.2 mM hypoxanthine and completed with 0.5 % (w/v) AlbuMAX II (Life Technologies, USA). AlbuMAX II is a lipid-rich bovine serum albumin substitute that serves as a replacement for human serum. Culture medium was replaced daily by collection of parasite pellets through centrifugation at 3 500 ×*g* for 5 min and aspiration of spent medium followed by resuspension in fresh medium. Cultures were incubated at 37 °C with shaking at 60 rpm and maintained under hypoxic conditions through supplementation of a hypoxic gas mixture (5 % O_2, 5 % CO_2 and 90 % N_2) (Afrox, South Africa). The parasitaemia of Rapi-Diff-stained thin smears of parasite cultures was evaluated daily at 1000 × magnification using a light microscope (Nikon, Japan), facilitating maintenance of parasitaemia at 2-6 % for ring- and 2-4 % for trophozoite-stage parasite cultures. This allowed optimal culture conditions for parasite proliferation and viability.

2.4.2. Synchronisation of asexual parasite cultures to the ring stage

Ring- and trophozoite-synchronised *P. falciparum* parasite cultures were obtained using D-sorbitol to selectively osmolyse trophozoite and schizont stages [108]. Parasites were collected at 4 000 ×*g* for 1 min, then resuspended in 5 % (w/v) D-sorbitol solution and incubated at 37 °C for 15 min. Parasites were again pelleted by centrifugation at 2 500 ×*g* for 5 min, aspiration of the supernatant, and washing the pellet twice by resuspension in pre-heated incomplete culture medium (AlbuMAX II negative), and centrifugation at 2 500 ×*g*. Synchronised parasite culture pellets were resuspended in pre-heated complete culture medium, gassed with a hypoxic gas mixture (5 % CO_2, 5 % O_2, 90 % N_2, Afrox, South Africa) and incubated at 37 °C with moderate shaking. Parasites were cultivated using routine culturing until the desired stages were attained, allowing for stage-specific studies in subsequent experiments. Where a greater level of synchronicity was required, synchronisation was repeated twice, once every 48 h when a majority of ring stages were observed.

2.4.3. *In vitro* induction and cultivation of *P. falciparum* gametocytes

To produce late-stage gametocytes, asexual parasite cultures were synchronised to ring-stage parasites for two consecutive cycles as in section 2.4.1., on days -7 and -5 relative to the day of gametocyte induction and maintained with routine culturing. Gametocyte cultures were initiated from a >90 % ring-stage synchronised culture on day -3 by the introduction of environmental stress conditions using gametocyte medium (culture medium without the addition of supplemental glucose) to a haematocrit of 6 % and parasitaemia of 0.5 % and incubated at 37 °C in a stationary incubator under hypoxic conditions, without replenishing the culture medium on day -2. Gametocytogenesis was induced on day 0 by decreasing the haematocrit to 4 %. Routine culturing was performed thereafter, maintaining the temperature at 37 °C throughout culturing using a heated platform and removing spent

medium by aspiration with a vacuum pump. Cultures were incubated at 37 °C in a stationary incubator under hypoxic conditions. Asexual-stage parasites were eliminated from gametocyte cultures from day 3 post-induction using glucose-supplemented culture medium with the addition of 50 mM N-acetyl glucosamine (NAG) to prevent merozoite reinvasion, until only gametocyte stages were seen, and maintained using glucose-supplemented medium thereafter.

2.5. Histone enrichment and immunoblot evaluation of PTM changes due to drug treatment

2.5.1. Parasite treatment and histone enrichment

P. falciparum NF54 parasites were cultivated *in vitro* as described in section 2.4. Cultures were treated at 5 × half-maximal inhibitory concentration (IC_{50}) (Scriptaid, Sirtinol and Oxamflatin, IC_{50} determined previously [77, 98]) or at 5 µM (ML324, f1iii, UNC0379 and UNC0638) for the indicated periods at 37 C under hypoxic conditions. Subsequent to treatment, parasite pellets were collected by centrifugation at 3 500 ×*g* for 5 min and released from erythrocytes by resuspension in 0.15 % or 0.06 % (w/v) saponin solution in phosphate-buffered saline (PBS) pH7.0 (137 mM NaCl, 2.7 mM KCl, 1.5 mM KH_2PO_4, 10 mM Na_2HPO_4) on ice for 10 min, for asexual stages and late-stage gametocyte stages, respectively. Residual erythrocyte debris and haemoglobin were removed through multiple wash steps by resuspension of pellets in PBS and collection at 3 500 ×*g*, followed by aspiration of the supernatant.

The acid-soluble histone fraction was enriched for immunoblot analysis of histone PTM changes consequent to epidrug treatment [78]. Isolated parasite pellets were ground in a hypotonic buffer containing 10 mM Tris-HCl pH 8.0, 3 mM $MgCl_2$, 0.25 M sucrose and 0.2 % (v/v) Nonidet P-40 in the presence of a protease inhibitor (cOmplete EDTA-free Protease Inhibitor Cocktail, Roche) using a dounce pestle, and the isolated nuclei were collected through centrifugation at 500 ×*g* for 10 min. This step was repeated once more, followed by a wash step using the same buffer without Nonidet P-40 detergent. Pelleted nuclei were carefully resuspended in a buffer containing 10 mM Tris-HCl pH 8.0, 0.8 mM NaCl and 1 mM ethylenediaminetetraacetic acid (EDTA) in the presence of a protease inhibitor cocktail and incubated on ice for 10 min, then collected again by centrifugation at 500 ×*g* for 5 min. Histones were extracted by resuspension of the resultant chromatin pellet in 750 µL of 0.25 M HCl and homogenisation using a dounce pestle, with overnight incubation at 4 °C on a rolling mixer. The supernatant was retained after centrifugation at 11 000 ×*g* for 30 min at 4 °C. Histones were precipitated from the supernatant through the introduction of an equal volume of 20 % (v/v) trichloroacetic acid (TCA) and mixing by inversion, followed by incubation for 15 min on ice and collection of the histone-enriched pellet through centrifugation for 30 min at 12 000 ×*g*. The pellet was washed once with 500 µL of acetone and retained by centrifugation at 12 000 ×*g*, then allowed to dry. The pellet was resuspended in PBS with protease inhibitor cocktail and centrifuged 5 000 ×*g*, retaining the histone-containing supernatant. Sample protein concentrations were determined according to a bovine serum albumin (BSA) standard curve using the bicinchoninic acid (BCA) assay method with the BCA Protein Assay kit from Pierce, according to the manufacturer's instructions.

2.5.2. Immunoblot evaluation of histone PTM changes consequent to epidrug treatment

The inhibition of writer and eraser proteins that effect changes to histone tail PTMs is expected to alter the abundance of these PTMs. These changes may be observed and quantified by immunoblotting, whereby antibodies specific to the PTMs of interest are used to probe for these PTMs. A secondary antibody conjugated to a reporter enzyme such as horseradish peroxidase (HRP), which acts on a substrate resulting in the emission of chemiluminescence, may then be used to generate a signal whose strength is dependent on the PTM abundance. This signal may be captured using X-ray film or a charge-coupled device. Changes in histone PTM status, namely histone tail lysine acetylation in the case of the HDACi (Scriptaid, Sirtinol and Oxamflatin) and lysine methylation in the case of the HDMi (UNC0379 and UNC0638) and HKMTi (ML324 and f1iii), were evaluated using dot-blot analyses. This was accomplished through the quantitative application (range 40-400 ng, consistent between compared conditions) of histone samples, as enriched from treated parasite cultures in section 2.5.1 above, by dot blotting directly onto NCP Porablot nitrocellulose membrane (Macherey-Nagel, Germany), followed by 1 h agitation of membranes in 5 % skim milk blocking buffer in Tris-buffered saline with TWEEN 20 (TBS-t) (50 mM Tris pH 7.5, 150 mM NaCl, 0.1 % (v/v) TWEEN 20). Membranes were then incubated overnight on a rolling mixer at 4 °C in primary antibodies (generated in rabbits), diluted in TBS-t, to probe for the marks of interest. General histone tail lysine acetylation was probed for using α-H3K9ac (ab4441 from Abcam; 1:10 000), while α-H3K9me3 was used to probe for general histone tail lysine methylation (ab8898 from Abcam; 1:10 000). A polyclonal antibody against H3K9ac, H3K14ac, H3K18ac, H3K23ac and H3K27ac was used to probe for pan acetylation (ab47915 from Abcam; 1:10 000). α-H3Core (ab1791 from Abcam; 1:10 000), which targets the core histone tail, was used as a control. Membranes were subsequently washed three times in TBS-t followed by incubation in a horseradish peroxidase-conjugated goat α-rabbit secondary antibody (ab6721 from Abcam; 1:5 000) whilst agitating on a rolling mixer for 1 h.

To visualise dot blot membranes, equal parts of peroxide and luminol from the SuperSignal West Pico PLUS Chemiluminescent Substrate kit (Thermo Scientific) were mixed and applied. Visualisation was performed using two methods, according to equipment availability; dot blot imaging for ML324 was performed by exposing chemiluminescent substrate-covered membranes to CL-XPosure X-ray film (Thermo Scientific) in an X-ray cassette in a dark room. Dot blot membranes for the remaining compounds were visualised with a ChemiDoc MP imaging system (Bio-Rad, USA) containing a charge-coupled device, with a Chemi/UV/Stain-Free sample tray (Bio-Rad, USA) and acquiring signal with the chemiluminescence application.

The relative abundances of the histone PTMs under investigation were assessed by evaluating the relative integrated density of each dot. To this end, images generated by X-ray film or charge-coupled device exposure to chemiluminescent substrate-coated dot blot membranes were imported onto ImageJ v. 1.52n (NIH, USA). Background signal was removed using a rolling ball algorithm with the *Subtract Background* command. Images were then inverted to set background to a zero value for integrated density. Using a circular selection, the integrated density value of each dot was measured

using the *Measure* function with “integrated density” enabled. Each compound could thus be compared to a vehicle control allowing the effect of each inhibitor on PTM abundance to be ascertained.

For each condition, two to three biological replicates, each containing three technical repeats, were performed. Statistical significance was evaluated by applying unpaired, two-tailed t-tests using GraphPad Prism 6 (GraphPad Software, USA).

2.6. Quantification of male gamete formation inhibition using exflagellation inhibition assays

Inhibition of male gamete formation is a useful measure of the potential of a compound for transmission blocking. As male gamete formation is visible microscopically as exflagellation centres, the number of exflagellation centres in a treated culture compared to an untreated one may be evaluated and expressed as a percentage of inhibition [109, 110].

To this end, mature gametocyte cultures (>90 % stage V) were prepared at approximately 4 % haematocrit, with a gametocytaemia >1 % and a male-to-female ratio of between 1:3 and 1:5, using glucose-supplemented complete culture medium. The test compound was evaluated at a 2 µM concentration and, in parallel, an untreated culture was prepared, as well as a methylene blue-treated culture at 10 µM as a positive control for inhibition. Cultures were incubated for 48 h at 37 °C in a stationary incubator and supplemented with a hypoxic gas mixture (5 % CO_2, 5 % O_2, 90 % N_2) (Afrox, South Africa). For each condition, a standard volume of 1 000 µL was pelleted and resuspended in 50 µL of ookinete medium (RPMI-1640 cell culture medium containing L-glutamine, 50 % (v/v) human serum, 100 µM xanthurenic acid, 23.81 mM sodium bicarbonate, 0.2 % (w/v) glucose, 0.024 $mg.mL^{-1}$ gentamycin, 25 mM HEPES, 0.2 mM hypoxanthine and 0.5 % (w/v) AlbuMAX II) and incubated at room temperature for 8 min. Of the resuspended mixture, 10 µL was loaded into a haemocytometer cell and incubated for a further 8 min. For each sample, exflagellation centres were viewed microscopically with a Carl Zeiss NT 6V/10W Stab microscope (Carl Zeiss, Germany) at 400 × magnification and recorded with a microcapture camera. One 8-10 sec video was recorded every 30 s over an 8 min period, with a new field for each, for a total of 16 videos. The number of exflagellation centres per field was evaluated through semi-automated enumeration using the Spot Detector utility from Icy v. 2.0.0 bioimage analysis software. Videos were imported into Icy and processed with the *Intensity Projection*, *Filter Toolbox* and *Spot Detector* plugins. The *Intensity Projection* plugin was set to use “Active Sequence” input and “Standard Deviation” type projection along the time axis, and the Filter Toolbox utility was set to use “Active Sequence” input, with a separable Gaussian filter type with one iteration and Gaussian blur set to sigma x = 5 and sigma y = 5. Spot detection was performed on a scale of 25 pixels, with bright spots detected over a dark background.

The percentage inhibition was calculated using the equation:

$$EI = \frac{E_u - E_t}{E_u} * 100$$

where *EI* is the percentage exflagellation inhibition, E_u is the average number of exflagellation centres per field in the untreated sample and E_t is the average number of exflagellation centres per field in the treated sample.

2.7. Quantification of transmission blocking using standard membrane-feeding assays

Standard membrane-feeding assays were performed by the Drug Discovery Program at the Malaria Parasite Molecular Laboratory at the University of Pretoria in collaboration with the Wits Research Institute for Malaria. Data analysis was performed independently as part of this MSc.

While compound activity against late-stage gametocytes and inhibition of male gamete formation are strong indicators of transmission blocking, it is necessary to confirm this by evaluating drug-treated culture oocyst formation in mosquitoes. The SMFA allows a robust, largely *in vitro* approach to this, and provides a measure of both transmission blocking (TBA, % inhibition of oocyst prevalence) and transmission-reducing activity (TRA, % reduction in oocyst intensity) [111, 112].

SMFAs were performed using treated late-stage gametocyte cultures fed to *Anopheles coluzzii* mosquitoes. Mosquitoes were reared at the Wits Research Institute for Malaria as previously described [78], and all insect-related work is covered by standard operating procedures approved and managed through Wits University. A late-stage gametocyte culture (majority stage V) at 1.5-2.5 % gametocytaemia and 4 % haematocrit was treated at 2 µM with the test compound, with an untreated culture prepared in parallel, and incubated at 37 °C for 48 h in a stationary incubator and supplemented with a 5 % CO_2, 5 % O_2, 90 % N_2 hypoxic gas mixture (Afrox, South Africa). Following the 48 h drug pressure, the blood meal was prepared by removing the spent medium and supplementing the infected erythrocytes with 1× volume of fresh, uninfected erythrocytes and 2× volume of human serum (male, AB^+). This was fed to 5–7-day old female *An. coluzzii* mosquitoes in the dark for 40 min using heated glass feeders covered with cow intestine to form a membrane. Only fully fed mosquitoes were retained for further evaluation. These were incubated for a further 8-10 days, whereupon they were dissected, removing the midgut. Midguts were rinsed in PBS and stained with 0.1 % (v/v) mercurochrome to allow microscopic oocyst visualisation and enumeration.

Findings were used to calculate oocyst prevalence and intensity as follows:

$$TBA = \frac{U_p - T_p}{U_p} * 100$$

$$TRA = \frac{U_i - T_i}{U_i} * 100$$

where *U* refers to the untreated condition, *T* refers to the drug-treated condition and *p* and *I* refer to oocyst prevalence and intensity, respectively.

Each condition was evaluated with three biological replicates, each containing two technical repeats, represented by two feeding cups for each condition. A Mann-Whitney non-parametric t-test was applied to evaluate statistical significance using GraphPad Prism 6 (GraphPad Software, USA).

Chapter 3: Results

3.1. HDACi targeting *P. falciparum* parasites

As indicated in Table 1.1, three HDACi were under investigation due to their prior potency described against multiple stages of *P. falciparum* parasites. This includes Sirtinol, active against both asexual blood-stage parasites (IC_{50} = 0.37 µM [77]) and late-stage gametocytes (IC_{50} = 0.130 µM [77]), Scriptaid (IC_{50} = 0.5 µM for asexual blood-stage parasites and 0.820 µM for late-stage gametocytes [77]) and Oxamflatin (IC_{50} = 3.7 µM for asexual blood-stage parasites and 3.001 µM for late-stage gametocytes [77]).

3.1.1. Modelling of HDACs for exploration of HDACi target indicators

For *in silico* evaluation of drug binding modes, putative targets of the three HDACi under investigation, Scriptaid, Sirtinol and Oxamflatin, were modelled, both by homology-based modelling using SwissModel and as generated by DeepMind's AlphaFold2, which follows machine-learning approach based on physical and chemical principles. First, targets of these epidrugs in *P. falciparum* were identified on the basis of sequence homology to their targets in human cell lines. For Sirtinol, PfSir2A was indicated to be the closest homologue in *P. falciparum* as predicted by the Expect (E) value using NCBI's protein Basic Local Alignment Search Tool (protein BLAST). This indicated PfSir2A as the most probable homologue of the Sirtinol target in humans, SIRT1 (E = 5e-19) and SIRT2 (E = 1e-18), compared to poor probabilities seen for PfSir2B (E = 0.37 and 0.058 for SIRT1 and SIRT2, respectively). Fortunately, the crystal structure for PfSir2A is available [102] and was used directly in docking studies, negating the requirement for any modelling of this target.

While both Scriptaid and Oxamflatin exhibit HDACi activity in human cell lines, the particular targets are unknown [85], and therefore all class I and II HDAC family members in *P. falciparum* (PfHDAC1, PfHDAC2 and PfHDAC3) were evaluated as potential targets. The proposed targets were subsequently used for model generation with SwissModel.

Templates were selected for the HDAC models based on the highest initial GMQE as an indicator of quality for the resultant model and with sequence identity mostly at >30 %. As such, PfHDAC1 was modelled in the *H. sapiens* HDAC2 as a template (Fig. 3.1 A), with close structural correlation observed (pruned Cα heavy atom RMSD of 0.07 Å for aligned Cα atoms) (Fig. 3.1 A). A high per-residue quality was indicated, and structural validation revealed good intramolecular steric interactions for both models. Moreover, Ramachandran analysis indicated that only 0.27 % of residues had unfavourable geometry and 97 % had favourable geometry for the SwissModel structure (Fig. S1 A). By comparison, the AlphaFold model obtained for PfHDAC1 (Fig. 3.1 B) showed 0.89 % of residues to be Ramachandran outliers, those residues with poor conformity to energetically allowable peptide backbone dihedral angles associated with particular secondary structures, with 95 % of residues indicated to have favoured peptide backbone geometry (Fig. S1 B). On these bases, the SwissModel structure was selected as a suitable model for *in silico* docking studies for PfHDAC1. In both models, an 8-stranded

parallel β-pleated sheet surrounded by 8 α helices, the canonical α/β HDAC fold in common with other class I and II HDACs [113] and part of the histone deacetylase domain (InterPro: IPR000286), was observed.

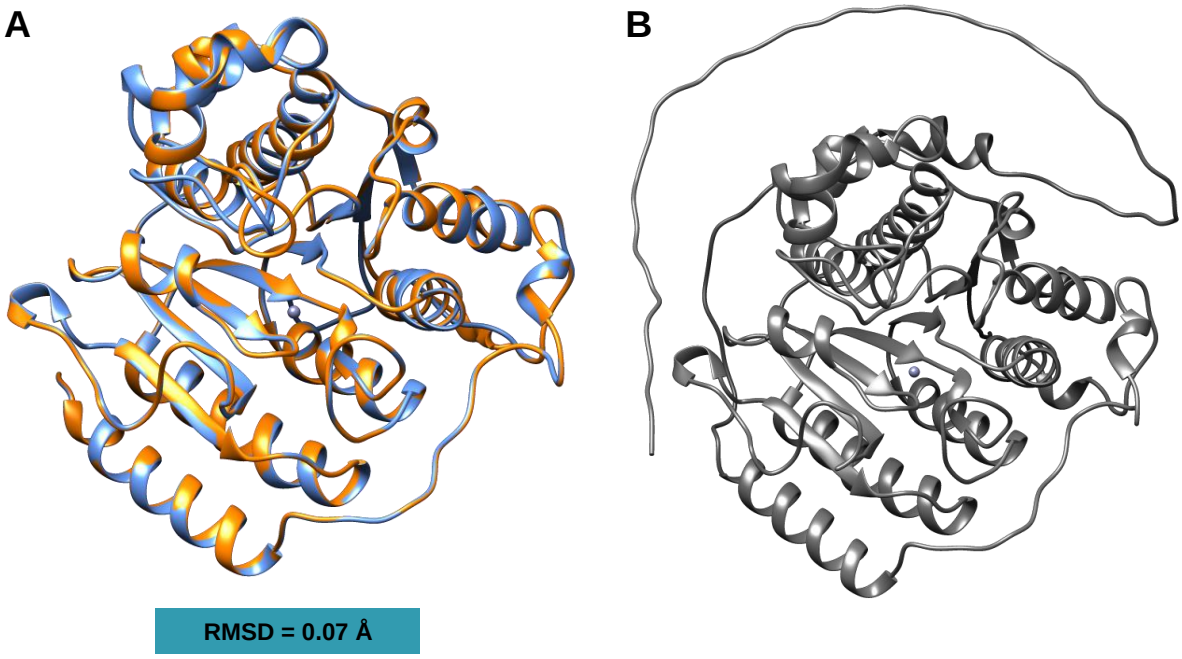

Figure 3.1: Structural model of PfHDAC1. (A) PfHDAC1 model generated using SwissModel and overlaid on the template, *H. sapiens* HDAC2. RMSD = 0.07 Å. PfHDAC1 structure in orange and template structure in blue. **(B)** PfHDAC1 model obtained from AlphaFold2.

For PfHDAC2, the obtained SwissModel model showed good correlation with the template structure (Alcagenaceae bacterium FB188 histone deacetylase-like amidohydrolase) with a Cα heavy chain RMSD of 0.44 Å for aligned Cα atoms (Fig. 3.2 A). The AlphaFold model (Fig. 3.2 B) had a slightly better evaluation of residues with favourable peptide backbone dihedral angles (94 %) compared to the homology model (91 %), while 0.63 % of residues had unfavourable geometry in the AlphaFold model compared to 1.42 % in the homology model (Fig. S2 B). Additionally, both models had favourable intramolecular steric interactions. However, based on its better geometric characteristics, the AlphaFold model was retained for docking studies. The α/β HDAC fold, within the histone deacetylase domain (IPR000286), is visible in both models, as for PfHDAC1.

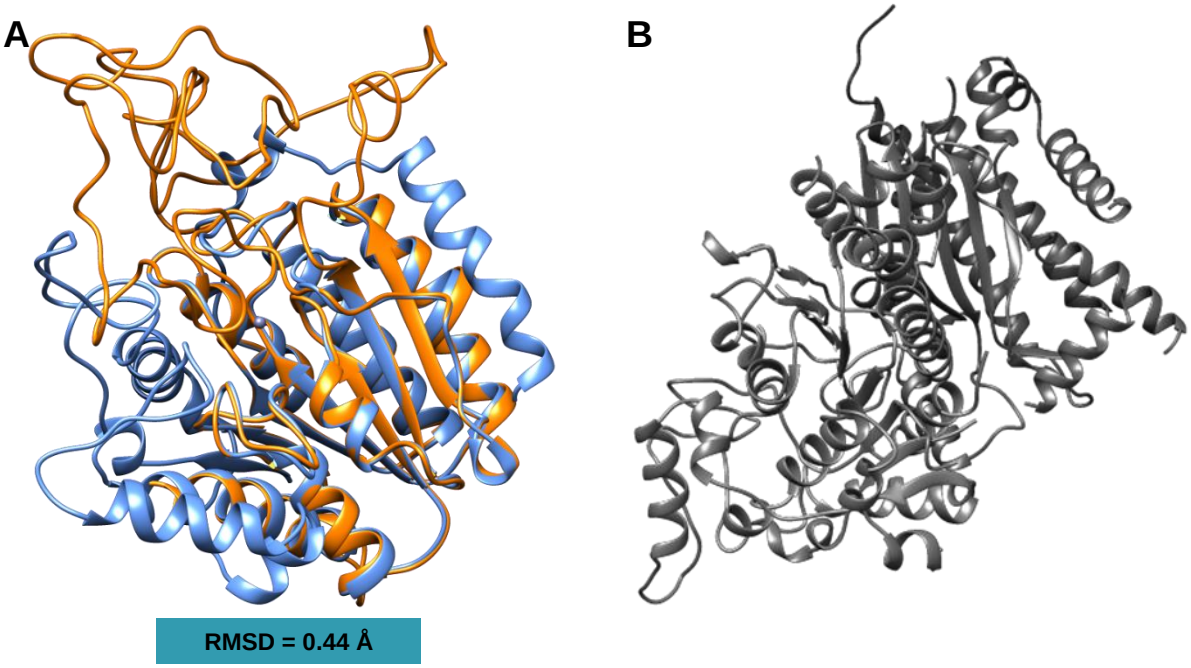

Figure 3.2: Structure of PfHDAC2. (A) PfHDAC2 model generated using SwissModel and overlaid on the template, Alcaligenaceae bacteria histone deacetylase-like amidohydrolase. RMSD = 0.44 Å. PfHDAC2 structure in orange and template structure in blue. **(B)** PfHDAC2 model obtained from AlphaFold2.

For the putative PfHDAC3, the homology model obtained showed good alignment with its FB188 histone deacetylase-like amidohydrolase template, with an RMSD of 0.23 Å for aligned Cα atoms (Fig. 3.3 A). However, model validation using MolProbity showed this model to have a very high number of serious intramolecular steric overlaps. Ramachandran analysis revealed 1.75 % of residues to be geometric outliers, with 93 % favoured (Fig. S3 A). By contrast, the intramolecular steric interactions in the AlphaFold model obtained for PFHDAC3 (Fig. 3.3 B) indicated good steric characteristics. Conversely, the AlphaFold structure revealed favourable geometry for 93 % of residues, with none in disallowed regions (Fig. S3 B). The AlphaFold structure was therefore used for subsequent docking studies. As for both of the class I PfHDAC1 and PfHDAC2 models, the α/β HDAC fold was visible in the models generated for this class II HDAC.

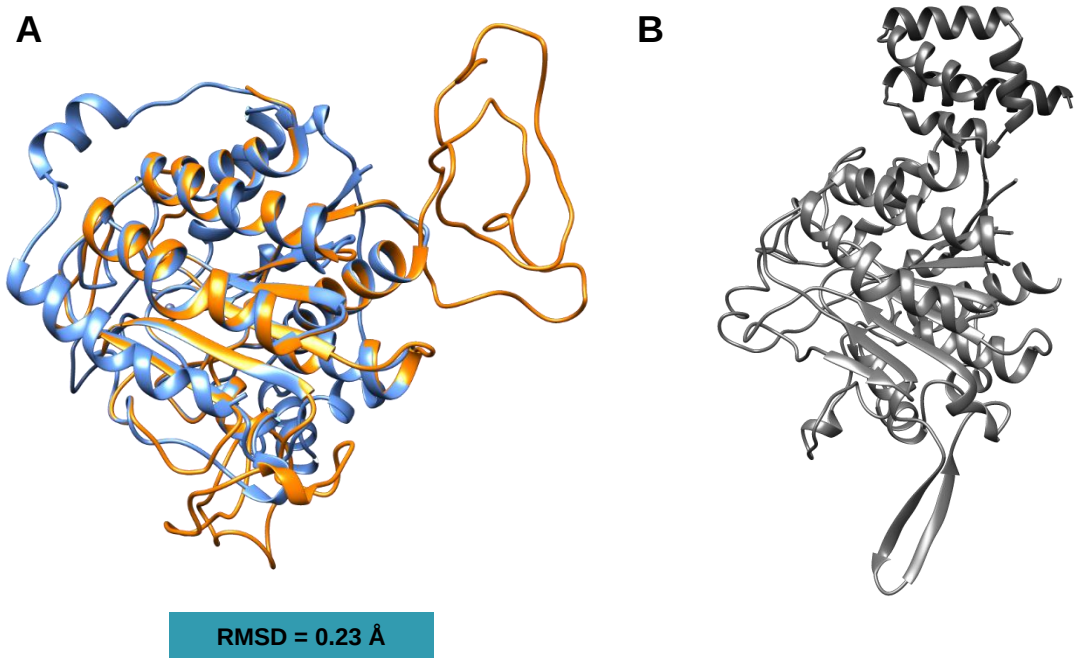

Figure 3.3: Structure of putative PfHDAC3. (A) Putative PfHDAC3 model generated using SwissModel and overlaid on the template, Alcaligenaceae bacteria histone deacetylase-like amidohydrolase. RMSD = 0.23 Å. Putative HDAC3 structure in orange and template structure in blue. **(B)** Putative PfHDAC3 model obtained from AlphaFold2.

3.1.2. Docking of HDACi to HDAC models for identification of target indicators

To evaluate the binding affinity and interactions of the epidrugs Sirtinol, Scriptaid and Oxamflatin to their putative targets, *in silico* molecular docking to the target models obtained above was performed using SwissDock. To note again, the crystal structure for PfSir2A was used as it was available, and Sirtinol was docked into this structure (Fig. 3.4).

The strongest binding mode for Sirtinol docked to Sir2A had a Gibb's free energy (ΔG) of -37.7 kJ.mol^{-1} (Fig. 3.4 A and B), indicating energetically favourable interactions. This binding mode involved direct occlusion of the active site, with Sirtinol binding observed to sterically overlap with both the NAD^+ cofactor (shown in yellow with coordinating residues in light blue), and a myristoylated H3K9 fragment (indicated in red and binding in the same active site as would H3K9ac, with coordinating residues indicated in orange). In studies of molecular interaction of Sirtinol with human SIRT1 and SIRT2, it has previously been reported that this is mediated in part through hydrogen bonding with the imine nitrogen, carbonyl oxygen and naphthol hydroxyl groups. Such hydrogen bonds including the imine nitrogen and carbonyl carbon to the NAD+ cofactor-coordinating residue R 49 are evident in the strongest observed binding mode of Sirtinol to PfSir2A, supporting this binding mode [114]. Sirtinol also bound in proximity to numerous other NAD+-coordinating factors, including Q114, N115 and H132, as well as the H3K9 substrate-coordinating residues V116, F181 and T211. These findings support PfSir2A as a possible target of Sirtinol.

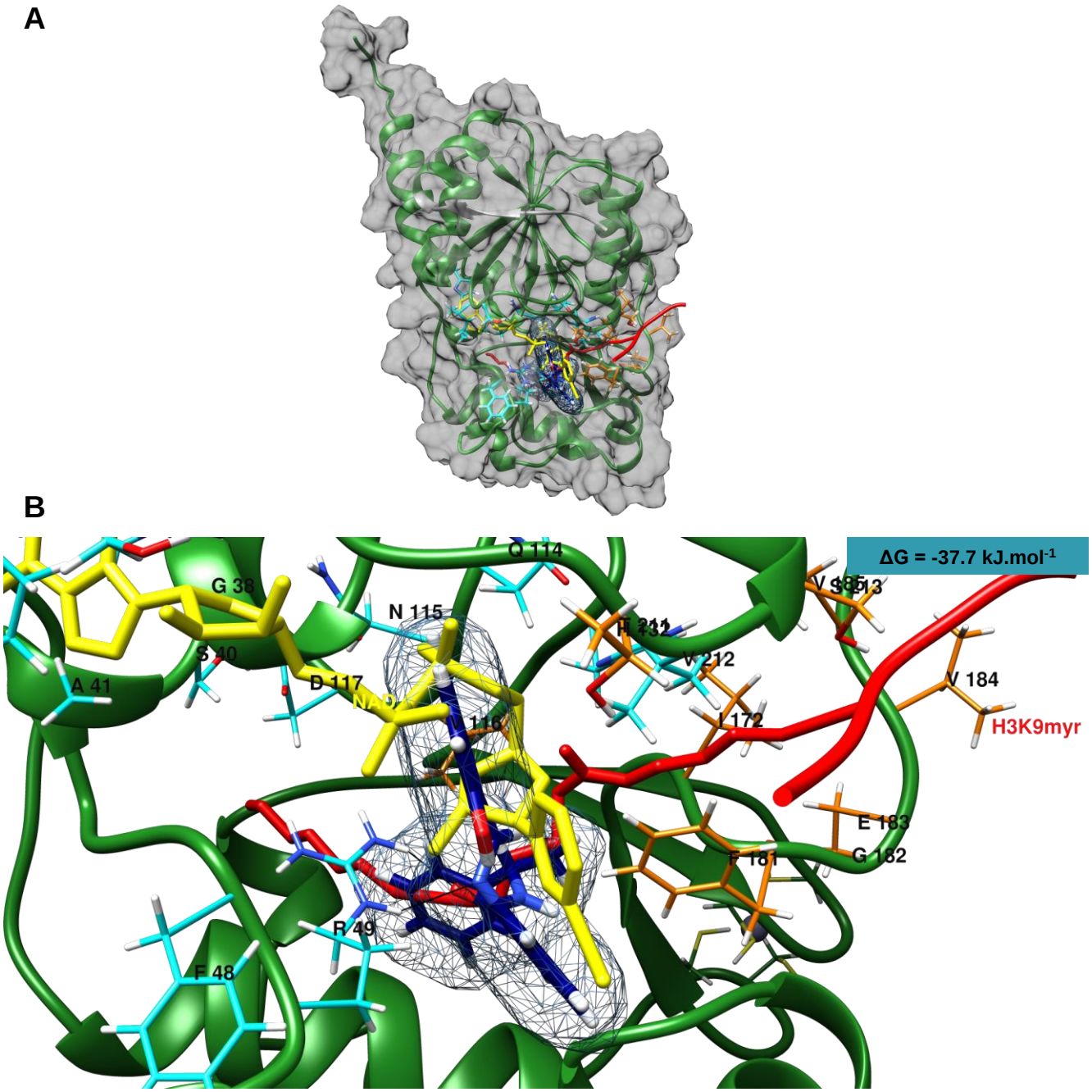

Figure 3.4: Mechanistic evaluation of targeting of PfSir2A by Sirtinol. (A) Sirtinol-PfSir2A complex. **(B)** Enlarged view of PfSir2A active site with complexed Sirtinol ligand. Bound NAD^+ cofactor is indicated in yellow with coordinating residues in light blue. A myristoylated H3K9 residue, occupying the same binding pocket as would an acetylated H3K9 residue, is shown in red with coordinating residues in orange. Sirtinol is shown in dark blue. The sirtuin domain is indicated in green and hydrogen bonds in black.

Of the three HDACs for which docking was evaluated, Oxamflatin was observed to bind to the active site of PfHDAC1 alone. The strongest observed binding mode was associated with a binding energy of -39.8 $kJ.mol^{-1}$ (Fig. 3.5 A and B), where Oxamflatin completely occluded the active site. Hydrogen bonding was observed between the bound ligand and the catalytic residue H138. Oxamflatin additionally sterically obstructs D174, H176 and D262, each Zn^{2+}-coordinating residues, and the catalytic residue H139. This binding mode would preclude the HDAC activity of this enzyme and is therefore supported as a possible target.

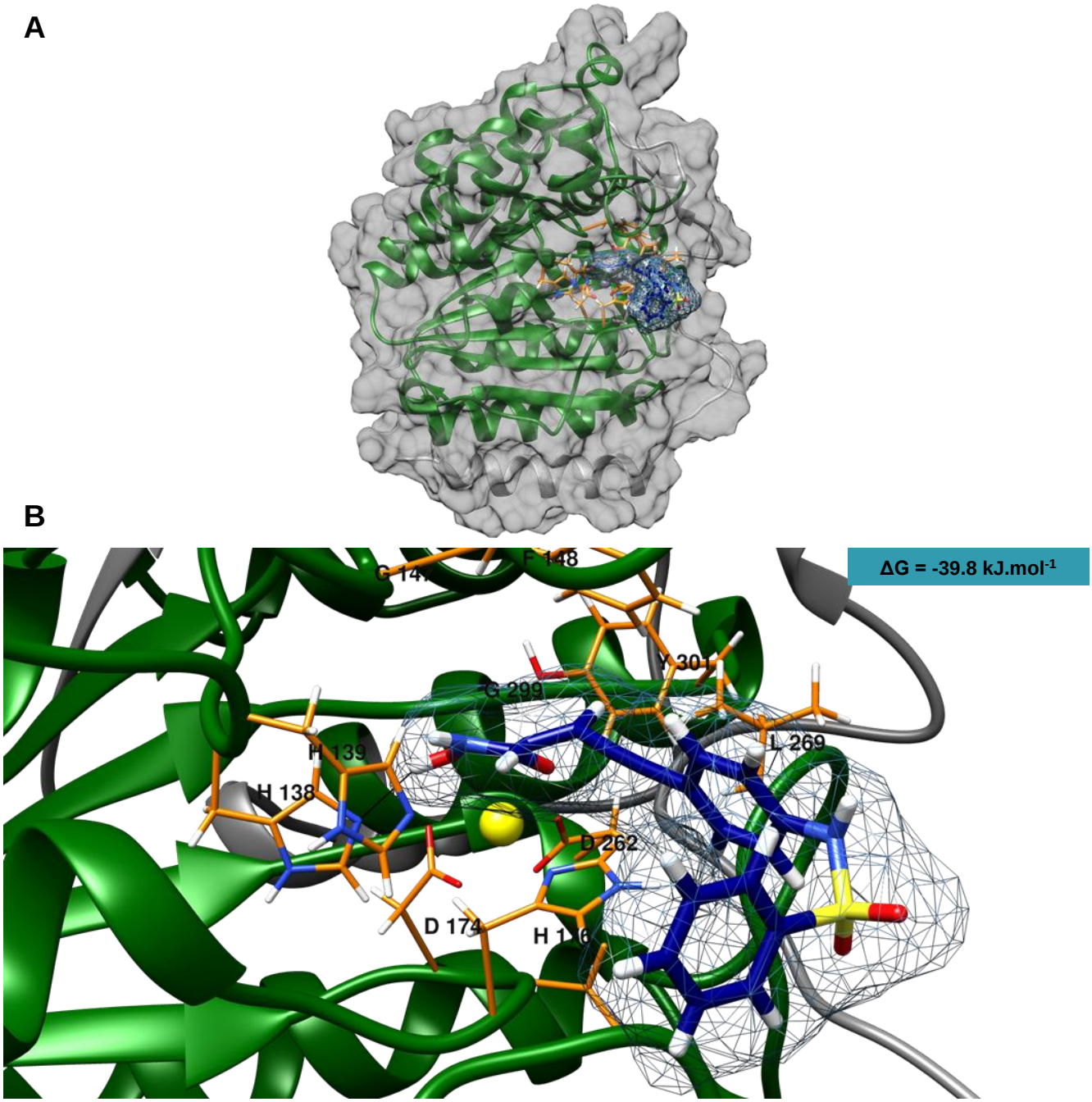

Figure 3.5: Mechanistic evaluation of targeting of PfHDAC1 by Oxamflatin. (A) Oxamflatin-PfHDAC1 complex. **(B)** Enlarged view of PfHDAC1 active site with complexed Oxamflatin ligand. Active site residues in orange. Oxamflatin is shown in dark blue. The histone deacetylase domain is shown in green. Hydrogen bonds are indicated in black and the Zn^{2+} cofactor is shown in yellow.

Scriptaid did not bind in proximity to active sites in either PfHDAC2 or the putative PfHDAC3. However, the strongest binding mode for Scriptaid docked to PfHDAC1 showed complete occlusion of the active site (Fig. 3.6 A and B) with a ΔG of -42.2 $kJ.mol^{-1}$. Steric overlap is observed between Scriptaid and the Zn^{+} cofactor. Intermolecular hydrogen bonding is indicated between Scriptaid and the catalytic residue H138, as for Oxamflatin, with additional hydrogen bonds formed with G147 and H176 (a Zn^{2+}-coordinating residue). These were previously predicted to be key binding residues involved in HDAC1-inhibitor complexes [115], with proximity to, and thus steric obstruction of, other key residues in common

with Oxamflatin, including the key catalytic residue H139 and the Zn^{2+}-coordinating residues D174 and D262, supporting PfHDAC1 as a possible target of Scriptaid.

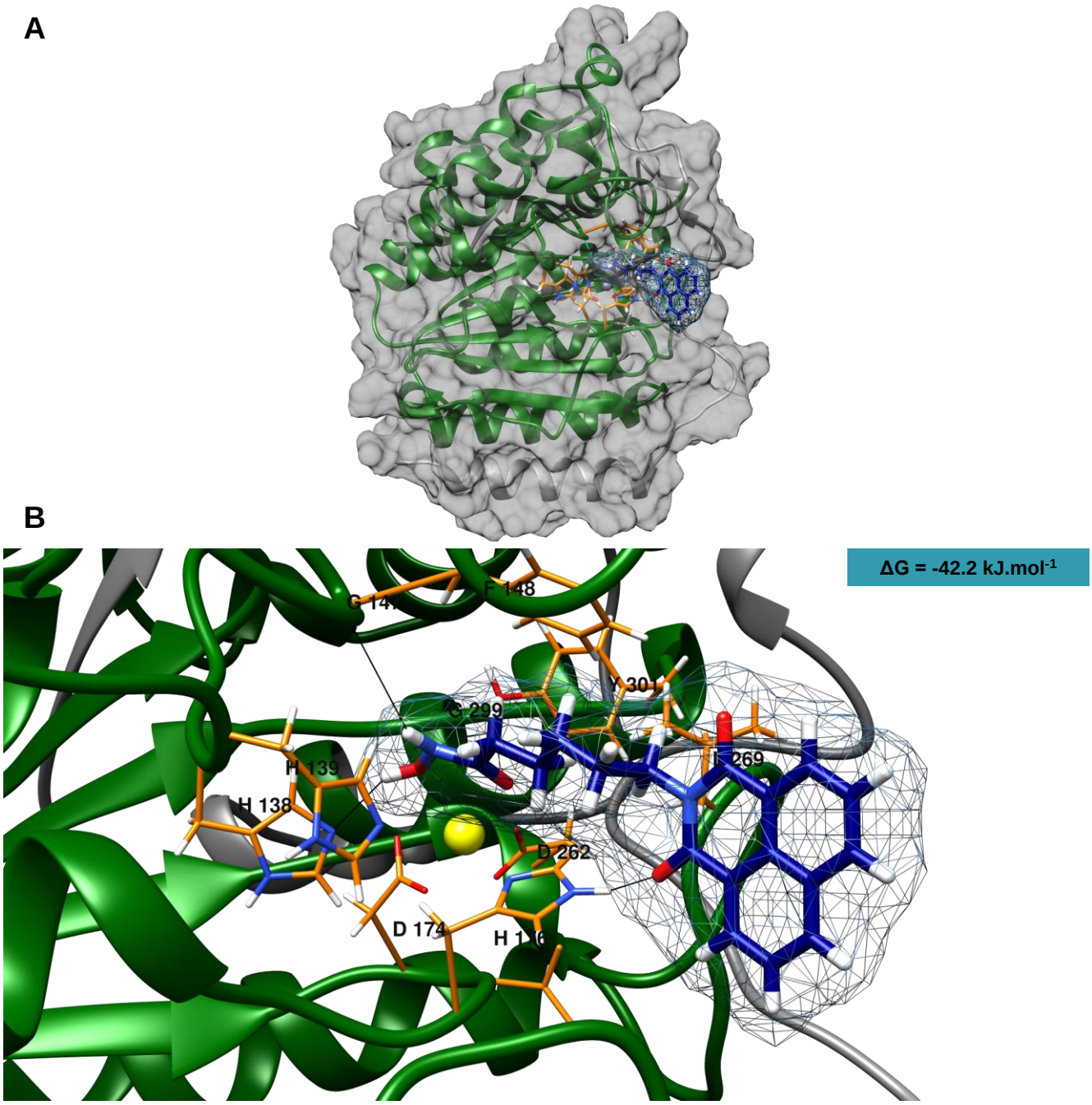

Figure 3.6: Mechanistic evaluation of targeting of PfHDAC1 by Scriptaid. (A) Scriptaid-PfHDAC1 complex. **(B)** Enlarged view of PfHDAC1 active site with complexed Scriptaid ligand. Active site residues in orange. Scriptaid is shown in dark blue. The histone deacetylase domain is shown in green. Hydrogen bonds are indicated in black and the Zn^{2+} cofactor is shown in yellow.

3.1.3. Immunoblot analysis of histone tail acetylation status changes resulting from HDACi treatment in asexual parasites

The three HDACi epidrugs (Scriptaid, Sirtinol and Oxamflatin), were previously shown to modulate histone acetylation levels in human cancer cells, thereby causing transcriptional dysregulation and subsequent cell death or senescence [81, 86, 89]. These compounds were subsequently interrogated

for their ability to alter histone acetylation, due to inhibition of HDAC activity, in *P. falciparum*. Asexual-stage parasites were evaluated after 6 h of drug pressure through immunoblotting (Fig. 3.7). This resulted in a pronounced 3.3-times increase in the general acetylation of H3K9 after Scriptaid treatment (Fig. 3.7 A). Sirtinol induced a less dramatic 2.3-times increase in H3K9ac after 6 h (Fig. 3.7 B), however, a concurrent 1.8-times increase in H3Core levels was also observed. Oxamflatin induced increases in both H3K9ac (1.9-times increase) and H3Core (2.4-times increase) abundance after 6 h of drug pressure (Fig. 3.7 C). This indicates that 6 h treatment of *P. falciparum* parasites with Sirtinol and Oxamflatin may induce general stress responses, resulting in unwanted changes of the core H3 levels. However, in all cases, the control methylation mark H3K9me3, did not change, indicating that the observed changes in H3K9ac were specific to the inhibition of HDACs with these inhibitors.

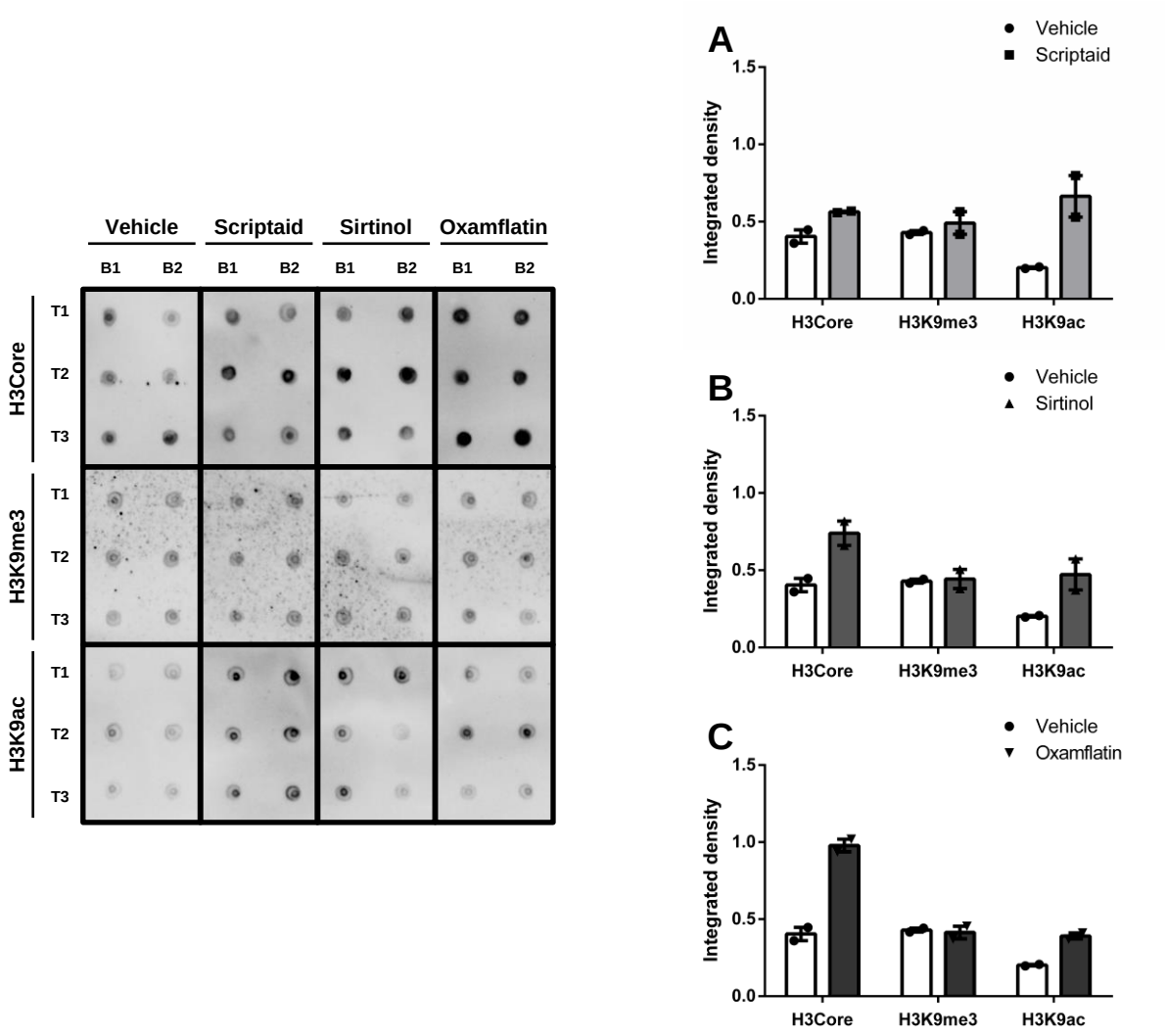

Figure 3.7: Post-translational modification changes in epidrug-treated asexual parasites after 6 h of drug pressure. Dot blots of parasite histone samples and relative histone post-translational modification abundance (α -H3Core, α -H3K9me3 and α -H3K9ac) for asexual parasites treated with **(A)** Scriptaid, **(B)** Sirtinol and **(C)** Oxamflatin for 6 h. Data are representative of two independent biological replicates (B1-2) performed in technical triplicate (T1-3), with mean ± S.E. indicated.

To evaluate any temporal influence in PTM acetylation with these three HDACi, *P. falciparum* parasites were evaluated after prolonged 12 h of drug pressure. This would additionally indicate if the changes in H3Core detected after 6 h were indeed due to general stress responses if they were maintained at 12 h. Similar to the increased acetylation of H3K9 seen after 6 h treatment of *P. falciparum* parasites with Scriptaid, this hyperacetylation was again seen at 12 h, with a 2.6-times increase in H3K9ac. This was without associated changes in the abundance of H3core or the general repressive mark H3K9me3 (Fig. 3.8 A). These findings provide mechanistic evidence that the activity of Scriptaid against asexual stages [77] is, as in human cell lines, due to HDAC inhibition This implies that Scriptaid could induce transcriptional dysregulation in asexual parasites, contributing to the observed parasite death phenotype.

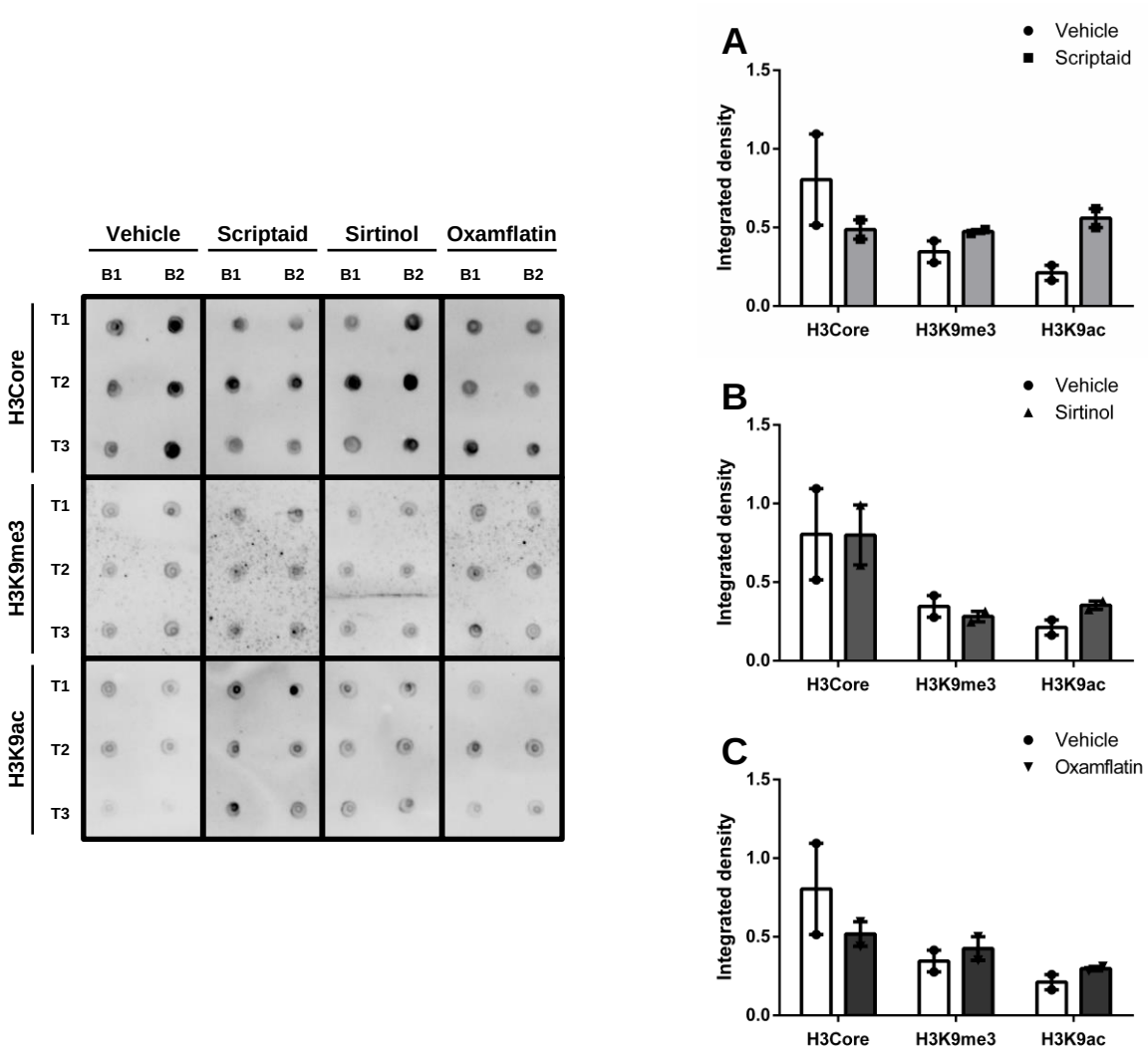

Figure 3.8: Post-translational modification changes in epidrug-treated asexual parasites after 12 h of drug pressure. Dot blots of parasite histone samples and relative histone post-translational modification abundance (α-H3Core, α-H3K9me3 and α-H3K9ac) for asexual parasites treated with **(A)** Scriptaid, **(B)** Sirtinol and **(C)** Oxamflatin for 12 h. Data are representative of two independent biological replicates (B1-2) performed in technical triplicate (T1-3), with mean ± S.E. indicated.

After treatment of *P. falciparum* parasites with Sirtinol for 12 h, only a 1.7-fold increase in H3K9ac was observed (Fig. 3.8 B). Moreover, although the average H3Core levels did not change, wide variability in H3Core abundance was seen after 12 h treatments with this compound. This observation, in combination with the altered H3Core abundance after 6 h treatments, indicated a possible general death response after treatment with Sirtinol. It is therefore unclear whether perturbation of H3K9ac is the sole MoA of this compound in asexual stages.

Treatment with Oxamflatin indicated a 0.4-times decrease in H3Core abundance and a 1.4-times increase in H3K9ac after 12 h drug pressure (Fig. 3.8 C), which is in contrast with the increased abundance of H3Core seen after 6 h treatment. These incongruous trends observed with this compound could support a general death response induced by Oxamflatin, independent of changes in histone acetylation levels.

3.1.4. Immunoblot analysis of histone acetylation after Scriptaid and Sirtinol treatment of gametocytes

Scriptaid has shown inhibitory activity against asexual stages as well as early- and late-stage gametocytes in previous studies [78] and, as evidenced above, results in hyperacetylation of histones which could dysregulate gene expression. Therefore, to determine whether observed histone acetylation changes in asexual stages are also apparent in late-stage gametocytes, immunoblotting was also used to investigate PTM changes in these late-stage gametocytes due to Scriptaid treatment. Even after 12 h of treatment, Scriptaid was found to induce only a slight, but significant 0.05-times decrease ($P = 0.0376$, $n = 3$) in histone tail methylation, with no concurrent changes in acetylation (Fig. 3.9). It is therefore evident that, in contrast to observations in asexual stages, Scriptaid may exhibit an alternative MoA to HDAC inhibition in late-stage gametocytes or that, if the same MoA is evident, this is not observed at 12 h of treatment.

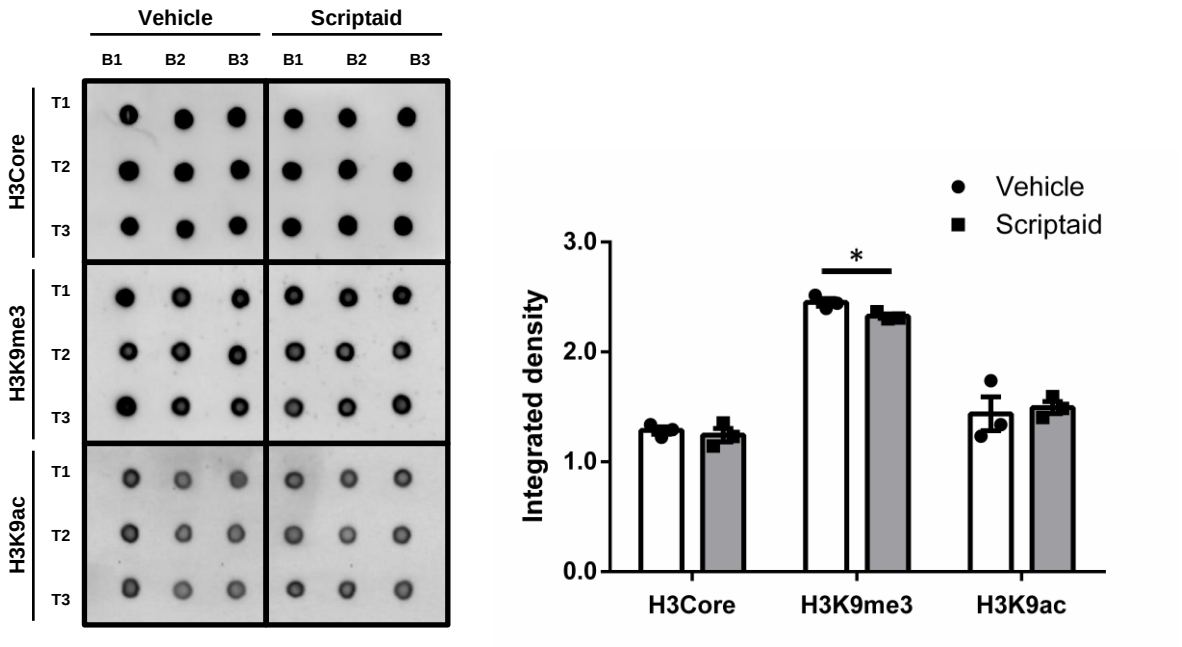

Figure 3.9: Post-translational modification changes in Scriptaid-treated late-stage gametocytes. Dot blots of parasite histone samples and relative histone post-translational modification abundance (α-H3Core, α-H3K9me3 and α-H3K9ac) for late-stage gametocytes treated with Scriptaid for 12 h. Data are representative of three independent biological replicates (B1-3) performed in technical triplicate (T1-3), with mean ± S.E. indicated. *P = 0.0376, unpaired, two-tailed t-test.

To evaluate whether the potent activity of Sirtinol against late-stage gametocytes is associated with an epigenetic MoA in these stages, histone PTM changes consequent to Sirtinol treatment in these stages were evaluated. After 6 h, Sirtinol induced 0.3-fold and 0.5-fold decreases in H3K9me3 and H3K9ac, respectively (Fig. 3.10). However, since both acetylation, as expected, and methylation (unexpected) histone PTMs were affected, the data point towards a possible general death response, rather than specific effects on histone PTMs. This is further supported by a 0.2-fold decrease in H3Core levels (Fig. 3.10).

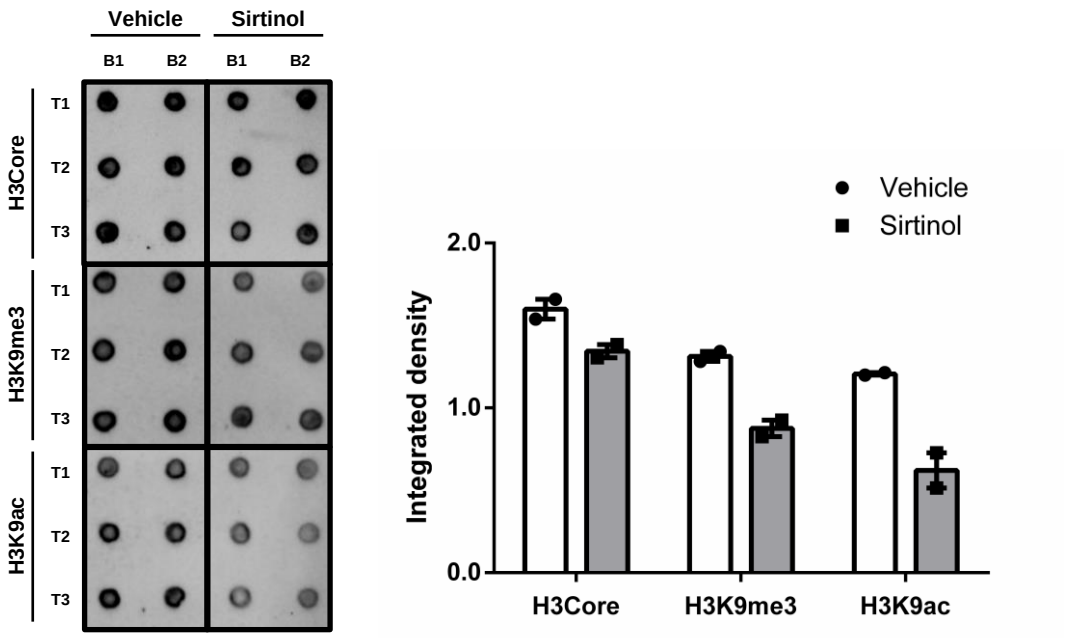

Figure 3.10: Post-translational modification changes in Sirtinol-treated late-stage gametocytes. Dot blots of parasite histone samples and relative histone post-translational modification abundance (α-H3Core, α-H3K9me3 and α-H3K9ac) for late-stage gametocytes treated with Sirtinol for 6 h. Data are representative of two independent biological replicates (B1-2) performed in technical triplicate (T1-3), with mean ± S.E. indicated.

It was therefore decided to evaluate changes in PTMs after Sirtinol treatment for a shorter, 3 h timeframe (Fig. 3.11). In addition, to attain a broader indication of the histone tail acetylation status, a polyclonal antibody preparation against H3K9ac, H3K14ac, H3K18ac, H3K23ac and H3K27ac was used to evaluate pan acetylation. After only 3 h of exposure to Sirtinol in late-stage gametocytes, no significant changes could be detected in any of the histone PTMs or the histone core control (Fig. 3.11). Whilst this indicates that the overt stress observed after 6 h treatment was alleviated, it also shows that there was no observable effect on histone PTMs over a shorter time period. This could be due either to the need for an intermediate timepoint, or Sirtinol not changing acetylation to an extent detectable with dot-blot analysis in late-stage gametocytes. Conclusive evidence as to the MoA of Sirtinol affecting histone acetylation in late-stage gametocytes could therefore not be established.

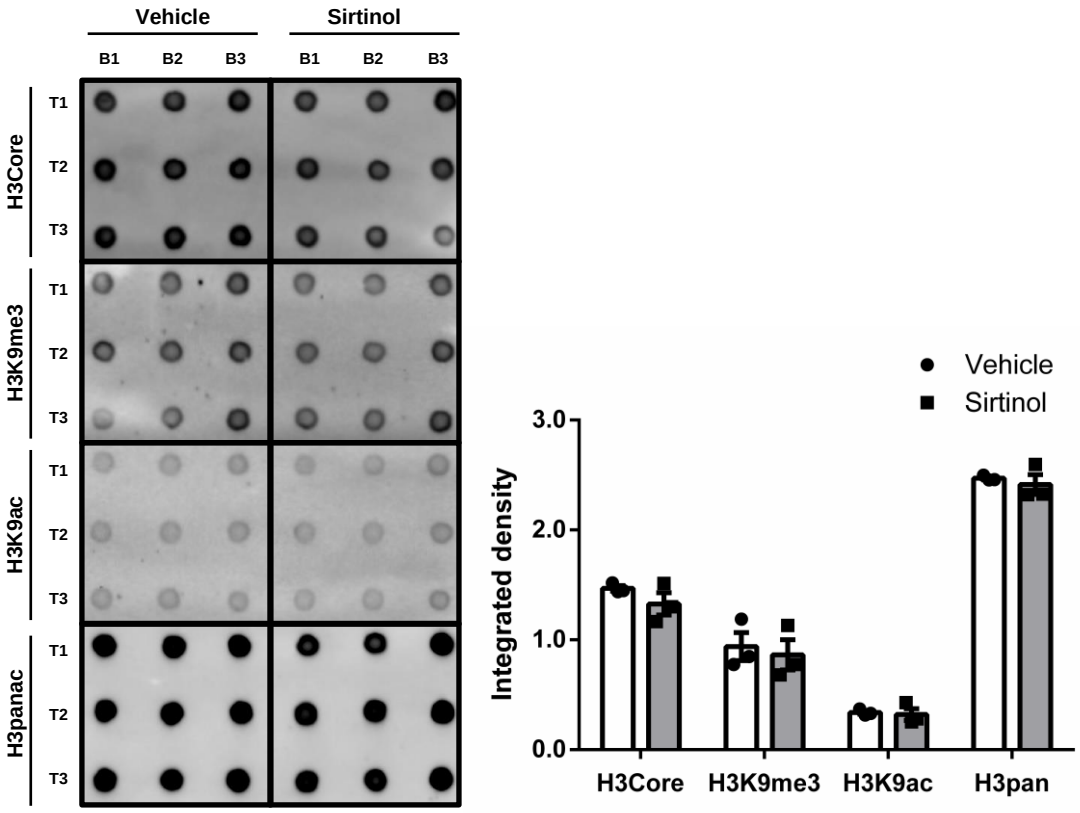

Figure 3.11: Post-translational modification changes in Sirtinol-treated late-stage gametocytes. (A) Dot blots of parasite histone samples and relative histone post-translational modification abundance (α-H3Core, α-H3K9me3 and α-H3K9ac) for asexual parasites treated with Sirtinol for 3 h. Data are representative of three independent biological replicates (B1-3) performed in technical triplicate (T1-3), with mean ± S.E. indicated. Unpaired, two-tailed t-test.

Since Sirtinol displays late-stage gametocyte selectivity (3.8-times increase), this compound indeed has potential as a transmission-blocking candidate. However, to confirm its transmission-blocking potential, in the absence of conclusive proof that this killing of gametocytes is due to specific effects on histone acetylation levels, the ability of Sirtinol to inhibit gamete and oocyst formation was evaluated. Scriptaid, by contrast, has activity against asexual parasites and early-stage gametocytes in addition to late-stage gametocytes and, as a compound with broader stage activity profiles, was included as a comparative control (Fig. 3.12).

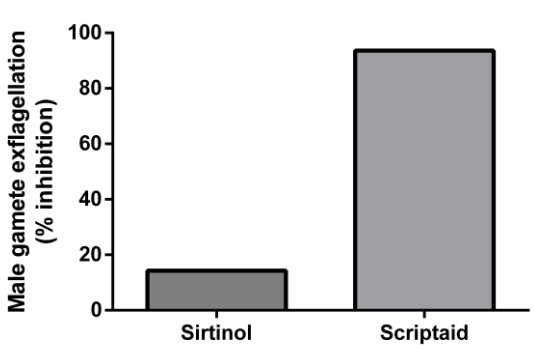

Figure 3.12: Inhibition of male gamete exflagellation by HDACi 48 h post-treatment. Data representative of one biological repeat.

Sirtinol was found to poorly inhibit male gamete exflagellation, by only 14.3 % (Fig. 3.12) compared to a methylene blue positive control for inhibition (100 %) and a vehicle control for full viability (0 %). Scriptaid, by contrast, induced a profound decrease in exflagellation at 93.6 %. These data indicate likely transmission-blocking activity by Scriptaid, but Sirtinol does not appear to target male gametes, and its transmission-blocking therefore needed further confirmation. As such, to confirm the transmission-blocking activity of Scriptaid and Sirtinol, standard membrane-feeding assays (SMFAs) were performed (Fig. 3.13). These assays evaluate the reduction in oocyst intensity (Fig. 3.13 A), the average number of oocysts per mosquito, as a measure of transmission-reducing activity (TRA), or oocyst prevalence (Fig. 3.13 B), the number of mosquitoes in which oocysts are found, as a measure of transmission-blocking activity (TBA), compared to vehicle controls [111]. Interestingly, despite previously having shown poor inhibition of male gametes, Sirtinol significantly decreased oocyst intensity (P<0.0001, n = 3) and prevalence (P = 0.0003) by 96 % and 80 %, respectively, indicating potent transmission-blocking capability (Fig. 3.13). Treatment with Scriptaid significantly reduced both oocyst intensity (89 %) and oocyst prevalence (77 %) (P<0.0001, n = 3), thus revealing a favourable transmission-blocking profile. Therefore, the gametocytocidal activity of both compounds results in confirmed transmission-blocking capabilities, although the MoA of the compounds as affecting acetylation in late-stage gametocytes could not be established.

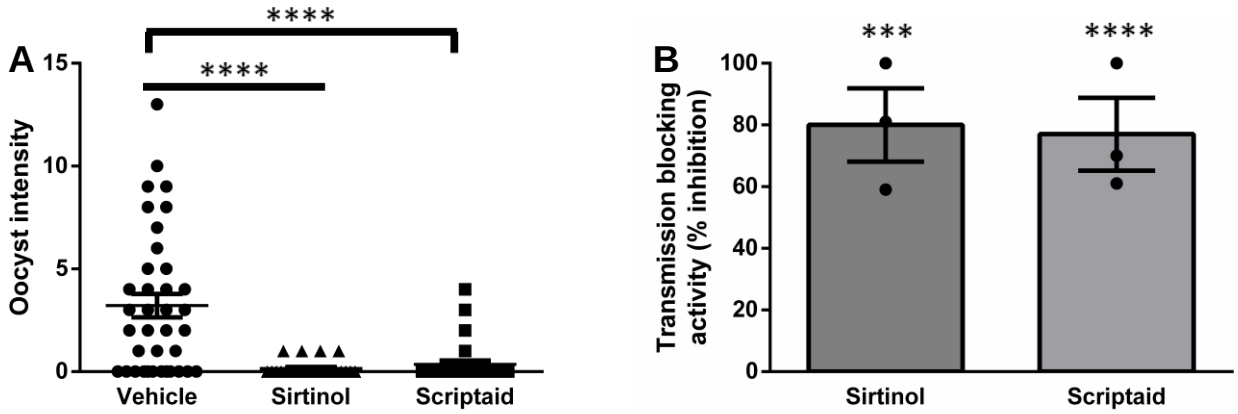

Figure 3.13: Transmission-reducing and transmission-blocking activity of HDACi against *P. falciparum* parasites. Treatments were performed at 2 µM for 48 h. **(A)** Oocyst intensity as measured by the number of oocysts per mosquito, with mean ± S.E.M indicated. **(B)** Transmission-blocking activity as a percentage decrease in the number of mosquitoes containing oocysts. Data are representative of three independent biological repeats performed in technical duplicate, with mean ± S.E. indicated. *** P = 0.003, **** P<0.0001, Mann-Whitney non-parametric t-test.

3.2. HDMi targeting *P. falciparum* parasites

The HDMi inhibitor ML324, as indicated in Table 1.1, was evaluated due to observed late-stage specific activity in *P. falciparum* parasites (IC_{50} = 0.08 µM).

3.2.1. Modelling of HDMs for exploration of HDMi target indicators

To confirm the potential targets for ML324, putative drug targets were predicted based on homology to the known target proteins of this compound in mammalian cells, KDM4A, KDM4B and KDM4E [91, 99]. PfJmjC1 was the most homologous protein to the human KDM4 target (~2e-13) but, because ML324 was previously observed to inhibit recombinantly expressed PfJmj3 *in vitro* [80], models of PfJmjC2 and PfJmj3 were also modelled to confirm docking to Jmj3 and preclude docking to JmjC1 and JmjC2.

An RMSD of 0.37 Å for aligned Cα atoms points to good alignment of the homology model generated for PfJmjC1 to its *A. thaliana* JMJ14 template (Fig. 3.14 A). Neither the AlphaFold model (Fig.3.14 B) nor the homology model were found to have unacceptable intramolecular steric interactions upon structural validation with MolProbity. A Ramachandran plot of peptide backbone dihedral angles revealed that, for the SwissModel structure, 92 % of residues had favourable geometry while 1.06 % had unfavourable geometry (Fig. S4 A). In contrast, the AlphaFold structure had a favourable geometry for 95 % of residues while 0.71 % of residues proved to have unfavourable geometry (Fig. S4 B), revealing moderately better conformity to energetically allowed backbone dihedral angles and supporting progression of this model to docking studies.

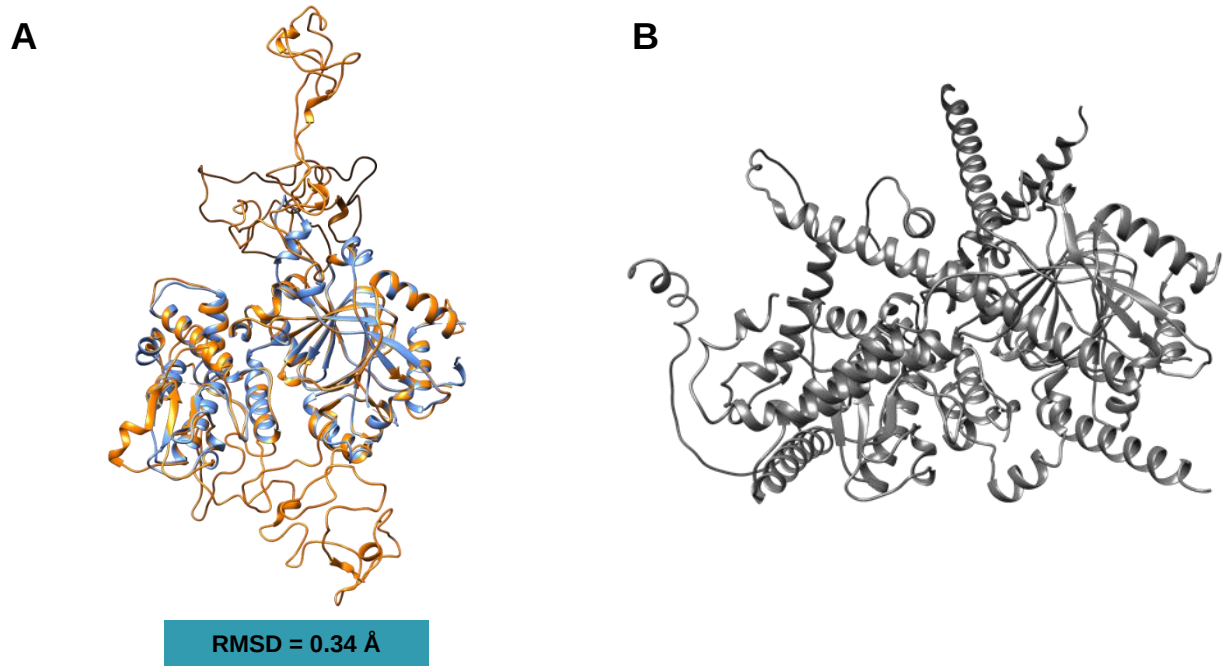

Figure 3.14: Structure of PfJmjC1. (A) JmjC1 model generated using SwissModel and overlaid on the template, *A. thaliana* probable lysine-specific demethylase JMJ14. RMSD = 0.34 Å. JmjC1 structure in orange and template structure in blue. **(B)** PfJmjC1 model obtained from AlphaFold2.

Evident in this structure is a JmjC domain (InterPro: IPR003347), necessary for substrate-specificity. The cupin domain-like beta barrel tertiary structure typical of JmjC domains [116], with residues for binding of α-ketoglutarate and Fe^{2+} cofactors important for protein function, are visible. In addition, a JmjN domain (InterPro: IPR003349), predicted to occur only in PfJmjC1 within the *P. falciparum* histone demethylases, is seen [117]. A C5HC2-type zinc finger domain (InterPro: IPR004198) is present [80], in common with the JARID1 subgroup of human Jumonji demethylases, which is known to bind AT-rich DNA stretches [116].

PfJmjC2 was modelled on the human JmjC domain-containing protein C2orf60, with close correlation indicated by a Cα heavy chain RMSD of 0.37 Å for aligned Cα atoms (Fig. 3.15 A). Although MolProbity validations indicated favourable intramolecular steric interactions for both the homology model and the AlphaFold model (Fig. 3.15 B), the latter had much better energetically allowed dihedral angle distributions (96 % of residues favoured and 0.23 % outliers) (Fig. S5 B), compared to the SwissModel structure (88 % of residues with favourable geometry and 2.43 % as outliers, Fig. S5 A). The AlphaFold structure was therefore retained for docking evaluation of ML324. As for PfJmjC1, a JmjC beta barrel domain (InterPro: IPR003347) was evident in both PfJmjC2 structures. This protein has neither zinc-finger nor JmjN domains, as is evident in these models [117].

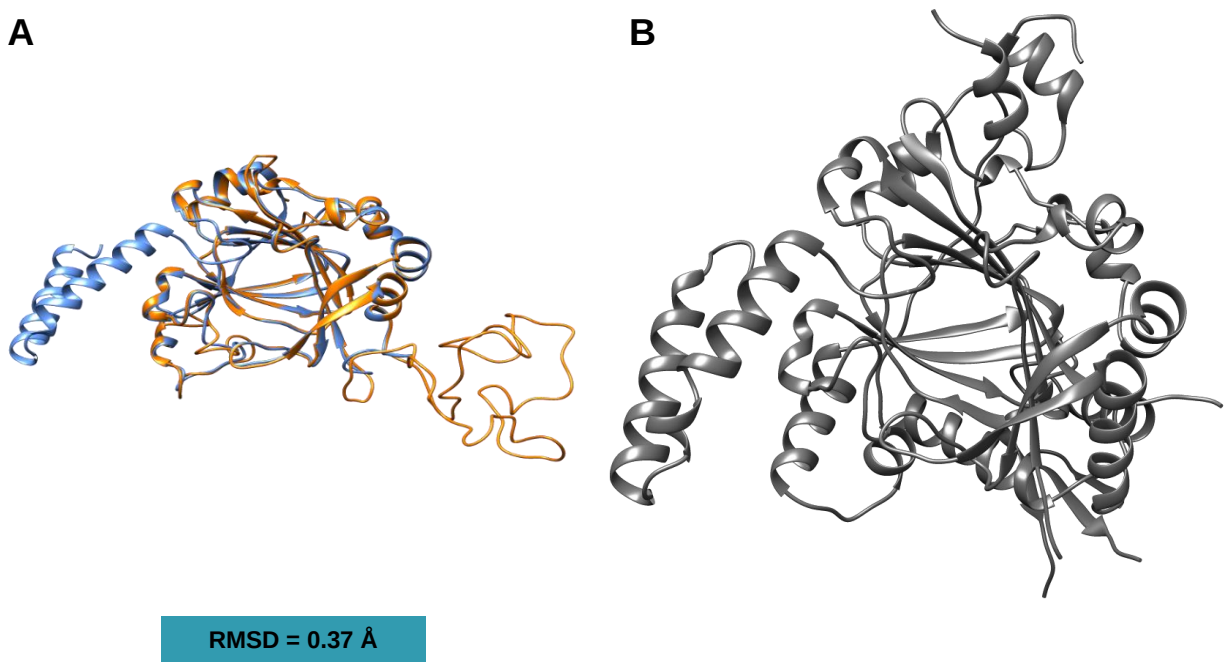

Figure 3.15: Structure of PfJmjC2. (A) JmjC2 model generated using SwissModel and overlaid on the template, *H. sapiens* JmjC domain-containing protein C2orf60. RMSD = 0.37 Å. JmjC2 structure in orange and template structure in blue. **(B)** PfJmjC2 model obtained from AlphaFold2.

PfJmj3 was modelled using homology-based modelling on factor inhibiting HIF-1 (FIH-1), a negative regulator of the oxygen homeostasis mediator hypoxia inducible factor 1 [118]. This protein contains a JmjC domain (InterPro: IPR003347) that forms the active site of the Jmj3 protein and allows it to coordinate α-ketoglutarate and Fe^{2+} cofactors involved in the demethylase activity. The model correlated well with its template, yielding a Cα heavy chain RMSD of 0.34 Å for aligned Cα atoms (Fig.

3.16 A). However, this model had an extremely poor per-residue quality and was therefore not retained for docking. MolProbity structural validation of the AlphaFold model (Fig. 3.16 B) indicated favourable intramolecular steric interactions as well as an acceptable dihedral angle geometry (97 % of residues favoured and 0.24 % outliers) (Fig. S6). The AlphaFold model was therefore retained for exploration of ML324 targets.

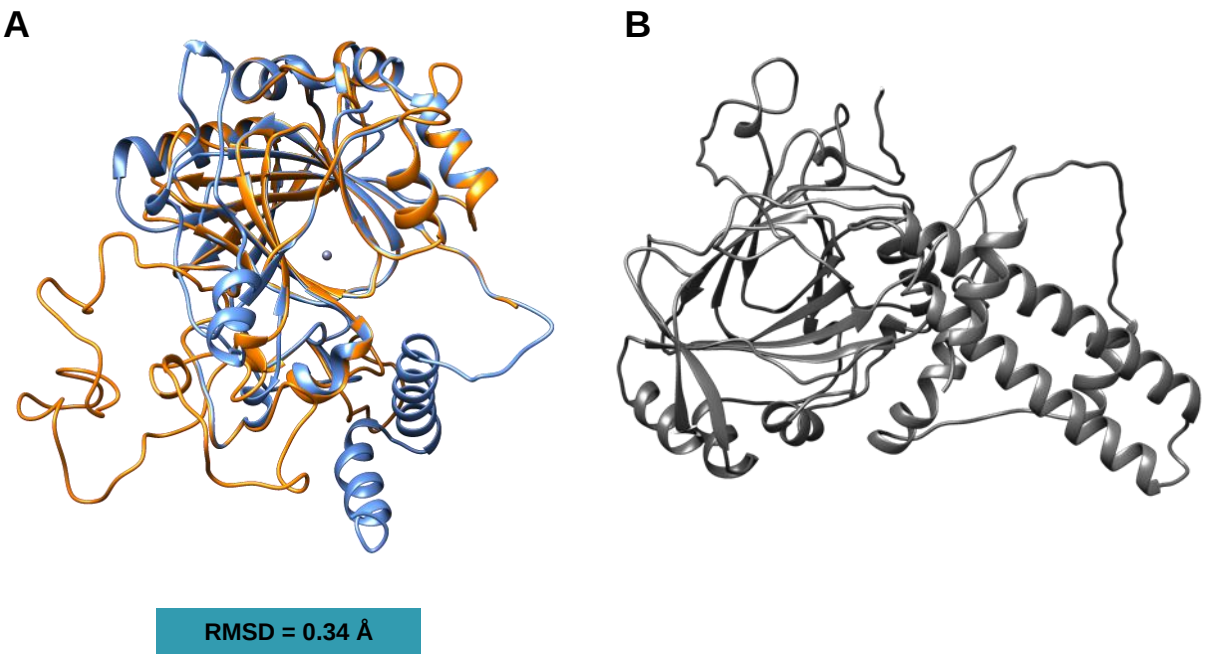

Figure 3.16: Structure of PfJmj3. (A) Jmj3 model generated using SwissModel and overlaid on the template, *H. sapiens* Hypoxia-inducible factor 1-alpha inhibitor. RMSD = 0.34 Å. Jmj3 structure in orange and template structure in blue. **(B)** PfJmj3 model obtained from AlphaFold2.

3.2.2. Docking of HDMi to HDM models for identification of target indicators

To confirm the *in vitro* activity of ML324 against the *P. falciparum* JmjC domain-containing proteins [80], *in silico* docking of ML324 was performed to each of the models created for PfJmjC1, PfJmjC2 and PfJmj3. Docking against the first two protein models revealed no binding of ML324 in proximity to the active sites of either PfJmjC1 (Fig. 3.17 A) or to PfJmjC2 (Fig. 3.17 B). This therefore excludes these two proteins as the targets of ML324 based on the molecular docking strategy applied. By contrast, docking of ML324 to PfJmj3 showed complete occlusion of the JmjC domain active site in this protein by ML324 with a ΔG of -35.1 $kJ.mol^{-1}$ (Fig. 3.17 C and D). ML324 is observed to occlude the Fe^{2+}-coordinating residues H166, D168 and H342, as well as Y106, N172 and K181, each involved in 2-oxoglutarate (2-OG) binding. Both of these binding partners are integral to the function of PfJmj3 through the formation of succinate and iron intermediates by oxidative decarboxylation, which are subsequently used for lysine demethylation [80]. Occlusion of these would therefore preclude activity. These *in silico* data therefore support the *in vitro* observations by Matthews *et al.* that ML324 inhibits recombinant PfJmj3 activity [80] and indicate that PfJmj3 is the sole Jmj family member targeted by this compound.

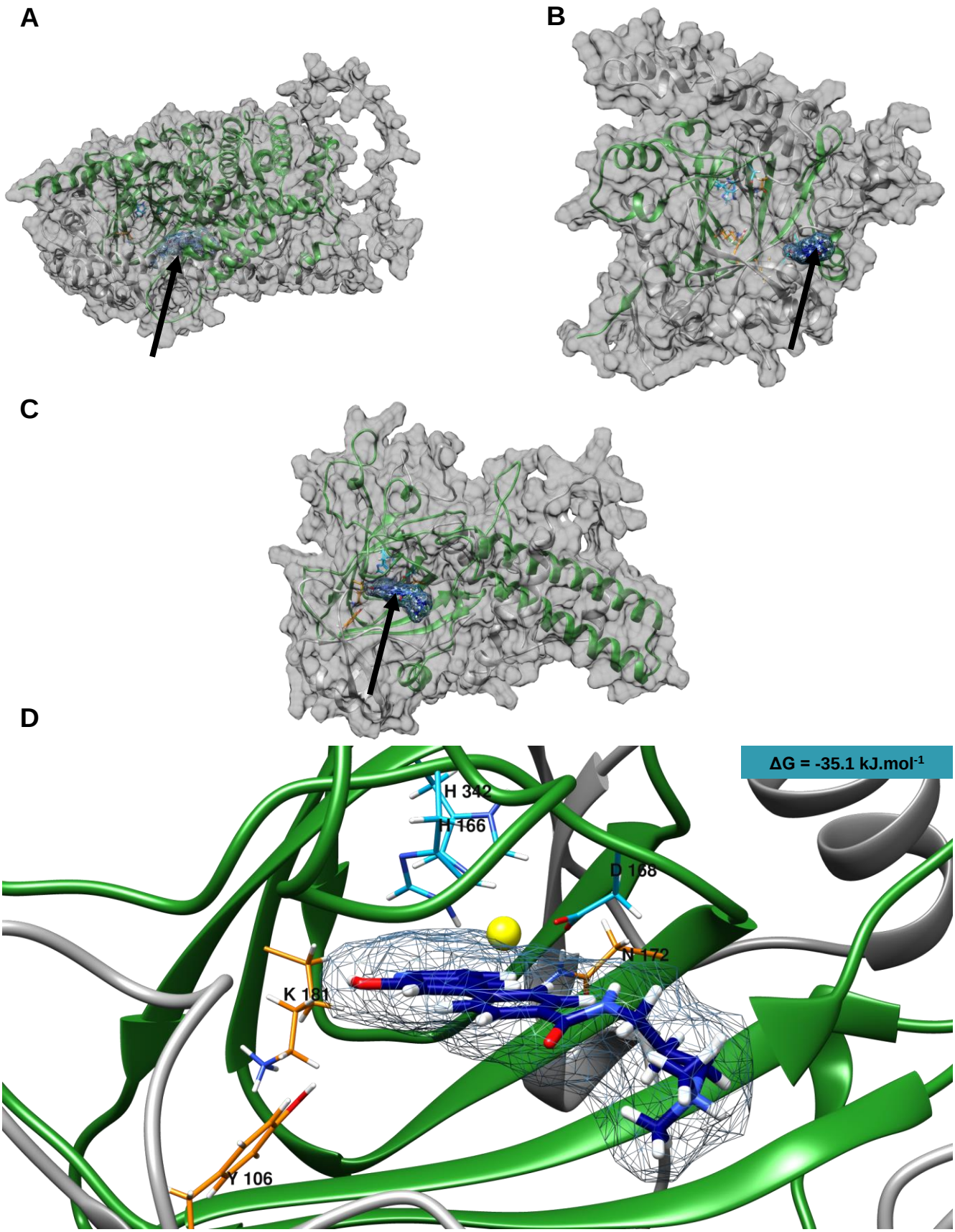

Figure 3.17: Mechanistic evaluation of targeting of JmjC domain-containing proteins by ML324. **(A)** ML324-PfJmjC1 complex. No proximity to the active site is observed **(B)** ML324-PfJmjC2 complex. No proximity to the active site is observed. **(C)** ML324-PfJmj3 complex. **(D)** Enlarged view of PfJmj3 with complexed ML324 ligand. ML324 is observed to intercalate directly into the active site, entirely occluding it. 2-OG-coordinating residues are shown in orange and Fe^{2+}-coordinating residues in light blue. ML324 is shown in dark blue. JmjC domains are shown in green. Fe^{2+} cofactor is shown in yellow. Black arrows indicate predicted binding sites

As a control for specificity of ML324 binding against PfJmj3, another KDM4 inhibitor, f1iii, was included. This compound is structurally dissimilar to ML324 (see Table 1.1). Compound f1iii also showed potent inhibition of late-stage gametocytes with an IC_{50} of 9 nM (J. Reader, unpublished). Like ML324, the strongest binding mode of f1iii to PfJmj3 (Fig. 3.18 A and B) was observed to sterically block the Fe^{2+}-coordinating residues H166 and D168 as well as the 2-OG-coordinating residues Y106, N172 and K181, binding with a ΔG of -31.8 $kJ.mol^{-1}$. This binding mode would therefore, like ML324, prevent activity by PfJmj3.

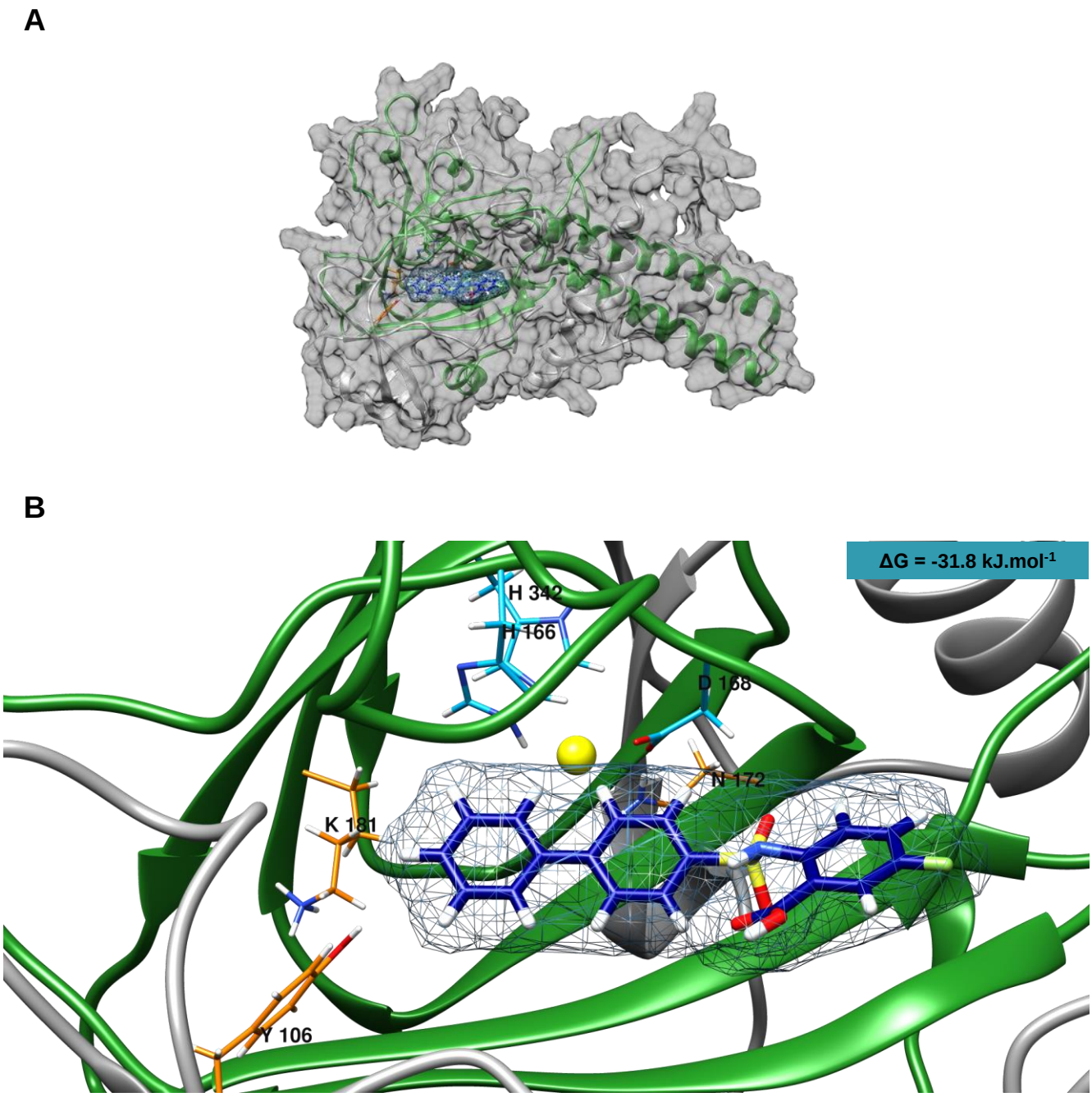

Figure 3.18: Mechanistic evaluation of targeting of PfJmj3 by f1iii. (A) f1iii-PfJmj3 complex. **(B)** Enlarged view of PfJmj3 active site with complexed f1iii ligand. 2-OG-coordinating residues are shown in orange and Fe^{2+}-coordinating residues in light blue. F1iii is shown in dark blue. JmjC domains are shown in green. Fe^{2+} cofactor is shown in yellow.

3.2.3. MoA determination of ML324 through dot-blot analysis

To evaluate whether inhibition of PfJmj3, as the indicated target for ML324, results in changes in lysine methylation on histones as part of the MoA in *P. falciparum*, immunoblot analysis was performed. Asexual parasites were not evaluated as this compound shows stage-selectivity towards late-stage gametocytes as a differential phenotype. Methylation of the key mark H3K9me3 was evaluated after treatment of late-stage gametocytes with ML324 (Fig. 3.19). This revealed a statistically significant 1.4-times increase in H3K9me3 (P = 0.0282, n = 3) without corresponding changes to H3Core or H3K9ac controls. This therefore supports PfJmj3 as the target of ML324 and confirms an epigenetic MoA by ML324 in *P. falciparum* parasites, as is observed in human cancer cells, mediated through inhibition of Jumonji demethylase PfJmj3 function.

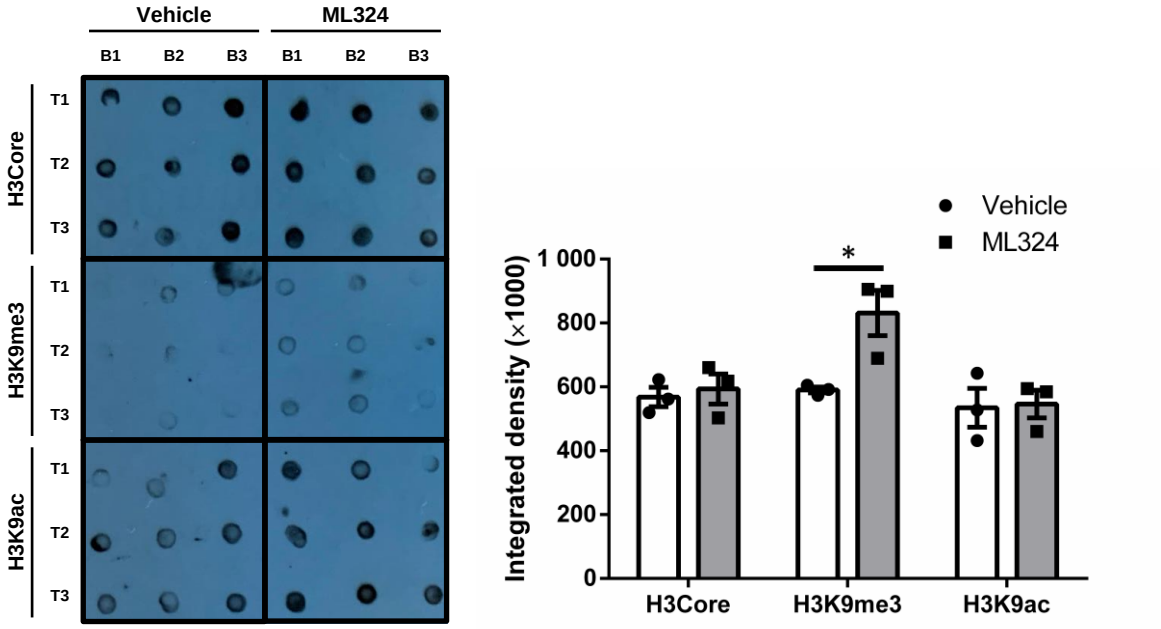

Figure 3.19: Post-translational modification changes in ML324-treated late-stage gametocytes. Dot blots of parasite histone samples and relative histone post-translational modification abundance (α-H3core, α-H3K9me3 and α-H3K9ac) for late-stage gametocytes treated with 5 µM ML324 for 24 h. Data are representative of three independent biological replicates (B1-3) performed in technical triplicate (T1-3), with mean ± S.E. indicated. *P = 0.0282, unpaired, two-tailed t-test.

F1iii was investigated for perturbation of histone tail methylation, but no statistically significant changes in H3K9me3 abundance (Fig. 3.20) or in the H3K9ac controls could be observed. Since the direct homologues of KDM4 in humans are PfJmjC1 and PfJmjC2 in *P. falciparum*, the fact that a KDM4 inhibitor did not result in perturbation of histone methylation indicates that the effect seen with ML324 as a PfJmj3 inhibitor is specific and important in late-stage gametocytes.

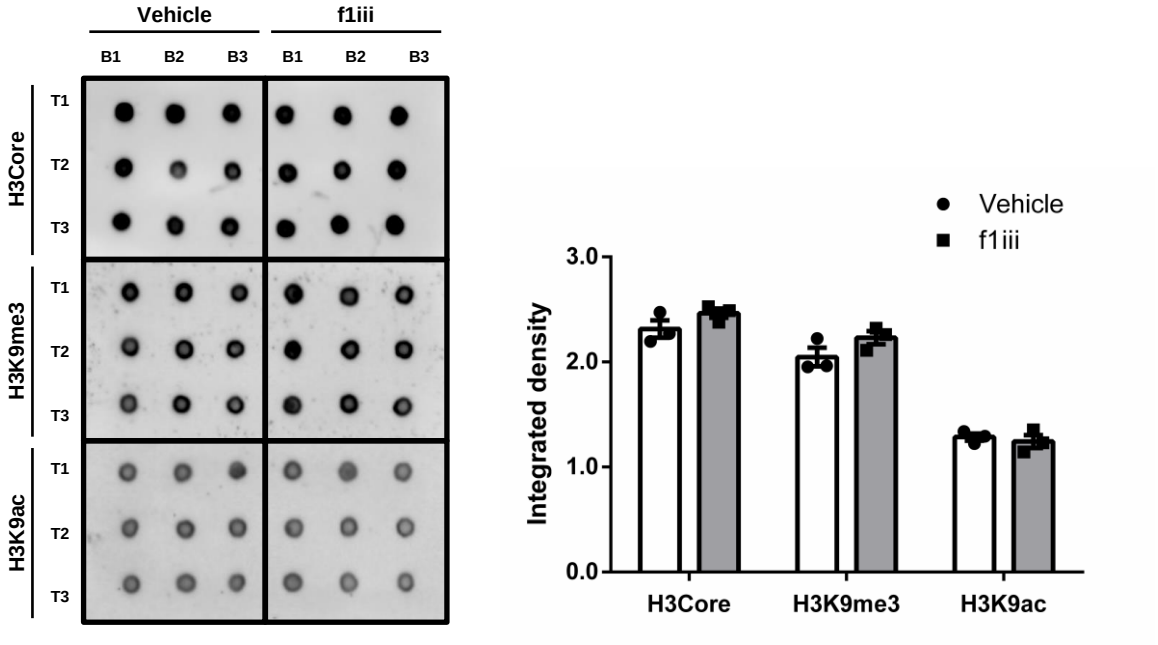

Figure 3.20: Post-translational modification changes in f1iii-treated late-stage gametocytes. Dot blots of parasite histone samples and relative histone post-translational modification abundance (α-H3core, α-H3K9me3 and α-H3K9ac) for late-stage gametocytes treated with 5 µM ML324 for 24 h. Data are representative of three independent biological replicates (B1-3) performed in technical triplicate (T1-3), with mean ± S.E. indicated. Unpaired, two-tailed t-test.

3.3. HKMTi targeting *P. falciparum* parasites

Two HKMTi, indicated in Table 1.1, were investigated based on activity against *P. falciparum* parasites. The compound UNC0638 potently targeted asexual stages (IC_{50} = 0.028 µM [77]) with more moderate inhibition of late-stage gametocytes (0.442 µM), with UNC0379 included to expand the HKMTi chemical footprint.

3.3.1. Modelling of HKMTs for exploration of HKMTi target indicators

Putative targets for both the HKMTi UNC0638 and a close analogue UNC0379 were identified as before on the basis of homology to their targets in human cells. Both of these compounds have specific targets in mammalian cells, and single target indicators for UNC0638 of PfSET2 (homologue of G9a, [93]) and UNC0370 of PfSET8 (homologue of mammalian SET8 [96]) were observed with high confidence (E-values of 2e-15 and 5e-28, respectively). To create homology models of PfSET2 and PfSET8, templates that provided the highest initial GMQE were selected, with sequence identities at >30 % in both instances.

PfSET8 was subsequently modelled on a *Cryptosporidium parvum* Iowa II lysine methyltransferase CpSET8 template with an RMSD of 0.24 Å for aligned Cα atoms (Fig. 3.21 A), indicating good conformity, with model validation showing few intramolecular steric clashes. The peptide backbone showed highly favourable peptide backbone geometry, with 99 % of residues favoured and no outliers (Fig. S7 A). However, the active site was poorly captured, with key substrate-coordinating residues showing poor per-residue quality. By contrast the AlphaFold model (Fig. 3.21 B), though it too showed

acceptable intramolecular steric interactions, had a less favourable distribution of peptide backbone dihedral angles (92 % favoured and 2.23 % outliers) (Fig. S7 B).

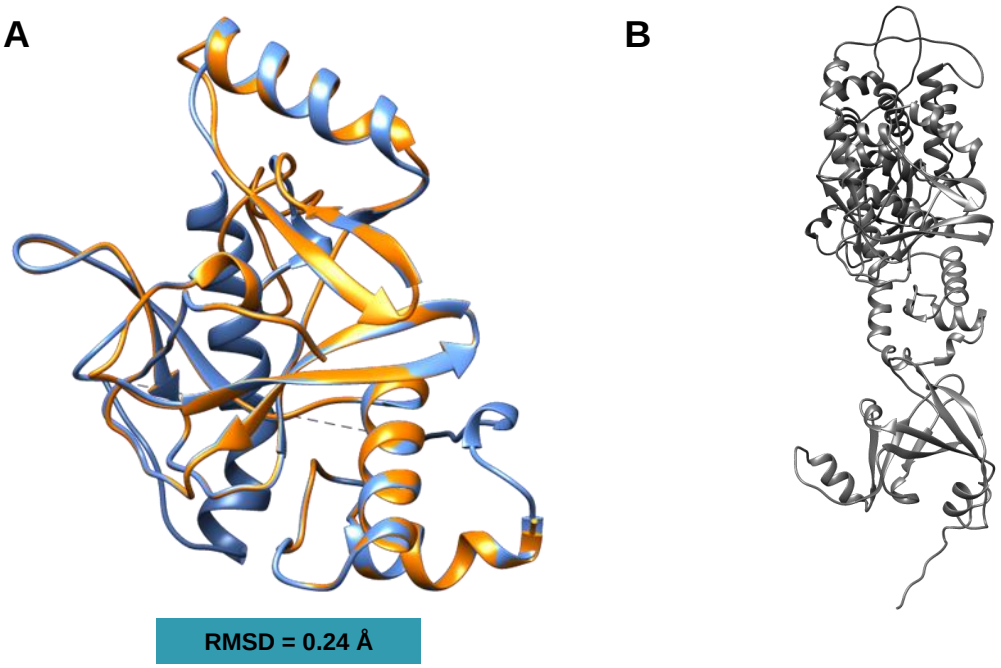

Figure 3.21: Structure of PfSET8. (A) PfSET8 model generated using SwissModel and overlaid on the template, *Cryptosporidium parvum* Iowa II lysine methyltransferase CpSET8. RMSD = 0.24 Å. PfSET8 structure in orange and template structure in blue. **(B)** PfSET8 model obtained from AlphaFold2.

The core active site-containing SET domain (InterPro: IPR001214) was, however, modelled with high confidence, and this model was therefore progressed to molecular docking for exploration of UNC0379 targets. Characteristic of the conserved SET domain is a “pseudo knot” structure surrounded by three discreet anti-parallel β-pleated sheets [119]. This was visible in both of the models generated.

PfSET2 was modelled on *H. sapiens* lysine methyltransferase SETD2 as a template, to which it conformed closely, with a Cα heavy chain RMSD of 0.25 Å for aligned Cα atoms (Fig. 3.22 A). However, an inadequate per-residue score was obtained using homology-based modelling and this model was therefore not progressed to docking. By contrast, the AlphaFold model (Fig. 3.22 B) showed high per-residue confidence, particularly in the active site-containing domain. MolProbity validation of this model revealed favourable intramolecular steric interactions. Ramachandran analysis of peptide backbone dihedral angle distributions showed geometric favourability for 92 % of residues, while 2.23 % of residues were found to be outliers (Fig. S8), indicating poor conformity of the peptide backbone to energetically allowed regions. However, as the core active site-containing SET domain was captured with high confidence, this model was retained for docking evaluation. As for PfSET8, three anti-parallel β-pleated sheets surrounding a pseudo knot structure were observed within the SET domain ((InterPro: IPR001214) in each model.

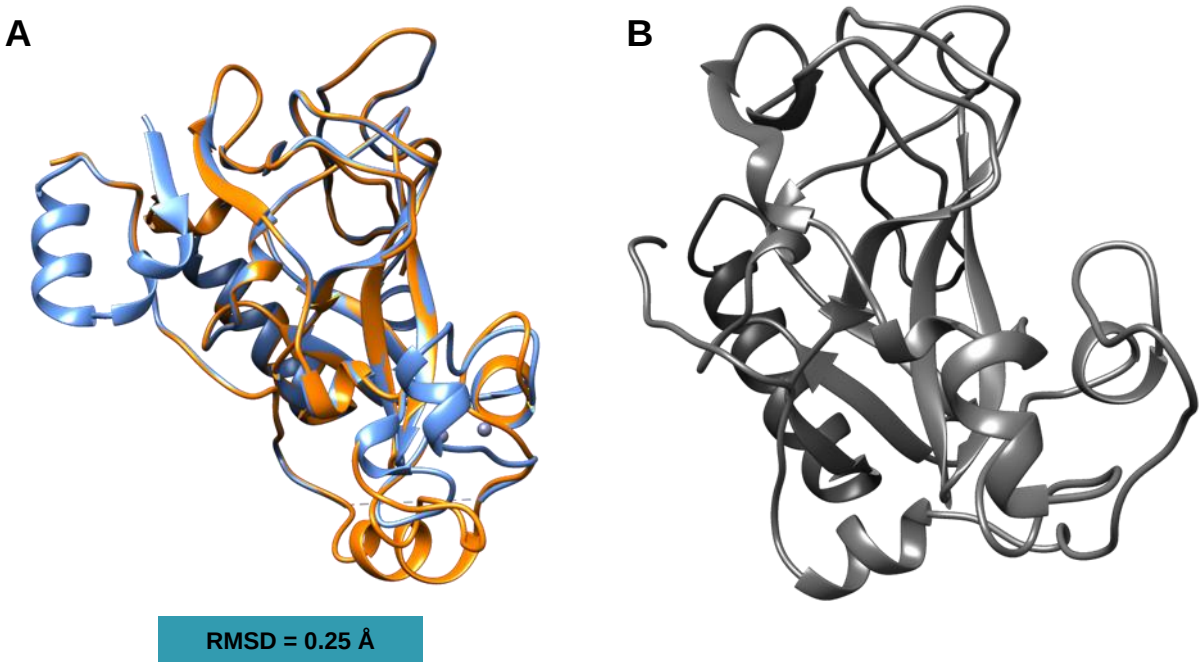

Figure 3.22: Structure of PfSET2. (A) PfSET model generated using SwissModel and overlaid on the template, *H. sapiens* lysine methyltransferase SETD2. RMSD = 0.25 Å. PfSET2 structure in orange and template structure in blue. **(B)** PfSET2 model obtained from AlphaFold2.

3.3.2. Docking of HKMTi to HKMT models for identification of target indicators

UNC0379 was observed in *in silico* molecular docking simulations to intercalate directly into the active site of the SET8 domain with a ΔG of -35.1 kJ.mol^{-1} associated with the strongest binding mode (Fig. 3.23 A and B).

Hydrogen bonds are indicated between UNC0379 and the substrate-coordinating residue E1172, with possible pi stacking between the quinazoline core and the substrate-coordinating residue Y1170, and steric occlusion of numerous other substrate-coordinating residues such as E1075, K1079 and Y1090 and S-adenosylmethionine (SAM) co-substrate-coordinating residues such as F1087 and V1130. This would preclude binding of PfSET8 to its histone tail substrate through obstruction of the histone tail lysine-binding channel, inhibiting its function.

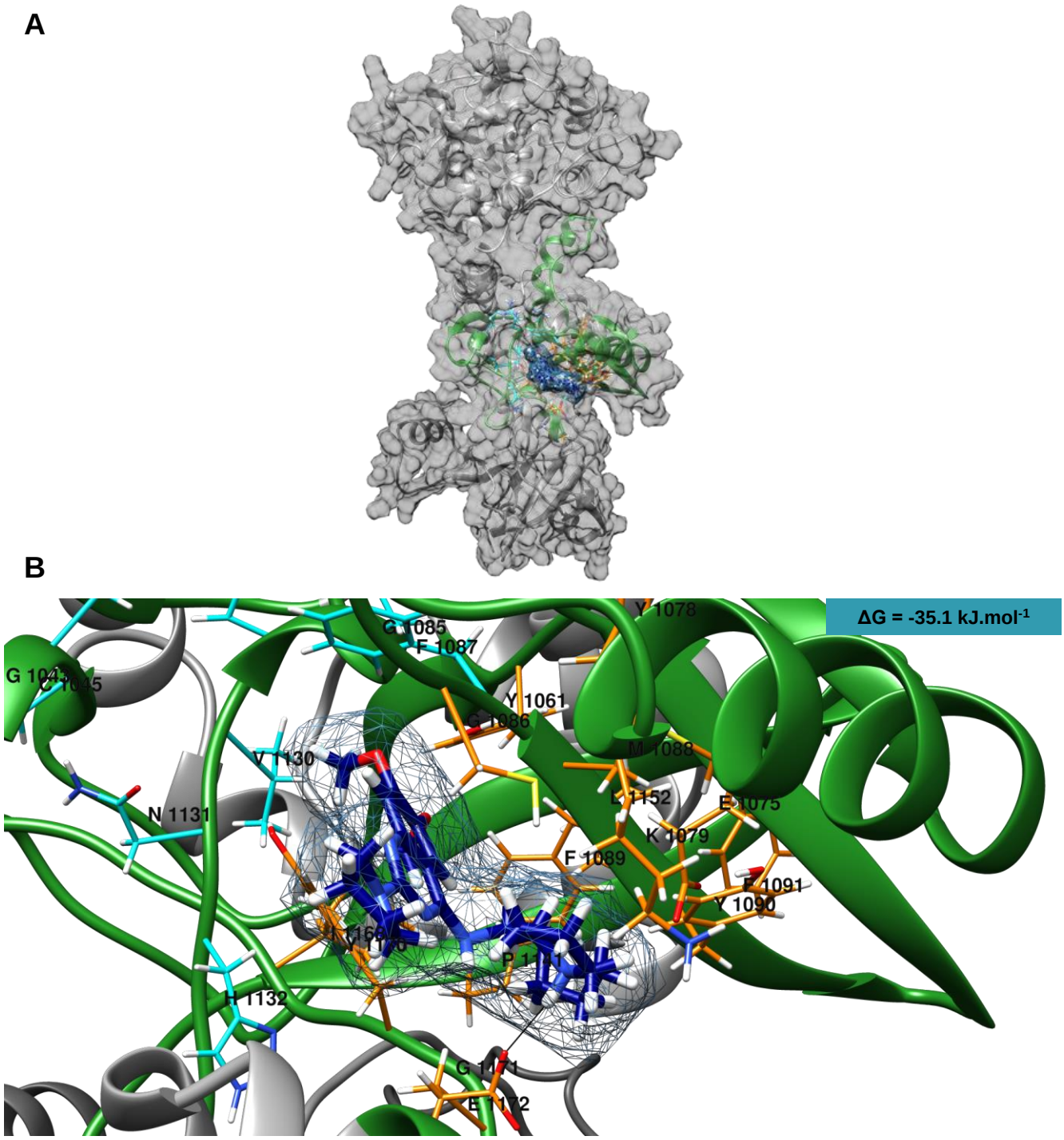

Figure 3.23: Mechanistic evaluation of targeting of PfSET8 by UNC0379. (A) UNC0379-PfSET8 complex. **(B)** Enlarged view of PfSET8 active site with complexed UNC0379 ligand. The SET domain is shown in green with active site residues shown in orange. S-adenosylmethionine co-substrate-coordinating residues are shown in light blue. UNC0379 is shown in dark blue and hydrogen bonds are indicated in black.

UNC0638 was observed to bind directly into the SET domain active site of PfSET2 in the strongest binding mode (Fig.3.24 A and B) with a ΔG of -45.4 kJ.mol^{-1}. A hydrogen bond was observed to form between the substrate-coordinating residue W2177 and UNC0638 in this binding mode, with steric occlusion of numerous other active site residues and SAM co-substrate-coordinating residues (Fig. 3.24 B) including the key catalytic residue Y 2239, conserved in the human methyltransferase G9a [93, 120].

These interactions would prevent binding of PfSET2 to its substrate to effect histone methylation PTM changes, resulting in transcriptional dysregulation.

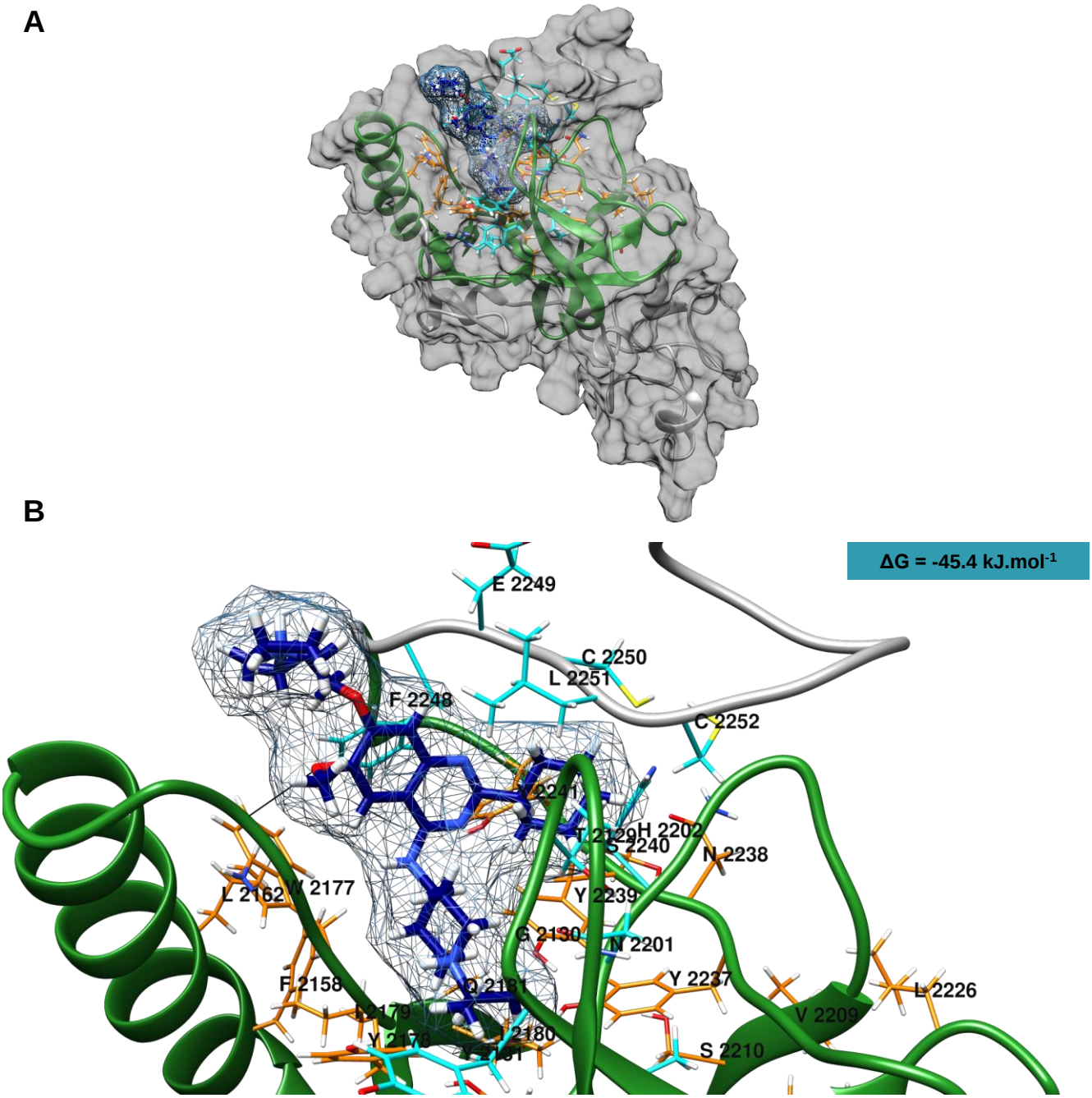

Figure 3.24: Mechanistic evaluation of targeting of PfSET2 by UNC0638. (A) UNC0638-PfSET2 complex. **(B)** Enlarged view of PfSET2 active site with complexed UNC0638 ligand. The SET domain is shown in green with active site residues shown in orange. S-adenosylmethionine co-substrate-coordinating residues are shown in light blue. UNC0638 is shown in dark blue and hydrogen bonds are indicated in black.

3.3.3. Dot-blot analysis of histone tail methylation status resulting from treatment with a selection of HKMTi

Both HKMTi were subsequently evaluated for their potential ability to target SET2 and SET8 by assessing changes in histone methylation levels. H3K9me3 was significantly decreased upon treatment

with both UNC0379 (0.3-times decrease, Fig. 3.25 A, *P* = 0.0268, n = 3) and UNC0638 (0.3-times decrease, Fig. 3.25 B, *P* = 0.0140, n = 3) without associated increases in the H3Core control.

It is therefore evident that these two compounds do perturb histone methylation PTM status and could exert their inhibitory activity against *P. falciparum* through targeting of SET histone methyltransferases, possibly by consequent dysregulation of gene expression.

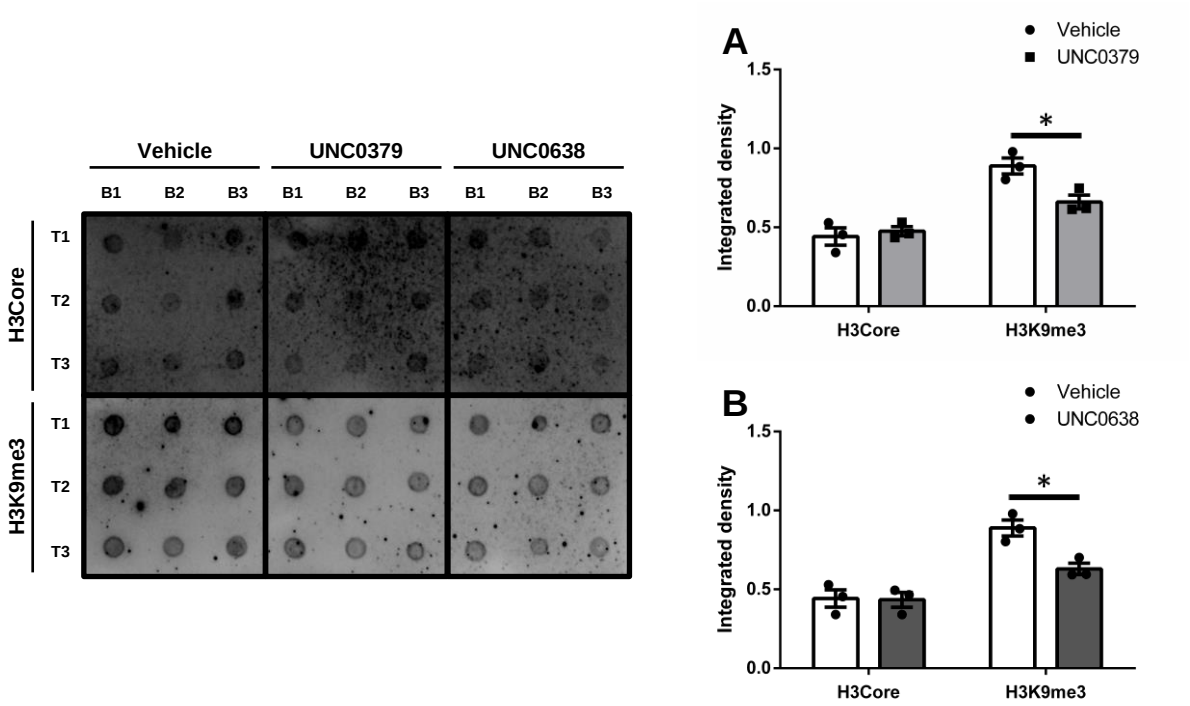

Figure 3.25: Post-translational modification changes in UNC0379 and UNC0638-treated asexual parasites. Dot blots of parasite histone samples and relative histone post-translational modification abundance (α-H3core, α-H3K9me3 and α-H3K9ac) for late-stage gametocytes treated at 5 µM concentrations of **(A)** UNC0379 and **(B)** UNC0638 for 24 h. Data are representative of three independent biological replicates (B1-3) performed in technical triplicate (T1-3), with mean ± S.E. indicated. Unpaired, two-tailed t-test. UNC0379 **P* = 0.0268. UNC0638 **P* = 0.0140

While both UNC0638 and UNC0379 show selectivity towards asexual stages, both compounds also exhibit activity against late-stage gametocytes. To elucidate to what extent this translates to transmission blocking in mosquito stages, SMFAs were performed. UNC0638 reduced oocyst intensity by 90 % (Fig. 3.26 A) and oocyst prevalence by 73 % (Fig. 3.26 C, both significant, *P*<0.0001, n = 3), indicating good transmission blocking capabilities. UNC0379 too showed potent transmission reduction, decreasing oocyst intensity by 87 % (Fig. 3.26 B, *P*<0.0001, n = 3). However, transmission-blocking activity was more modest but significant, reducing oocyst prevalence by 58 % (Fig. 3.26 C, *P* = 0.001). Together these data indicate good transmission blocking by both HKMTi.

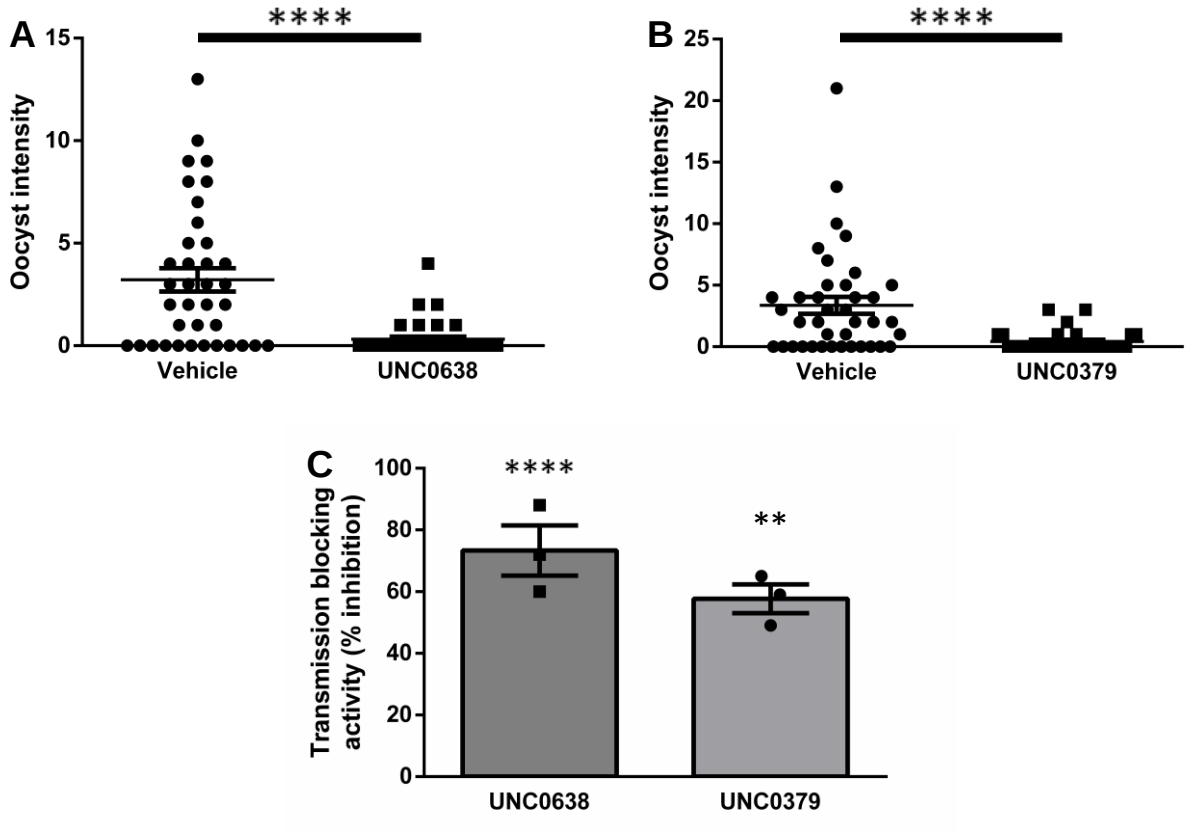

Figure 3.26: Transmission-reducing and transmission-blocking activity of HKMTi against *P. falciparum* parasites. Treatments were performed at 2 µM for 48 h **(A)** Oocyst intensity after UNC0638 treatment as measured by the number of oocysts per mosquito, with mean ± S.E.M indicated. **(B)** Oocyst intensity after UNC0379 treatment. **(C)** Transmission blocking activity as a percentage decrease in the number of mosquitoes containing oocysts. Data are representative of three indpendent biological repeats performed in technical duplicate, with mean ± S.E. indicated. **** *P*<0.0001, Mann-Whitney non-parametric t-test.

Chapter 4: Discussion

The increasingly urgent threat of drug resistance in malaria parasites necessitates bringing transmission-blocking drugs to clinical use with the aim of achieving malaria elimination, and the development of drugs targeting relevant parasite biology is of utmost importance. The parasite epigenome has proven to be an important regulator of gene expression, and thus of progression through the complex parasite life cycle [56, 121], and has presented a feasible target of chemotherapeutics both in *P. falciparum* [77, 78] and in Apicomplexan parasites at large [95, 122].

In this dissertation, epigenetic inhibitors that have previously shown activity in human cell lines were investigated for target indicators and MoA in *P. falciparum*. The activity of epidrugs in human cancers has been well characterised, with a number of compounds, for example Vorinostat, having progressed to clinical use [123]. Epigenetic regulation has also been substantively validated as a targetable biology in *P. falciparum*, with some, such as BIX-012944 and JIB-04, having progressed in the drug discovery pipeline [79, 80]. A number of these compounds show favourable pharmacokinetic profiles [124]. Epigenetic inhibitors have also been investigated in other Apicomplexans and have demonstrated an epigenetic MoA [95]

This dissertation presents the use of complimentary experimental and *in silico* approaches to confirm perturbation of epigenetic regulation. Favourable indicators of transmission blocking were ascertained for several of these compounds, emphasising their potential in meeting targets for new chemotherapeutics against malaria and contributing to the elimination of this disease [48, 49]. Although convincing docking modes were observed for the compounds under investigation, limitations to the modelling and docking approach exist. For example, crystallisation conditions, both for crystal structures used directly for docking and for structures used as templates for homology modelling, may not correspond to *in vivo* conditions [125]. In addition, protein flexibility within the active site is a factor, which may have implications for binding modes yielded by molecular docking simulations. While this may reflect in inaccurate determination of the exact binding pose of the docked ligand, value still exists in the use of molecular modelling to explore potential drug targets [126]. To further examine the MoA of these compounds, mechanistic evaluation is essential. While it is possible to heterologously express proteins and assay directly for inhibition, this has certain drawbacks, especially as it pertains to *P. falciparum* proteins. Proteins from this parasite have proven exceedingly difficult to purify, due, for example, to a disproportionately high rate of inclusion body formation in expression systems [127]. In addition, value exists in evaluating *in situ* epigenetic perturbation consequent to inhibition of these epigenetic effectors. These factors therefore support the use of immunoblotting to evaluate these changes.

Due to the semi-quantitative nature of immunoblotting, sensitivity issues may arise in evaluating PTM changes consequent to epigenetic effector inhibition. Alternative approaches for the evaluation of histone tail PTM changes with a higher sensitivity include enzyme-linked immunosorbent assays (ELISA) and liquid chromatography-mass spectrometry (LC-MS) [128, 129]. However, biological

repeats and stringent analyses and statistical validations were included in this study to support conclusions made.

One of the HDACi evaluated, Scriptaid, was observed to perturb H3K9ac in asexual parasites, with *in silico* indications that this is mediated by specific inhibition of PfHDAC1. In support of PfHDAC1 as the target of Scriptaid, Mukherjee *et al.* [115] investigated *in silico* docking of HDACi to PfHDAC1, wherein numerous coordinating residues were observed in common with those found in the present study. PfHDAC1 shows favourable indications as a targetable protein, with other specific inhibitors of this epigenetic effector having been observed, including Quisinostat which, like Scriptaid, shows dual stage activity [130], the multi-stage inhibitor JX21108 [131] and a number of amino acid derivatives [132].

While an epigenetic MoA for Scriptaid against asexual stages was confirmed, this did not translate to late-stage gametocytes. This indicates that the MoA in late-stage gametocytes may differ from that in asexual stages, supported by an observed decrease in *pfhdac1* transcript abundance in late-stage gametocytes [55] and a lower sensitivity to this compound in these stages. It is conceivable, however, that the sensitivity of immunoblot analysis is such that changes in histone tail acetylation status were not captured in gametocytes, and it may therefore be prudent to explore histone tail PTM changes with more sensitive approaches. Further, male gamete exflagellation assays and SMFAs confirmed potent transmission-blocking activity by this compound, a valuable attribute towards malaria elimination goals. However, as evidenced by the observed paucity of acetylation changes in late-stage gametocytes, this too may be mediated by an MoA other than HDAC inhibition. The observation that acetylation changes are seen in asexuals but not in late-stage gametocytes may be a consequence of the respective importance of the H3K9ac PTM in these stages. This is supported by the general euchromatic permissiveness characterising asexual parasite stages, associated with high H3K9ac occupancy in active gene promotors, and the overall higher abundance of H3K9ac in these stages, compared to the heterochromatic status observed in gametocytes, associated with, for example the silencing H3K9me3 mark [68, 69] (Fig. 1.5).

These findings corroborate the hypothesis that the activity seen by Scriptaid in previous reports [87] against asexual stages is, as in human cell lines, consequent to histone deacetylase inhibition. It is evident, therefore, that this compound may induce transcriptional dysregulation in asexual parasites, leading to the observed parasite death phenotype, with *in silico* evidence to support that this is mediated by inhibition of PfHDAC1. In previous studies evaluating inhibitors of PfHDAC1, a potent blockade in asexual stage progression was discovered [132]. It is predicted that the same may be true for Scriptaid and this will be explored in future studies. This, in combination with the potent transmission-blocking activity observed upon Scriptaid treatment, highlight the potential of this compound as an antiproliferative and transmission-blocking chemotherapeutic. However, as poor selectivity over human cells is exhibited by this compound [77], a derivatisation strategy is indicated for selectivity improvement, which will allow for an expansion of the footprint of PfHDAC1-targeting compounds.

While immunoblot analyses showed changes to histone acetylation in asexual stages upon treatment with Sirtinol, this was not true in late-stage gametocytes. As for Scriptaid, this may be a matter of the sensitivity associated with immunoblot analysis. Despite these acetylation status changes in asexual parasites, Sirtinol exhibits poor inhibition of these stages [77]. This is not unexpected as, while PfSir2A is implicated in transcriptional silencing of *var* genes in asexual stages, such perturbation is not expected to be lethal *in vitro* due to the role of this protein in cytoadherence and immune evasion through antigenic variation [133, 134]. In addition, PfSir2A has proven to be dispensable in asexual stages *in vitro*. It has, however, been postulated that targeting of PfSir2A may still result in therapeutic effect in clinical use due to targeting of cytoadhesion and diminishing the ability of the parasite to evade the host immune system by disruption of *var* gene regulation [135, 136].

Sir2A inhibitors have previously been described as having poor antiparasitic activity against asexual stages [136], correlating to observations of Sirtinol activity [77]. However, the present study showed potent transmission blocking using SMFAs. This was observed in the face of poor inhibition of male gamete formation, identified through exflagellation inhibition assays, indicating a possible female-specific activity. It has previously been reported that male gametocytes are more susceptible to drug inhibition. These observations therefore present an interesting deviation from the norm and necessitate further examination of the activity of Sirtinol against female late-stage gametocytes, for example through female gametocyte activation assays [84]. Intriguingly, these observations may allude to the possible importance of Sir2A in the regulation of genes involved in female gametogenesis, supported by the observed increase in abundance of *sir2a* transcript levels in stage V gametocytes [55]. Sirtinol, on the basis of its potent transmission-blocking ability and strong parasite selectivity over human cells [77], is therefore indicated for progression in drug development efforts as a transmission-blocking antimalarial.

Present studies revealed that ML324 is likely to specifically target PfJmj3, with no valid binding modes observed for either of the other Jmj domain-containing proteins identified within the *P. falciparum* proteome. ML324 was also previously revealed to confer potent transmission blocking, greatly decreasing both male exflagellation and oocyst intensity [78]. While ML324 does not appear to have activity against asexual stages *in vitro*, microarray analyses revealed perturbation of genes related to cytoadhesion and pathogenesis, and, like Sirtinol, may therefore exhibit *in vivo* therapeutic activity. ML324 has been shown to chelate the Fe^{2+} cofactor in target active sites through the phenolic group and imine nitrogen [91]. However, iron loading experiments (Reader, unpublished) have revealed no change in IC_{50}, indicating that the inhibition of PfJmj3 is specific and not consequent to chelation of the Fe^{2+} cofactor. Future studies will also attempt to empirically prove this target. ML324 does not appear to have activity against asexual stages, thus precluding *in vitro* resistance selection and next-generation sequencing as a means of target identification [137]. Therefore, alternative means of target identification are necessitated, such as conditional knockdown studies to evaluate consequent epigenetic perturbations and correlate these with changes resulting from chemical inhibition with ML324. While this compound has favourable inhibitory indicators, pharmacological parameters are also an important consideration. Favouring this compound over other inhibitors of Jmj domain-containing proteins, ML324

shows superior cell permeability, in addition to favourable pharmacological characteristics, such as plasma and microsomal stability, with a proven amenability to chemical derivatisation [91]. This supports progression of this compound through the drug discovery pipeline and the employment of a derivatisation strategy for improvement of selectivity. This will allow the development of this scaffold as a possible transmission-blocking drug exploiting a unique biology.

UNC0638 is an inhibitor of G9a in human cancer cells [93, 94]. Molecular docking revealed potential binding of this compound to the most likely homologue of this protein in *P. falciparum* parasites, PfSET2. Further validating the targeting of SET domain-containing proteins, the G9a inhibitor BIX01294 was shown by Ngwa *et al.* to inhibit asexual parasite stages as well as male exflagellation and zygote formation. It would thereby diminish transmission [79], in common with UNC0638, which demonstrated potent inhibition of male gamete formation [77]. In the present study, SMFAs confirmed this good transmission blocking ability by UNC0638. In addition, BIX01294 and UNC0638 have been shown to occupy similar binding poses in G9a [93], and it is surmised that the same may be true in the *P. falciparum* homologue PfSET2. Supporting an epigenetic MoA of this compound in asexual parasites, immunoblotting revealed a significant decrease in histone tail methylation in UNC0638-treated parasites.

To more precisely characterise the epigenetic perturbation consequent to treatment by these HKMTi, subsequent studies may focus on evaluation of specific histone PTMs known to be effected by their putative targets. For example, PfSET8, the putative target of UNC0379, is known to mono-, di- and trimethylate H3K20 [117], and future studies will assess changes to these PTMs. Likewise, UNC0379, predicted to target PfSET2, would be expected to alter di- and trimethylation of H3K36 and evaluation of these changes is therefore indicated.

While efforts presented in this dissertation have revealed strong indicators of compound MoA and specific targets, further target deconvolution efforts are required for conclusive target identification. This may be achieved, for example, through affinity chromatography [138] or drug affinity responsive target stability (DARTS). DARTS, which exploits the stability of a target against protease degradation upon compound binding, thereby allowing negative selection of the compound target, has benefits over a strategy such as affinity chromatography, as it does not require chemical derivatisation of the compound, which is both complex and may alter drug activity and disrupt the compound pharmacophore, and is independent of mechanism of action associated with the compound [139]. This, in addition to techniques described above, may allow empirical identification of compound targets.

While each of the compounds selected have previously demonstrated some level of activity against human cell lines, some, for example Sirtinol, show major selectivity for the parasite [77]. Where this is not the case, derivatisation of these compounds may improve selectivity. Subsequent efforts will also endeavour to conclusively identify the targets of these proteins using the abovementioned techniques. In addition, the observed PTM changes will be linked to perturbation of gene expression using microarray analysis of gene transcript levels or RNA-seq in treated parasite populations, as well as

evaluating changes to other relevant PTMs. The importance of arginine methylation as a means of effecting epigenetic control is also becoming increasingly apparent, and evaluation of these PTMs and inhibitors of their effector proteins is therefore a priority.

These findings provide substantial support for the hypothesised epigenetic MoA of the investigated epidrugs in *P. falciparum* parasites and have demonstrated potential targets of these compounds. This work has the potential to substantially increase the footprint of epigenetic compounds in the drug discovery pipeline, thereby furthering efforts to exploit this novel targetable biology. These data also serve as a firm foundation for further target deconvolution studies. The compounds explored in this dissertation constitute a number of potential scaffolds for future drug development efforts, with potential for addressing the pressing need for transmission-blocking drugs and contributing to advancement towards the grander aim of malaria elimination.

Chapter 5: Conclusion

Malaria, as one of the most severe diseases afflicting humankind due to the devastating health and socioeconomic burdens it imparts on those who suffer it, necessitates extreme measures to mitigate its effects. Because of the high level of complexity presented by the causative organism, parasites of the genus *Plasmodium*, and the rapidity with which the organism develops resistance, a continuous drug development pipeline is essential.

While great strides have been made towards malaria elimination in many countries, and eradication in general, there is a long path ahead to reach this ultimate goal. Various strategies are employed to achieve malaria control and elimination and may include vector control, surveillance and chemotherapeutic approaches. Historically, the focus on the development of chemotherapeutics has been the targeting of asexual stages of the parasite, as these are the clinically relevant, symptom-causing stages, but more recently there has been a move towards investigating the targeting of the transmissible stages. This may aid progress towards malaria elimination in multiple ways; most importantly, this would go some way towards directly decreasing transmission. Additionally, the propensity for the parasite to develop resistance may be somewhat mitigated as a result of preventing resistant parasite populations from being transmitted.

The use of epigenetic compounds has been investigated for numerous diseases. These were initially screened for use against human cancers, as such compounds are able to disrupt the transcriptional profile of rapidly proliferating cells, thus selectively targeting cancer cells, with some, such as Vorinostat, already approved for clinical use. Such novel chemotypes and drug targets are of great importance to address the development of drug resistance.

Given the *in silico* and mechanistic validation of putative targets of the investigated epidrugs, this body of work presents an advancement of our understanding of the MoA of these compounds in *P. falciparum* parasites and the role that epidrugs may play in addressing the increasingly pressing matter of the development of resistance in this disease. Further, favourable transmission-blocking profiles are revealed by several epidrugs with diverse epigenetic modifier targets, constituting groundwork upon which subsequent studies may build and contributing towards our knowledge base as pertains to targetable parasite biology.

References

1 World Health Organization. (2020) World malaria report 2020: 20 years of global progress and challenges.
2 Teklehaimanot and Paola Mejia, A. (2008) Malaria and poverty. Annals of the New York Academy of Sciences. **1136**, 32-37
3 Blasco, B., Leroy, D. and Fidock, D. A. (2017) Antimalarial drug resistance: linking *Plasmodium falciparum* parasite biology to the clinic. Nature medicine. **23**, 917
4 Howes, R. E., Battle, K. E., Mendis, K. N., Smith, D. L., Cibulskis, R. E., Baird, J. K. and Hay, S. I. (2016) Global epidemiology of *Plasmodium vivax*. The American journal of tropical medicine and hygiene. **95**, 15-34
5 Cowman, A. F., Healer, J., Marapana, D. and Marsh, K. (2016) Malaria: biology and disease. Cell. **167**, 610-624
6 Antinori, S., Galimberti, L., Milazzo, L. and Corbellino, M. (2013) *Plasmodium knowlesi*: the emerging zoonotic malaria parasite. Acta tropica. **125**, 191-201
7 Arisue, N. and Hashimoto, T. (2015) Phylogeny and evolution of apicoplasts and apicomplexan parasites. Parasitology international. **64**, 254-259
8 World Health Organization. (2019) World malaria report 2019.
9 Trampuz, A., Jereb, M., Muzlovic, I. and Prabhu, R. M. (2003) Clinical review: Severe malaria. Critical care. **7**, 315
10 Takken, W., Smallegange, R. C., Vigneau, A. J., Johnston, V., Brown, M., Mordue-Luntz, A. J. and Billingsley, P. F. (2013) Larval nutrition differentially affects adult fitness and *Plasmodium* development in the malaria vectors *Anopheles gambiae* and *Anopheles stephensi*. Parasites & vectors. **6**, 345
11 Gupta, A. P., Chin, W. H., Zhu, L., Mok, S., Luah, Y.-H., Lim, E.-H. and Bozdech, Z. (2013) Dynamic epigenetic regulation of gene expression during the life cycle of malaria parasite *Plasmodium falciparum*. PLoS pathogens. **9**, e1003170
12 Rosenberg, R., Wirtz, R. A., Schneider, I. and Burge, R. (1990) An estimation of the number of malaria sporozoites ejected by a feeding mosquito. Transactions of the Royal Society of Tropical Medicine and Hygiene. **84**, 209-212
13 Tavares, J., Formaglio, P., Thiberge, S., Mordelet, E., Van Rooijen, N., Medvinsky, A., Ménard, R. and Amino, R. (2013) Role of host cell traversal by the malaria sporozoite during liver infection. Journal of experimental medicine. **210**, 905-915
14 Sturm, A., Amino, R., Van de Sand, C., Regen, T., Retzlaff, S., Rennenberg, A., Krueger, A., Pollok, J.-M., Menard, R. and Heussler, V. T. (2006) Manipulation of host hepatocytes by the malaria parasite for delivery into liver sinusoids. science. **313**, 1287-1290
15 Wright, G. J. and Rayner, J. C. (2014) *Plasmodium falciparum* erythrocyte invasion: combining function with immune evasion. PLoS pathogens. **10**, e1003943
16 Weiss, G. E., Gilson, P. R., Taechalertpaisarn, T., Tham, W.-H., de Jong, N. W., Harvey, K. L., Fowkes, F. J., Barlow, P. N., Rayner, J. C. and Wright, G. J. (2015) Revealing the sequence and resulting cellular morphology of receptor-ligand interactions during *Plasmodium falciparum* invasion of erythrocytes. PLoS pathogens. **11**, e1004670
17 Gilson, P. R. and Crabb, B. S. (2009) Morphology and kinetics of the three distinct phases of red blood cell invasion by *Plasmodium falciparum* merozoites. International journal for parasitology. **39**, 91-96
18 Chugh, M., Sundararaman, V., Kumar, S., Reddy, V. S., Siddiqui, W. A., Stuart, K. D. and Malhotra, P. (2013) Protein complex directs hemoglobin-to-hemozoin formation in *Plasmodium falciparum*. Proceedings of the National Academy of Sciences. **110**, 5392-5397
19 Salmon, B. L., Oksman, A. and Goldberg, D. E. (2001) Malaria parasite exit from the host erythrocyte: a two-step process requiring extraerythrocytic proteolysis. Proceedings of the National Academy of Sciences. **98**, 271-276
20 Arnot, D. and Gull, K. (1998) The *Plasmodium* cell-cycle: facts and questions. Annals of Tropical Medicine & Parasitology. **92**, 361-365

21 Arnot, D. E., Ronander, E. and Bengtsson, D. C. (2011) The progression of the intra-erythrocytic cell cycle of *Plasmodium falciparum* and the role of the centriolar plaques in asynchronous mitotic division during schizogony. International journal for parasitology. **41**, 71-80
22 Josling, G. A. and Llinas, M. (2015) Sexual development in *Plasmodium* parasites: knowing when it's time to commit. Nature Reviews Microbiology. **13**, 573
23 Talman, A. M., Domarle, O., McKenzie, F. E., Ariey, F. and Robert, V. (2004) Gametocytogenesis: the puberty of *Plasmodium falciparum*. Malaria journal. **3**, 24
24 Aguilar, R., Magallon-Tejada, A., Achtman, A. H., Moraleda, C., Joice, R., Cisteró, P., Suen, C. S. L. W., Nhabomba, A., Macete, E. and Mueller, I. (2014) Molecular evidence for the localization of *Plasmodium falciparum* immature gametocytes in bone marrow. Blood. **123**, 959-966
25 Nacher, M. (2004) Does the shape of *Plasmodium falciparum* gametocytes have a function? Medical hypotheses. **62**, 618-619
26 Billker, O., Lindo, V., Panico, M., Etienne, A., Paxton, T., Dell, A., Rogers, M., Sinden, R. and Morris, H. (1998) Identification of xanthurenic acid as the putative inducer of malaria development in the mosquito. Nature. **392**, 289
27 Babiker, H., Ranford-Cartwright, L. C., Currie, D., Charlwood, J., Billingsley, P., Teuscher, T. and Walliker, D. (1994) Random mating in a natural population of the malaria parasite *Plasmodium falciparum*. Parasitology. **109**, 413-421
28 Alano, P. (2007) *Plasmodium falciparum* gametocytes: still many secrets of a hidden life. Molecular microbiology. **66**, 291-302
29 Dorin-Semblat, D., Sicard, A., Doerig, C., Ranford-Cartwright, L. and Doerig, C. (2008) Disruption of the PfPK7 gene impairs schizogony and sporogony in the human malaria parasite *Plasmodium falciparum*. Eukaryotic cell. **7**, 279-285
30 Balaji, S., Babu, M. M., Iyer, L. M. and Aravind, L. (2005) Discovery of the principal specific transcription factors of Apicomplexa and their implication for the evolution of the AP2-integrase DNA binding domains. Nucleic acids research. **33**, 3994-4006
31 Painter, H. J., Campbell, T. L. and Llinás, M. (2011) The Apicomplexan AP2 family: integral factors regulating *Plasmodium* development. Molecular and biochemical parasitology. **176**, 1-7
32 Lim, S. S., Fullman, N., Stokes, A., Ravishankar, N., Masiye, F., Murray, C. J. and Gakidou, E. (2011) Net benefits: a multicountry analysis of observational data examining associations between insecticide-treated mosquito nets and health outcomes. PLoS medicine. **8**, e1001091
33 Toé, K. H., Jones, C. M., N'Fale, S., Ismail, H. M., Dabiré, R. K. and Ranson, H. (2014) Increased pyrethroid resistance in malaria vectors and decreased bed net effectiveness, Burkina Faso. Emerging infectious diseases. **20**, 1691
34 World Health Organization. (2018) Global report on insecticide resistance in malaria vectors: 2010–2016.
35 Moody, A. and Chiodini, P. (2000) Methods for the detection of blood parasites. Clinical & Laboratory Haematology. **22**, 189-201
36 Murray, C. K., Gasser, R. A., Magill, A. J. and Miller, R. S. (2008) Update on rapid diagnostic testing for malaria. Clinical microbiology reviews. **21**, 97-110
37 World Health Organization. (2015) Guidelines for the treatment of malaria. World Health Organization
38 Dobaño, C., Sanz, H., Sorgho, H., Dosoo, D., Mpina, M., Ubillos, I., Aguilar, R., Ford, T., Díez-Padrisa, N. and Williams, N. A. (2019) Concentration and avidity of antibodies to different circumsporozoite epitopes correlate with RTS, S/AS01E malaria vaccine efficacy. Nature communications. **10**, 1-13
39 Penny, M. A., Verity, R., Bever, C. A., Sauboin, C., Galactionova, K., Flasche, S., White, M. T., Wenger, E. A., Van de Velde, N. and Pemberton-Ross, P. (2016) Public health impact

and cost-effectiveness of the RTS, S/AS01 malaria vaccine: a systematic comparison of predictions from four mathematical models. The Lancet. **387**, 367-375
40 Datoo, M. S., Natama, M. H., Somé, A., Traoré, O., Rouamba, T., Bellamy, D., Yameogo, P., Valia, D., Tegneri, M. and Ouedraogo, F. (2021) Efficacy of a low-dose candidate malaria vaccine, R21 in adjuvant Matrix-M, with seasonal administration to children in Burkina Faso: a randomised controlled trial. The Lancet. **397**, 1809-1818
41 Lyke, K. E., Ishizuka, A. S., Berry, A. A., Chakravarty, S., DeZure, A., Enama, M. E., James, E. R., Billingsley, P. F., Gunasekera, A. and Manoj, A. (2017) Attenuated PfSPZ Vaccine induces strain-transcending T cells and durable protection against heterologous controlled human malaria infection. Proceedings of the National Academy of Sciences. **114**, 2711-2716
42 Draper, S. J., Sack, B. K., King, C. R., Nielsen, C. M., Rayner, J. C., Higgins, M. K., Long, C. A. and Seder, R. A. (2018) Malaria vaccines: recent advances and new horizons. Cell host & microbe. **24**, 43-56
43 Packard, R. M. (2014) The origins of antimalarial-drug resistance. New England Journal of Medicine. **371**, 397-399
44 Bray, P. G., Martin, R. E., Tilley, L., Ward, S. A., Kirk, K. and Fidock, D. A. (2005) Defining the role of PfCRT in *Plasmodium falciparum* chloroquine resistance. Molecular microbiology. **56**, 323-333
45 Dondorp, A. M., Nosten, F., Yi, P., Das, D., Phyo, A. P., Tarning, J., Lwin, K. M., Ariey, F., Hanpithakpong, W. and Lee, S. J. (2009) Artemisinin resistance in *Plasmodium falciparum* malaria. New England Journal of Medicine. **361**, 455-467
46 Dondorp, A. M., Fairhurst, R. M., Slutsker, L., MacArthur, J. R., Guerin, P. J., Wellems, T. E., Ringwald, P., Newman, R. D. and Plowe, C. V. (2011) The threat of artemisinin-resistant malaria. New England Journal of Medicine. **365**, 1073-1075
47 Balikagala, B., Fukuda, N., Ikeda, M., Katuro, O. T., Tachibana, S.-I., Yamauchi, M., Opio, W., Emoto, S., Anywar, D. A., Kimura, E., Palacpac, N. M. Q., Odongo-Aginya, E. I., Ogwang, M., Horii, T. and Mita, T. (2021) Evidence of Artemisinin-Resistant Malaria in Africa. New England Journal of Medicine. **385**, 1163-1171
48 Burrows, J. N., van Huijsduijnen, R. H., Möhrle, J. J., Oeuvray, C. and Wells, T. N. (2013) Designing the next generation of medicines for malaria control and eradication. Malaria journal. **12**, 187
49 Burrows, J. N., Duparc, S., Gutteridge, W. E., van Huijsduijnen, R. H., Kaszubska, W., Macintyre, F., Mazzuri, S., Möhrle, J. J. and Wells, T. N. (2017) New developments in anti-malarial target candidate and product profiles. Malaria journal. **16**, 26
50 Guiguemde, W. A., Shelat, A. A., Garcia-Bustos, J. F., Diagana, T. T., Gamo, F.-J. and Guy, R. K. (2012) Global phenotypic screening for antimalarials. Chemistry & biology. **19**, 116-129
51 Salcedo-Amaya, A. M., Hoeijmakers, W. A., Bártfai, R. and Stunnenberg, H. G. (2010) Malaria: could its unusual epigenome be the weak spot? The international journal of biochemistry & cell biology. **42**, 781-784
52 Adjalley, S. H., Johnston, G. L., Li, T., Eastman, R. T., Ekland, E. H., Eappen, A. G., Richman, A., Sim, B. K. L., Lee, M. C. and Hoffman, S. L. (2011) Quantitative assessment of *Plasmodium falciparum* sexual development reveals potent transmission-blocking activity by methylene blue. Proceedings of the National Academy of Sciences. **108**, E1214-E1223
53 Horrocks, P., Wong, E., Russell, K. and Emes, R. D. (2009) Control of gene expression in *Plasmodium falciparum*–ten years on. Molecular and biochemical parasitology. **164**, 9-25
54 Bozdech, Z., Llinás, M., Pulliam, B. L., Wong, E. D., Zhu, J. and DeRisi, J. L. (2003) The transcriptome of the intraerythrocytic developmental cycle of *Plasmodium falciparum*. PLoS biology. **1**, e5
55 Van Biljon, R., Van Wyk, R., Painter, H. J., Orchard, L., Reader, J., Niemand, J., Llinás, M. and Birkholtz, L.-M. (2019) Hierarchical transcriptional control regulates *Plasmodium falciparum* sexual differentiation. BMC genomics. **20**, 1-16

56 Duffy, M. F., Selvarajah, S. A., Josling, G. A. and Petter, M. (2012) The role of chromatin in *Plasmodium* gene expression. Cellular microbiology. **14**, 819-828
57 Lyko, F. (2018) The DNA methyltransferase family: a versatile toolkit for epigenetic regulation. Nature Reviews Genetics. **19**, 81-92
58 Miao, J., Fan, Q., Cui, L., Li, J., Li, J. and Cui, L. (2006) The malaria parasite *Plasmodium falciparum* histones: organization, expression, and acetylation. Gene. **369**, 53-65
59 Cosgrove, M. S. and Wolberger, C. (2005) How does the histone code work? Biochemistry and Cell Biology. **83**, 468-476
60 Grewal, S. I. and Moazed, D. (2003) Heterochromatin and epigenetic control of gene expression. science. **301**, 798-802
61 Cui, L. and Miao, J. (2010) Chromatin-mediated epigenetic regulation in the malaria parasite *Plasmodium falciparum*. Eukaryotic cell. **9**, 1138-1149
62 Treviño, L. S., Wang, Q. and Walker, C. L. (2015) Phosphorylation of epigenetic “readers, writers and erasers”: implications for developmental reprogramming and the epigenetic basis for health and disease. Progress in biophysics and molecular biology. **118**, 8-13
63 Grunstein, M. (1997) Histone acetylation in chromatin structure and transcription. Nature. **389**, 349-352
64 Dastidar, E. G., Dzeyk, K., Krijgsveld, J., Malmquist, N. A., Doerig, C., Scherf, A. and Lopez-Rubio, J.-J. (2013) Comprehensive histone phosphorylation analysis and identification of Pf14-3-3 protein as a histone H3 phosphorylation reader in malaria parasites. PloS one. **8**, e53179
65 Fan, Q., Miao, J., Cui, L. and Cui, L. (2009) Characterization of PRMT1 from *Plasmodium falciparum*. Biochemical Journal. **421**, 107-118
66 Trelle, M. B., Salcedo-Amaya, A. M., Cohen, A. M., Stunnenberg, H. G. and Jensen, O. N. (2009) Global histone analysis by mass spectrometry reveals a high content of acetylated lysine residues in the malaria parasite *Plasmodium falciparum*. Journal of proteome research. **8**, 3439-3450
67 Issar, N., Roux, E., Mattei, D. and Scherf, A. (2008) Identification of a novel post-translational modification in *Plasmodium falciparum*: protein sumoylation in different cellular compartments. Cellular microbiology. **10**, 1999-2011
68 Coetzee, N., Sidoli, S., Van Biljon, R., Painter, H., Llinás, M., Garcia, B. A. and Birkholtz, L.-M. (2017) Quantitative chromatin proteomics reveals a dynamic histone post-translational modification landscape that defines asexual and sexual *Plasmodium falciparum* parasites. Scientific reports. **7**, 607
69 Cui, L., Miao, J., Furuya, T., Li, X., Su, X.-z. and Cui, L. (2007) PfGCN5-mediated histone H3 acetylation plays a key role in gene expression in *Plasmodium falciparum*. Eukaryotic cell. **6**, 1219-1227
70 Lopez-Rubio, J. J., Gontijo, A. M., Nunes, M. C., Issar, N., Hernandez Rivas, R. and Scherf, A. (2007) 5′ flanking region of var genes nucleate histone modification patterns linked to phenotypic inheritance of virulence traits in malaria parasites. Molecular microbiology. **66**, 1296-1305
71 Kafsack, B. F., Rovira-Graells, N., Clark, T. G., Bancells, C., Crowley, V. M., Campino, S. G., Williams, A. E., Drought, L. G., Kwiatkowski, D. P. and Baker, D. A. (2014) A transcriptional switch underlies commitment to sexual development in malaria parasites. Nature. **507**, 248-252
72 Connacher, J., Josling, G. A., Orchard, L. M., Reader, J., Llinás, M. and Birkholtz, L.-M. (2021) H3K36 methylation reprograms gene expression to drive early gametocyte development in *Plasmodium falciparum*. Epigenetics & chromatin. **14**, 1-15
73 Heerboth, S., Lapinska, K., Snyder, N., Leary, M., Rollinson, S. and Sarkar, S. (2014) Use of epigenetic drugs in disease: an overview. Genetics & epigenetics. **6**, GEG. S12270
74 Yoo, C. B. and Jones, P. A. (2006) Epigenetic therapy of cancer: past, present and future. Nature reviews Drug discovery. **5**, 37

75 Andrews, K. T., Fisher, G. and Skinner-Adams, T. S. (2014) Drug repurposing and human parasitic protozoan diseases. International Journal for Parasitology: Drugs and Drug Resistance. **4**, 95-111
76 Engel, J. A., Jones, A. J., Avery, V. M., Sumanadasa, S. D., Ng, S. S., Fairlie, D. P., Adams, T. S. and Andrews, K. T. (2015) Profiling the anti-protozoal activity of anti-cancer HDAC inhibitors against *Plasmodium* and *Trypanosoma* parasites. International Journal for Parasitology: Drugs and Drug Resistance. **5**, 117-126
77 Coetzee, N., von Grüning, H., Opperman, D., van der Watt, M., Reader, J. and Birkholtz, L.-M. (2020) Epigenetic inhibitors target multiple stages of *Plasmodium falciparum* parasites. Scientific Reports. **10**, 1-11
78 Reader, J., van der Watt, M. E., Taylor, D., Le Manach, C., Mittal, N., Ottilie, S., Theron, A., Moyo, P., Erlank, E. and Nardini, L. (2021) Multistage and transmission-blocking targeted antimalarials discovered from the open-source MMV Pandemic Response Box. Nature communications. **12**, 1-15
79 Ngwa, C. J., Kiesow, M. J., Orchard, L. M., Farrukh, A., Llinás, M. and Pradel, G. (2019) The G9a histone methyltransferase inhibitor BIX-01294 modulates gene expression during *Plasmodium falciparum* gametocyte development and transmission. International journal of molecular sciences. **20**, 5087
80 Matthews, K. A., Senagbe, K. M., Notzel, C., Gonzalez, C. A., Tong, X., Rijo-Ferreira, F., Natarajan, B. V., Miguel-Blanco, C., Lafuente-Monasterio, M. J. and Garcia, B. A. (2020) Disruption of the *Plasmodium falciparum* life cycle through transcriptional reprogramming by inhibitors of Jumonji demethylases. ACS Infectious Diseases
81 Kim, Y. B., Lee, K.-H., Sugita, K., Yoshida, M. and Horinouchi, S. (1999) Oxamflatin is a novel antitumor compound that inhibits mammalian histone deacetylase. Oncogene. **18**, 2461-2470
82 Faghihloo, E., Araei, Y., Mohammadi, M., Mirzaei, H., Mohammadi, H. and Mokhtari-Azad, T. (2016) The effect of oxamflatin on the E-cadherin expression in gastric cancer cell line. Cancer gene therapy. **23**, 396-399
83 Jiang, S., Dowdy, S. C., Meng, X. W., Wang, Z., Jones, M. B., Podratz, K. C. and Jiang, S.-W. (2007) Histone deacetylase inhibitors induce apoptosis in both type I and type II endometrial cancer cells. Gynecologic oncology. **105**, 493-500
84 Delves, M. J., Ruecker, A., Straschil, U., Lelièvre, J., Marques, S., López-Barragán, M. J., Herreros, E. and Sinden, R. E. (2013) Male and female *Plasmodium falciparum* mature gametocytes show different responses to antimalarial drugs. Antimicrobial agents and chemotherapy. **57**, 3268-3274
85 Lee, E. J., Lee, B. B., Kim, S.-J., Park, Y.-D., Park, J. and Kim, D.-H. (2008) Histone deacetylase inhibitor scriptaid induces cell cycle arrest and epigenetic change in colon cancer cells. International journal of oncology. **33**, 767-776
86 Keen, J. C., Yan, L., Mack, K. M., Pettit, C., Smith, D., Sharma, D. and Davidson, N. E. (2003) A novel histone deacetylase inhibitor, scriptaid, enhances expression of functional estrogen receptor α (ER) in ER negative human breast cancer cells in combination with 5-aza 2′-deoxycytidine. Breast cancer research and treatment. **81**, 177-186
87 Grozinger, C. M., Chao, E. D., Blackwell, H. E., Moazed, D. and Schreiber, S. L. (2001) Identification of a class of small molecule inhibitors of the sirtuin family of NAD-dependent deacetylases by phenotypic screening. Journal of Biological Chemistry. **276**, 38837-38843
88 Akam, E. A., Gautam, R. and Tomat, E. (2016) Metal-binding effects of sirtuin inhibitor sirtinol. Supramolecular Chemistry. **28**, 108-116
89 Ota, H., Tokunaga, E., Chang, K., Hikasa, M., Iijima, K., Eto, M., Kozaki, K., Akishita, M., Ouchi, Y. and Kaneki, M. (2006) Sirt1 inhibitor, Sirtinol, induces senescence-like growth arrest with attenuated Ras–MAPK signaling in human cancer cells. Oncogene. **25**, 176-185
90 Mittal, N., Muthuswami, R. and Madhubala, R. (2017) The mitochondrial SIR2 related protein 2 (SIR2RP2) impacts *Leishmania donovani* growth and infectivity. PLoS neglected tropical diseases. **11**, e0005590

91 Rai, G., Kawamura, A., Tumber, A., Liang, Y., Vogel, J. L., Arbuckle, J. H., Rose, N. R., Dexheimer, T. S., Foley, T. L. and King, O. N. (2013) Discovery of ML324, a JMJD2 demethylase inhibitor with demonstrated antiviral activity. In Probe Reports from the NIH Molecular Libraries Program [Internet], National Center for Biotechnology Information (US)
92 Kleszcz, R., Skalski, M., Krajka-Kuźniak, V. and Paluszczak, J. (2021) The inhibitors of KDM4 and KDM6 histone lysine demethylases enhance the anti-growth effects of erlotinib and HS-173 in head and neck cancer cells. European Journal of Pharmaceutical Sciences. **166**, 105961
93 Vedadi, M., Barsyte-Lovejoy, D., Liu, F., Rival-Gervier, S., Allali-Hassani, A., Labrie, V., Wigle, T. J., DiMaggio, P. A., Wasney, G. A. and Siarheyeva, A. (2011) A chemical probe selectively inhibits G9a and GLP methyltransferase activity in cells. Nature chemical biology. **7**, 566-574
94 Liu, X. R., Zhou, L. H., Hu, J. X., Liu, L. M., Wan, H. P. and Zhang, X. Q. (2018) UNC0638, a G9a inhibitor, suppresses epithelial-mesenchymal transition-mediated cellular migration and invasion in triple negative breast cancer. Molecular medicine reports. **17**, 2239-2244
95 Vanheer, L. N. and Kafsack, B. r. F. (2021) Activity comparison of epigenetic modulators against the hemoprotozoan parasites *Babesia divergens* and *Plasmodium falciparum*. ACS Infectious Diseases
96 Julien, E., Herviou, L., Izard, F., Karmous-Gadacha, O., Gourzones, C., Bellanger, C., Desmedt, E., Ma, A., Vincent, L. and Cartron, G. (2020) Targeting the methyltransferase SETD8 impairs tumor cell survival and overcomes drug resistance independently of p53 status in multiple myeloma.
97 Wada, M., Kukita, A., Sone, K., Hamamoto, R., Kaneko, S., Komatsu, M., Takahashi, Y., Inoue, F., Kojima, M. and Honjoh, H. (2020) Epigenetic Modifier SETD8 as a Therapeutic Target for High-Grade Serous Ovarian Cancer. Biomolecules. **10**, 1686
98 Opperman, D. (2019) Epi-drugs kill asexual *Plasmodium falciparum* parasites through global changes in histone acetylation status and confer transmission blocking. University of Pretoria
99 Kirkpatrick, J. E., Kirkwood, K. L. and Woster, P. M. (2018) Inhibition of the histone demethylase KDM4B leads to activation of KDM1A, attenuates bacterial-induced pro-inflammatory cytokine release, and reduces osteoclastogenesis. Epigenetics. **13**, 557-572
100 Ma, A., Yu, W., Li, F., Bleich, R. M., Herold, J. M., Butler, K. V., Norris, J. L., Korboukh, V., Tripathy, A. and Janzen, W. P. (2014) Discovery of a selective, substrate-competitive inhibitor of the lysine methyltransferase SETD8. Journal of medicinal chemistry. **57**, 6822-6833
101 Waterhouse, A., Bertoni, M., Bienert, S., Studer, G., Tauriello, G., Gumienny, R., Heer, F. T., de Beer, T. A. P., Rempfer, C. and Bordoli, L. (2018) SWISS-MODEL: homology modelling of protein structures and complexes. Nucleic acids research. **46**, W296-W303
102 Zhu, A. Y., Zhou, Y., Khan, S., Deitsch, K. W., Hao, Q. and Lin, H. (2012) *Plasmodium falciparum* Sir2A preferentially hydrolyzes medium and long chain fatty acyl lysine. ACS chemical biology. **7**, 155-159
103 Jumper, J., Evans, R., Pritzel, A., Green, T., Figurnov, M., Ronneberger, O., Tunyasuvunakool, K., Bates, R., Žídek, A. and Potapenko, A. (2021) Highly accurate protein structure prediction with AlphaFold. Nature. **596**, 583-589
104 Pettersen, E. F., Goddard, T. D., Huang, C. C., Couch, G. S., Greenblatt, D. M., Meng, E. C. and Ferrin, T. E. (2004) UCSF Chimera—a visualization system for exploratory research and analysis. Journal of computational chemistry. **25**, 1605-1612
105 Williams, C. J., Headd, J. J., Moriarty, N. W., Prisant, M. G., Videau, L. L., Deis, L. N., Verma, V., Keedy, D. A., Hintze, B. J. and Chen, V. B. (2018) MolProbity: More and better reference data for improved all-atom structure validation. Protein Science. **27**, 293-315
106 Grosdidier, A., Zoete, V. and Michielin, O. (2011) Fast docking using the CHARMM force field with EADock DSS. Journal of computational chemistry. **32**, 2149-2159

107 Grosdidier, A., Zoete, V. and Michielin, O. (2011) SwissDock, a protein-small molecule docking web service based on EADock DSS. Nucleic acids research. **39**, W270-W277
108 Lambros, C. and Vanderberg, J. P. (1979) Synchronization of *Plasmodium falciparum* erythrocytic stages in culture. The Journal of parasitology, 418-420
109 Colmenarejo, G., Lozano, S., González-Cortés, C., Calvo, D., Sanchez-Garcia, J., Matilla, J.-L. P., Leroy, D. and Rodrigues, J. (2018) Predicting transmission blocking potential of anti-malarial compounds in the mosquito feeding assay using *Plasmodium falciparum* male gamete inhibition assay. Scientific reports. **8**, 1-13
110 Ruecker, A., Mathias, D., Straschil, U., Churcher, T., Dinglasan, R., Leroy, D., Sinden, R. and Delves, M. (2014) A male and female gametocyte functional viability assay to identify biologically relevant malaria transmission-blocking drugs. Antimicrobial agents and chemotherapy. **58**, 7292-7302
111 Churcher, T. S., Blagborough, A. M., Delves, M., Ramakrishnan, C., Kapulu, M. C., Williams, A. R., Biswas, S., Da, D. F., Cohuet, A. and Sinden, R. E. (2012) Measuring the blockade of malaria transmission–an analysis of the standard membrane feeding assay. International journal for parasitology. **42**, 1037-1044
112 Miura, K., Deng, B., Tullo, G., Diouf, A., Moretz, S. E., Locke, E., Morin, M., Fay, M. P. and Long, C. A. (2013) Qualification of standard membrane-feeding assay with *Plasmodium falciparum* malaria and potential improvements for future assays. PloS one. **8**
113 Marmorstein, R. (2001) Structure of histone deacetylases: insights into substrate recognition and catalysis. Structure. **9**, 1127-1133
114 Peck, B., Chen, C.-Y., Ho, K.-K., Di Fruscia, P., Myatt, S. S., Coombes, R. C., Fuchter, M. J., Hsiao, C.-D. and Lam, E. W.-F. (2010) SIRT inhibitors induce cell death and p53 acetylation through targeting both SIRT1 and SIRT2. Molecular cancer therapeutics. **9**, 844-855
115 Mukherjee, P., Pradhan, A., Shah, F., Tekwani, B. L. and Avery, M. A. (2008) Structural insights into the *Plasmodium falciparum* histone deacetylase 1 (PfHDAC-1): A novel target for the development of antimalarial therapy. Bioorganic & medicinal chemistry. **16**, 5254-5265
116 Klose, R. J., Kallin, E. M. and Zhang, Y. (2006) JmjC-domain-containing proteins and histone demethylation. Nature reviews genetics. **7**, 715-727
117 Cui, L., Fan, Q., Cui, L. and Miao, J. (2008) Histone lysine methyltransferases and demethylases in *Plasmodium falciparum*. International journal for parasitology. **38**, 1083-1097
118 Mahon, P. C., Hirota, K. and Semenza, G. L. (2001) FIH-1: a novel protein that interacts with HIF-1α and VHL to mediate repression of HIF-1 transcriptional activity. Genes & development. **15**, 2675-2686
119 Qian, C. and Zhou, M.-M. (2006) SET domain protein lysine methyltransferases: Structure, specificity and catalysis. Cellular and molecular life sciences CMLS. **63**, 2755-2763
120 Charles, M. R. C., Mahesh, A., Lin, S.-Y., Hsieh, H.-P., Dhayalan, A. and Coumar, M. S. (2020) Identification of novel quinoline inhibitor for EHMT2/G9a through virtual screening. Biochimie. **168**, 220-230
121 Duffy, M. F., Selvarajah, S. A., Josling, G. A. and Petter, M. (2013) Epigenetic regulation of the *Plasmodium falciparum* genome. Briefings in functional genomics. **13**, 203-216
122 Saksouk, N., Bhatti, M. M., Kieffer, S., Smith, A. T., Musset, K., Garin, J., Sullivan Jr, W. J., Cesbron-Delauw, M.-F. and Hakimi, M.-A. (2005) Histone-modifying complexes regulate gene expression pertinent to the differentiation of the protozoan parasite *Toxoplasma gondii*. Molecular and cellular biology. **25**, 10301-10314
123 Mann, B. S., Johnson, J. R., Cohen, M. H., Justice, R. and Pazdur, R. (2007) FDA approval summary: vorinostat for treatment of advanced primary cutaneous T-cell lymphoma. The oncologist. **12**, 1247-1252
124 Malmquist, N. A., Sundriyal, S., Caron, J., Chen, P., Witkowski, B., Menard, D., Suwanarusk, R., Renia, L., Nosten, F. and Jiménez-Díaz, M. B. (2015) Histone methyltransferase inhibitors are orally bioavailable, fast-acting molecules with activity against

different species causing malaria in humans. Antimicrobial agents and chemotherapy. **59**, 950-959
125 Davis, A. M., St-Gallay, S. A. and Kleywegt, G. J. (2008) Limitations and lessons in the use of X-ray structural information in drug design. Drug Discovery Today. **13**, 831
126 Melesina, J., Robaa, D., Pierce, R. J., Romier, C. and Sippl, W. (2015) Homology modeling of parasite histone deacetylases to guide the structure-based design of selective inhibitors. Journal of Molecular Graphics and Modelling. **62**, 342-361
127 Birkholtz, L.-M., Blatch, G., Coetzer, T. L., Hoppe, H. C., Human, E., Morris, E. J., Ngcete, Z., Oldfield, L., Roth, R. and Shonhai, A. (2008) Heterologous expression of plasmodial proteins for structural studies and functional annotation. Malaria journal. **7**, 1-20
128 Freitas, M. A., Sklenar, A. R. and Parthun, M. R. (2004) Application of mass spectrometry to the identification and quantification of histone post-translational modifications. Journal of cellular biochemistry. **92**, 691-700
129 Hesping, E., Skinner-Adams, T. S., Fisher, G. M., Kurz, T. and Andrews, K. T. (2020) An ELISA method to assess HDAC inhibitor-induced alterations to *P. falciparum* histone lysine acetylation. International Journal for Parasitology: Drugs and Drug Resistance. **14**, 249-256
130 Li, R., Ling, D., Tang, T., Huang, Z., Wang, M., Ding, Y., Liu, T., Wei, H., Xu, W. and Mao, F. (2021) Discovery of Novel *Plasmodium falciparum* HDAC1 Inhibitors with Dual-Stage Antimalarial Potency and Improved Safety Based on the Clinical Anticancer Drug Candidate Quisinostat. Journal of Medicinal Chemistry. **64**, 2254-2271
131 Huang, Z., Li, R., Tang, T., Ling, D., Wang, M., Xu, D., Sun, M., Zheng, L., Zhu, F. and Min, H. (2020) A novel multistage antiplasmodial inhibitor targeting *Plasmodium falciparum* histone deacetylase 1. Cell discovery. **6**, 1-15
132 Andrews, K., Tran, T., Lucke, A., Kahnberg, P., Le, G., Boyle, G., Gardiner, D., Skinner-Adams, T. and Fairlie, D. (2008) Potent antimalarial activity of histone deacetylase inhibitor analogues. Antimicrobial agents and chemotherapy. **52**, 1454-1461
133 Pasternak, N. D. and Dzikowski, R. (2009) PfEMP1: an antigen that plays a key role in the pathogenicity and immune evasion of the malaria parasite *Plasmodium falciparum*. The international journal of biochemistry & cell biology. **41**, 1463-1466
134 Merrick, C. J., Dzikowski, R., Imamura, H., Chuang, J., Deitsch, K. and Duraisingh, M. T. (2010) The effect of *Plasmodium falciparum* Sir2a histone deacetylase on clonal and longitudinal variation in expression of the *var* family of virulence genes. International journal for parasitology. **40**, 35-43
135 Andrews, K. T., Haque, A. and Jones, M. K. (2012) HDAC inhibitors in parasitic diseases. Immunology and cell biology. **90**, 66-77
136 Hailu, G. S., Robaa, D., Forgione, M., Sippl, W., Rotili, D. and Mai, A. (2017) Lysine deacetylase inhibitors in parasites: past, present, and future perspectives. Journal of medicinal chemistry. **60**, 4780-4804
137 Anderson, T., Nkhoma, S., Ecker, A. and Fidock, D. (2011) How can we identify parasite genes that underlie antimalarial drug resistance? Pharmacogenomics. **12**, 59-85
138 Lomenick, B., Olsen, R. W. and Huang, J. (2011) Identification of direct protein targets of small molecules. ACS chemical biology. **6**, 34-46
139 Lomenick, B., Hao, R., Jonai, N., Chin, R. M., Aghajan, M., Warburton, S., Wang, J., Wu, R. P., Gomez, F. and Loo, J. A. (2009) Target identification using drug affinity responsive target stability (DARTS). Proceedings of the National Academy of Sciences. **106**, 21984-21989

Chapter 6: Supplementary

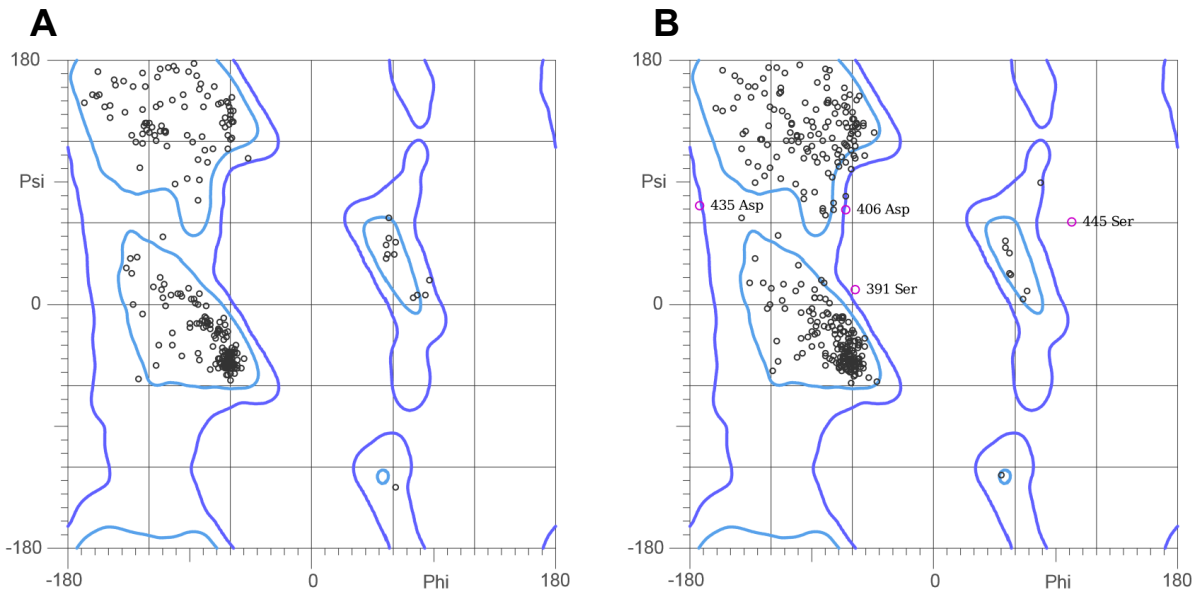

Figure S1: Ramachandran plots of energetically allowed peptide backbone dihedral angles for the general case of PfHDAC1 secondary structure. (A) SwissModel model secondary structure dihedral angle distribution. 97 % of residues indicated favourable dihedral angles while 0.27 % indicated unfavourable dihedral angles. **(B)** AlphaFold model secondary structure dihedral angle distribution. 95 % of residues indicated favourable dihedral angles while 0.89 % indicated unfavourable dihedral angles.

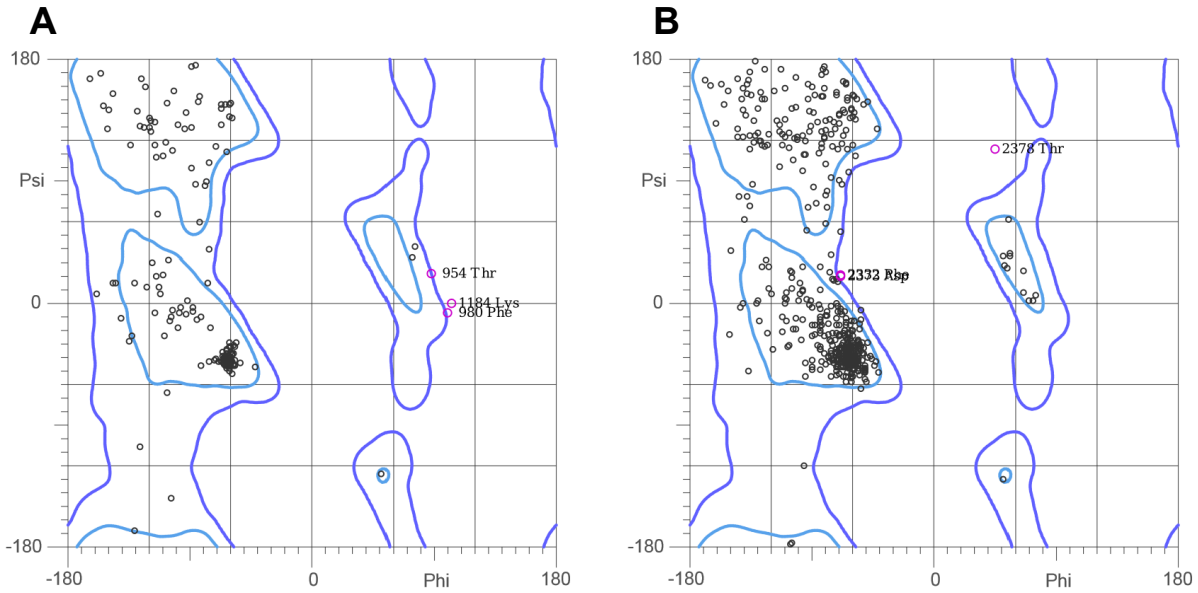

Figure S2: Ramachandran plots of energetically allowed peptide backbone dihedral angles for the general case of PfHDAC2 secondary structure. (A) SwissModel model secondary structure dihedral angle distribution. 91 % of residues indicated favourable dihedral angles while 1.42 % indicated unfavourable dihedral angles. **(B)** AlphaFold model secondary structure dihedral angle distribution. 94 % of residues indicated favourable dihedral angles while 0.63 % indicated unfavourable dihedral angles.

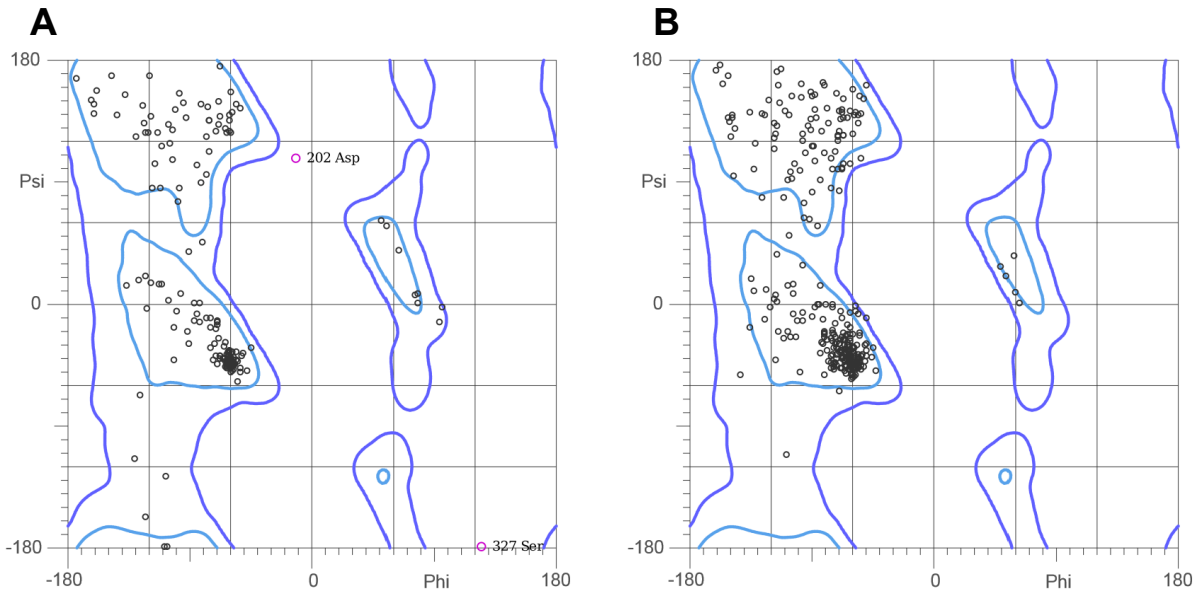

Figure S3: Ramachandran plots of energetically allowed peptide backbone dihedral angles for the general case of putative PfHDAC3 secondary structure. (A) SwissModel model secondary structure dihedral angle distribution. 93 % of residues indicated favourable dihedral angles while 1.75 % indicated unfavourable dihedral angles. **(B)** AlphaFold model secondary structure dihedral angle distribution. 93 % of residues indicated favourable dihedral angles while 0.00 % indicated unfavourable dihedral angles.

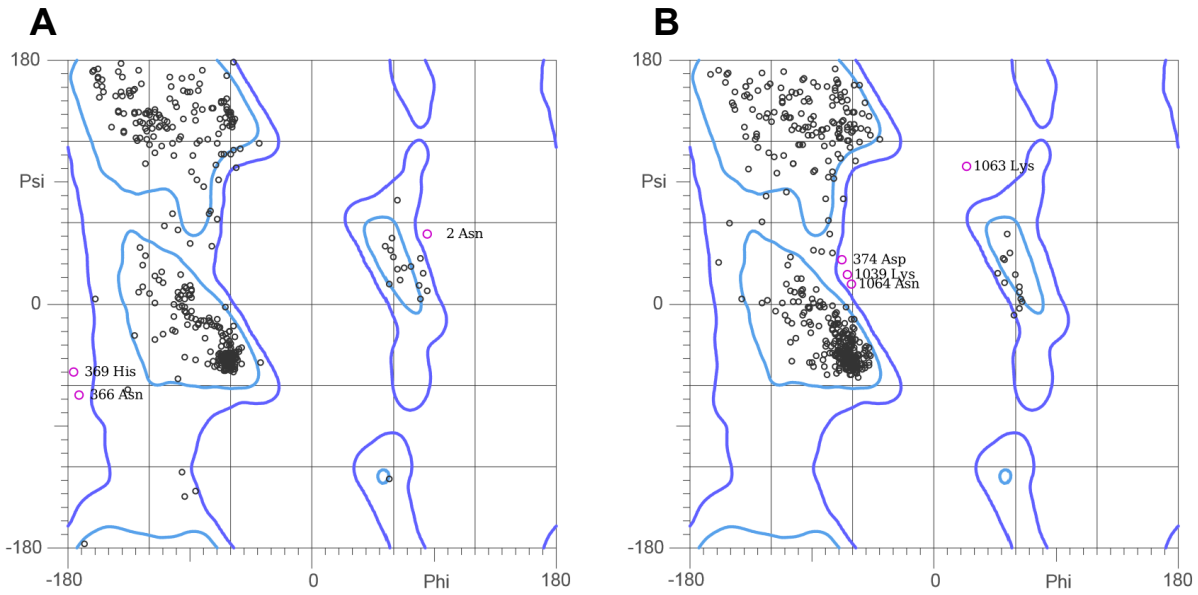

Figure S4: Ramachandran plots of energetically allowed peptide backbone dihedral angles for the general case of PfJmjC1 secondary structure. (A) SwissModel model secondary structure dihedral angle distribution. 92 % of residues indicated favourable dihedral angles while 1.06 % indicated unfavourable dihedral angles. **(B)** AlphaFold model secondary structure dihedral angle distribution. 95 % of residues indicated favourable dihedral angles while 0.71 % indicated unfavourable dihedral angles.

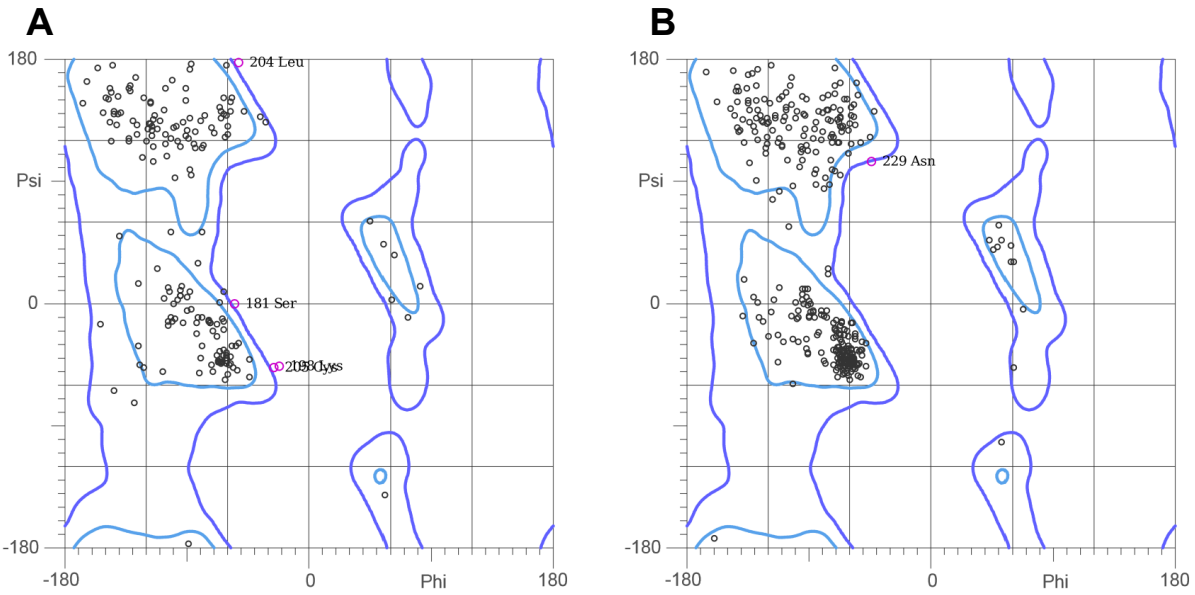

Figure S5: Ramachandran plots of energetically allowed peptide backbone dihedral angles for the general case of PfJmjC2 secondary structure. (A) SwissModel model secondary structure dihedral angle distribution. 88 % of residues indicated favourable dihedral angles while 2.43 % indicated unfavourable dihedral angles. **(B)** AlphaFold model secondary structure dihedral angle distribution. 96 % of residues indicated favourable dihedral angles while 0.23 % indicated unfavourable dihedral angles.

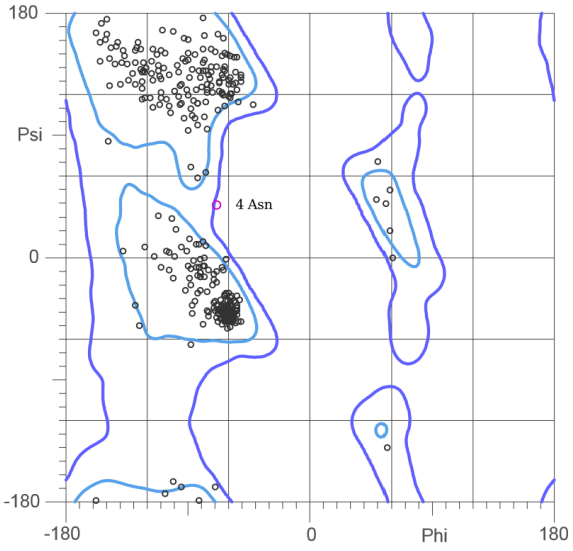

Figure S6: Ramachandran plots of energetically allowed peptide backbone dihedral angles for the general case of PfJmj3 secondary structure. AlphaFold model secondary structure dihedral angle distribution. 97 % of residues indicated favourable dihedral angles while 0.24 % indicated unfavourable dihedral angles.

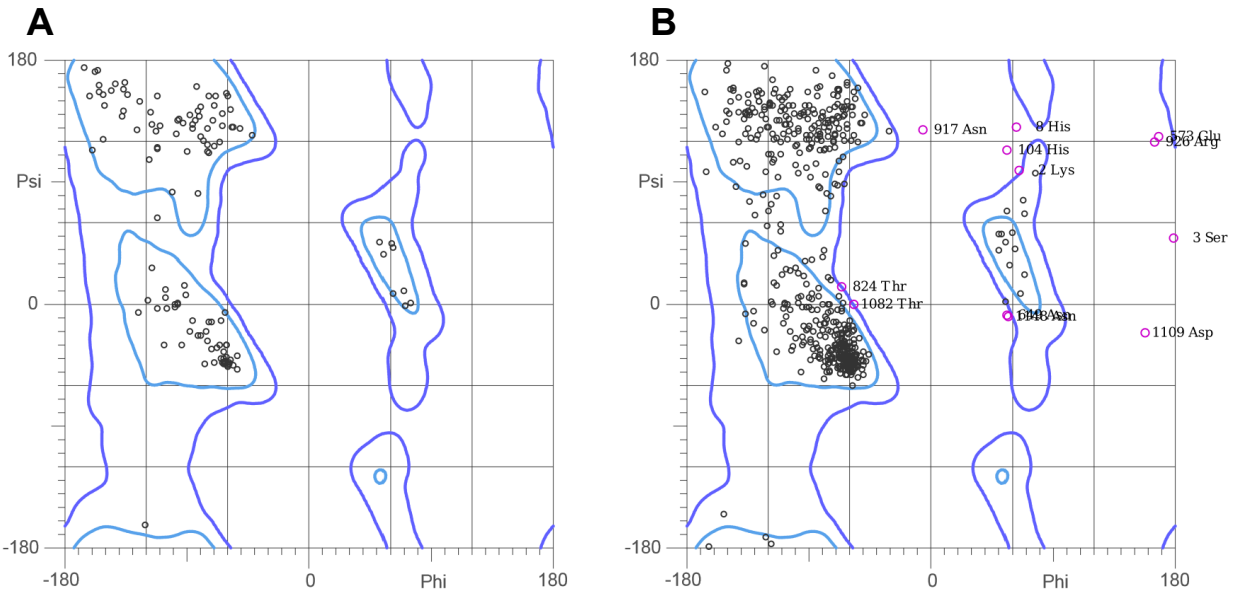

Figure S7: Ramachandran plots of energetically allowed peptide backbone dihedral angles for the general case of PfSET8 secondary structure. (A) SwissModel model secondary structure dihedral angle distribution. 99 % of residues indicated favourable dihedral angles while none indicated unfavourable dihedral angles. **(B)** AlphaFold model secondary structure dihedral angle distribution. 92 % of residues indicated favourable dihedral angles while 2.23 % indicated unfavourable dihedral angles.

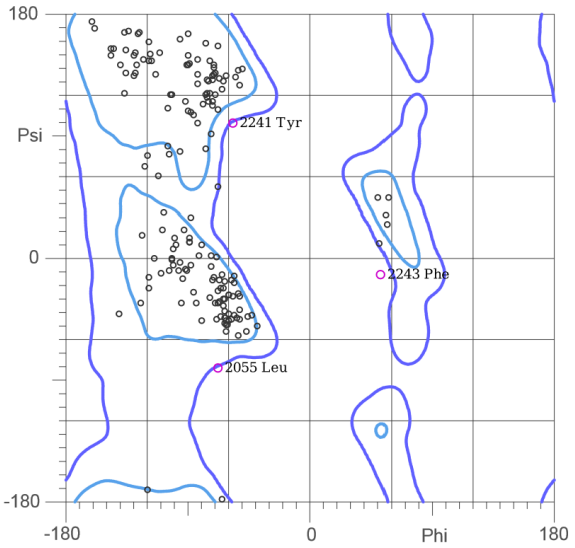

Figure S8: Ramachandran plots of energetically allowed peptide backbone dihedral angles for the general case of PfSET2 secondary structure. AlphaFold model secondary structure dihedral angle distribution. 92 % of residues indicated favourable dihedral angles while 1.39 % indicated unfavourable dihedral angles.